A Thesis Report

On

EVALUATION OF FRACTURE CHARACTERISTICS OF REACTOR PRESSURE VESSEL STEEL 20MnMoNi55 USING DAMAGE MECHANICS APPROACH

Submitted In partial fulfillment of the requirement for the award of

degree of

MASTER OF ENGINEERING

IN

CAD/CAM & ROBOTICS

Submitted By

HARDEEP SINGH

Roll No. 80681007

Under the guidance of

Dr. Rahul Chhibber
Lecturer
Mechanical Engineering Department.
Thapar University,
Patiala -147004

Dr. Bijan Kumar Dutta
Head,
Computational Mech. Section
Reactor Safety Division
BARC
Mumbai-400085

Mechanical Engineering Department

Thapar University

Patiala-147001 (INDIA)

CERTIFICATE

This is to certify that The Thesis titled, **"EVALUATION OF FRACTURE CHARACTERISTICS OF REACTOR PRESSURE VESSEL STEEL 20MnMoNi55 USING DAMAGE MECHANICS APPROACH",** being submitted by **Mr. Hardeep Singh,** in partial fulfillment of the requirement for the award of degree of **MASTER OF ENGINEERING (CAD/CAM & ROBOTICS) at THAPAR UNIVERSITY, PATIALA** is a bonafide work carried out by him under our guidance and supervision and no part of this thesis has been submitted for the award of any other degree.

Mr. Rahul Chhibber
Lecturer
Mechanical Engineering Department.
Thapar University,
Patiala -147004

Dr. Bijan Kumar Dutta
Head,
Computational Mech. Section
Reactor Safety Division
BARC
Mumbai-400085

Dr S.K. Mohapatra
Professor & Head,
Thapar University,
Patiala -147004

Dr R.K. Sharma
Dean, Academic Affairs
Thapar University
Patiala-147004

ACKNOWLEDGEMENT

I express my sincere gratitude to my supervisors-Dr. Rahul Chhibber, Lecturer, Mechanical Engineering Department at Thapar University, Patiala and Dr. B.K. Dutta, Head Computational Mechanics Section, Reactor Safety Division, BARC, Mumbai for their valuable guidance, proper advice, painstaking and constant encouragement during the course of my work.

I am grateful to Mr. Subhashish Guin, Scientific Officer (D), BARC. His suggestion and knowledge on the subject was invaluable throughout the thesis work. I am also grateful to Dr. Navneet Arora, Assoc. Professor Department of Mechanical Engineering IIT Roorkee for his help to perform experiments.

I feel very much obliged to Dr. S.K Mohapatra, Professor & Head, Department of Mechanical Engineering and Dr. Abhijit Mukherjee, Director, Thapar University for their encouragement and inspiration for my visit to BARC, Mumbai.

I am deeply indebted to my parents for their inspiration and ever encouraging moral support, which enabled me to pursue my studies.

I am also very thankful to the entire faculty and staff members of Mechanical engineering Department for their direct indirect help and cooperation.

Date:

HARDEEP SINGH

(ROLL NO. 80681007)

ABSTRACT

Material of Reactor Pressure Vessel (RPV) should have good enough fracture toughness to ensure safe operation of nuclear reactor. In order to be on safe side the fracture characteristics of RPV material have to be quantified. In this present work the fracture characteristics of 20MnMoNi55 steel – the material used for Indian PHWR – have been found using damage mechanics approach.

Fracture resistance of a ductile material is conventionally characterized by J-R curves. The original idea was that a unique fracture resistance curve would suffice to characterize the material. However, testing of different type of specimens revealed considerable different J-R curves due to different levels of triaxility imposed on the specimens. This raises the question of transferring fracture parameters from specimens to component level.

Under such circumstances it becomes advisable to use Damage Mechanics. The difficulty of geometry-dependency is largely overcome by Damage Mechanics, which models the drop in load carrying capacity of material with increase in plastic strain. Such modeling is done considering nucleation, growth and coalescence of the voids in a material following large scale plasticity. The constitutive model introduced by Gurson and modified by Tvergaard and Needleman is used in this work.

The model parameters are determined by using hybrid methodology of different tensile tests subsequent numerical analysis and curve fitting and finally comparison of analytical and experimental results. A parametric study on different Gurson parameters was carried out to experience the effect of different parameters on load ΔD curves for RNTS and J-R curves CT specimens. Later the model parameters were calibrated by fitting the analytical results in the experimental results.

CONTENTS

TITLE		PAGE NO.
CERTIFICATE		i
ACKNOWLEDGEMENT		ii
ABSTRACT		iii
CONTENTS		iv
LIST OF FIGURES		viii
LIST OF TABLES		xi
NOMENCLATURE		xii
CHAPTER - 1		
INTRODUCTION		**1**
1.1	Nuclear Reactor	1
1.2	Reactor Pressure Vessel	2
1.3	Fabrication of RPVs	2
1.4	Reactor Pressure Vessel material	5
CHAPTER - 2		
LITERATURE REVIEW		**6**
2.1	Fracture mechanics	6
2.2	Classification of Fracture Mechanics	7
2.2.1	Linear Elastic Fracture Mechanics (LEFM)	8
2.2.1.1	Plane stresses and Plain strains	9
2.2.1.2	Stress Intensity Factor and Crack Tip Stresses	11
2.2.1.3	Stress Intensity Factor and Fracture Toughness	12
2.2.1.4	Relationship between G and K	12
2.2.2	Elastic Plastic Fracture Mechanics (EPFM)	13
2.2.3	J-Integral	15
2.2.4	Crack Tip Opening Displacement (CTOD)	17

TITLE **PAGE NO.**

2.2.5 Relationship between J and CTOD 18

2.2.6 J-R Curve 18

2.3 Limitations of Single Parameter Characterization 19

2.4 Physical Significance of Crack Tip Constraint 20

2.5 Two Parameter Fracture Mechanics 20

2.5.1 J-T approach 21

2.5.2 J-h approach 22

2.5.3 J-A2 approach 22

2.5.4 J-Q approach 23

2.6 Micromechanical Modelling / Damage mechanics 23

2.6.1 Uncoupled Micromechanical Models 25

2.6.2 Coupled Micromechanical Models 26

2.7 Gurson Tvergaard Needleman model 27

2.7.1 Flow rule 29

2.8 GTN Model Parameters & Their Determination 32

2.9 Work reviewed 33

CHAPTER - 3

PROBLEM DEFINITION **45**

3.1 Introduction 45

3.2 Aim of thesis 45

CHAPTER-4

EXPERIMENTAL RESULTS **47**

4.1 Introduction 47

4.2 Material Properties 47

TITLE **PAGE NO.**

4.3 Experimental load – Diametric contraction curves of Round Notched Tensile specimens 48

4.3.1 Details of the Round Notched Tensile Specimens 49

4.3.2 Test results for RNTS 51

4.4 Testing of CT Specimen and TPB Specimen 53

4.4.1 Details of the Test Specimens 53

4.4.2 Details of the Testing Procedure 55

4.4.3 Test Results 57

CHAPTER: 5

FINITE ELEMENT ANALYSIS METHODOLOGY 59

5.1 Introduction 59

5.2 Generation of FE mesh 59

5.3 Generation of the input file 63

5.4 Running the FE code MADAM (Material Damage Modelling) 66

5.5 Post-processing the output from MADAM code 67

CHAPTER: 6

EVALUATION OF GURSON DAMAGE PARAMETERS 69

6.1 A Study on Effect of Gurson Parameters on Material Behaviour 69

6.2 Effect of Initial void volume fraction (f_0) 70

6.3 Effect of critical void volume fraction (f_c) 72

6.4 Effect of final void volume fraction (f_f) 73

6.5 Effect of mean strain of void nucleation (ε_n): 75

6.6 Effect of standard deviation of nucleation strain 'S_N': 76

6.7 Effect of void volume fraction at saturated nucleation, 'f_N' 78

6.8 Determination of damage parameters from experimental and analytical load- ΔD curves 79

TITLE **PAGE NO.**

6.8.1 Curve fitting of RNTS R2 79
6.8.2 Curve fitting of RNTS R4 83

CHAPTER: 7
VERIFICATION OF GURSON PARAMETERS **86**
7.1 Experimental vs Analytical J-R curves for CT specimen 86

CHAPTER: 8
CLOSURE **89**
8.1 Conclusions 89
8.2 Recommendations for Future Work 89

REFERENCES **90**

LIST OF FIGURES

FIGURE NO.	DESCRIPTION	PAGE NO.
1.1	A typical Nuclear reactor pressure vessel	3
1.2	Fabrication configurations of PWR beltline shells	4
2.1:	Linear elastic crack in tensile specimen	8
2.2:	Opening mode deformation	10
2.3:	Sliding mode deformation	10
2.4:	Tearing mode deformation	11
2.5:	Stress field near crack tip of an isotropic linear elastic material	11
2.6:	CT specimen with initial crack of length a	13
2.7:	Difference between LEFM, EPFM	14
2.8:	Elastic-plastic crack in tensile specimen	14
2.9	Crack in an arbitrary body—definition of *J*-integral	16
2.10a:	CTOD of original crack tip	17
2.10b:	CTOD of crack tip at intersection of 90 vertex	18
2.11	Void nucleation and growth in a tensile specimen of ductile material	24
2.12	Schematic path of a growing crack in a ductile material	25
4.1	Engineering stress-strain curve of 20MnMoNi55 steel	48
4.2	True stress strain curve of 20MnMoNi55 steel	48
4.3	Detail of smooth and notched tensile specimens	49
4.4	Photographs during testing (20MnMoNi55 R2)	50
4.5	The image processing using AutoCAD	51
4.6	Experimental Load-ΔD curve for R2	52
4.7	Experimental Load-ΔD curve for R4	53
4.8	CT specimens used for testing	53
4.9	Details of the CT specimens	54
4.10	TPB specimen used for testing	54
4.11	Details of the TPB specimen	55

FIGURE NO. DESCRIPTION PAGE NO.

4.12	Fractured CT specimen.	57
4.13	Fractured surface of broken CT specimen.	57
4.14	Fractured TPB specimen.	57
4.15	Experimental J-R curves for CT specimen (20MnMoNi55 steel)	58
4.16	Experimental J-R curve for TPB specimen (20MnMoNi55 steel)	58
5.1	Geometry of RNTS specimen	59
5.2	FE mesh for RNTS R2 specimen	60
5.3	FE mesh for RNTS R4 specimen	60
5.4	Geometry of TPB specimen	61
5.5	FE mesh for TPB specimen	61
5.6	Geometry of CT specimen	62
5.7	FE mesh for CT specimen	62
6.1	Load-ΔD curves for different f_o values	70
6.2	J-R curves for different f_o values	71
6.3	Load-ΔD curves for different f_c values	72
6.4	J-R curves for different f_c value	73
6.5	Load-ΔD curves for different f_f values	74
6.6	J-R curves for different f_f values	74
6.7	Load-ΔD curves for different ε_n values	75
6.8	J-R curves for different ε_n values	76
6.9	Load-ΔD curves for different S_n values	77
6.10	J-R curves for different S_n values	77
6.11	Load-ΔD curves for different f_n values	78
6.12	J-R curves for different f_n values	79
6.13	Experimental and Analytical load- ΔD curves for RNTS R2	80
6.14	Experimental and Analytical load- ΔD curves for RNTS R2	80
6.15	Experimental and Analytical load- ΔD curves for RNTS R2	81
6.16	Experimental and Analytical load- ΔD curves for RNTS R2	81

FIGURE NO. DESCRIPTION PAGE NO.

6.17 FEM mesh of RNTS R2 at load 2.2 KN and displacement 1.8mm 82

6.18 Experimental and Analytical load- ΔD curves for RNTS R4 83

6.19 Experimental and Analytical load- ΔD curves for RNTS R4 84

7.1 FEM mesh of CT specimen at load 3.32 KN and CTOD 3mm 86

7.2 Experimental vs Analytical J-R curves for CT Specimen for final set of Gurson parameters 87

7.3 Experimental vs Analytical J-R curves for TPB Specimen for final set of Gurson parameters. 87

7.4 FEM mesh of TPB specimen at load 1.3KN and CTOD 2.95mm 88

LIST OF TABLES

TABLE NO.	DESCRIPTION	PAGE NO.
4.1	Mechanical properties of 20MnMoNi55 steel at room temperature	47
4.2	Chemical composition of 20MnMoNi55 steel	47
4.3	Load – ΔD values of RNTS R2 specimen	51
4.4	Load – ΔD values of RNTS R4 specimen	52
6.1	Initial Gurson parameters and their values	69
6.2	Effect of f_o on ΔD (at sudden load drop), Slope Load-ΔD, Ji (initiation) and slope of J-R curve	71
6.3	Effect of f_c on ΔD (at sudden load drop), Slope Load-ΔD, Ji (initiation) and slope of J-R curve	73
6.4	Effect of f_f on ΔD (at sudden load drop), Slope Load-ΔD, Ji (initiation) and slope of J-R curve	75
6.5	Effect of ε_n on ΔD (at sudden load drop), Slope Load-ΔD, Ji (initiation) and slope of J-R curve	76
6.6	Effect of S_n on ΔD (at sudden load drop), Slope Load-ΔD, Ji (initiation) and slope of J-R curve	78
6.7	Effect of f_n on ΔD (at sudden load drop), Slope Load-ΔD, Ji (initiation) and slope of J-R curve	79
6.8	Set of Gurson parameters that best approximate material behaviour for R2	82
6.9	Set of Gurson parameters that best approximate material behaviour for R4	84
6.9	Final set of Gurson parameters that best approximate material behaviour	85

NOMENCLATURE

SYMBOLS	MEANING
a	Crack length
A	Crack-face area, constant
A_2	Constraint indexing parameter
A_i	Area of inclusion and void
A_T	Total area under observation
A_V	Area fraction of voids
b	Ligament length of specimen
B	Specific width, constant
CTOD	Crack tip opening displacement
D	Damage parameter/Diameter
ΔD	Contraction in diameter
E	Young's Modulus
E_t	Tangent modulus of stress- strain
f	Void volume fraction
f_o	Initial void volume fraction
f_c	Critical void volume fraction
f_f	Final void volume fraction
f_n	Void volume fraction at saturated nucleation
f	Void increment rate
f	Modified void volume fraction
f_u	Modified ultimate void volume fraction
f_{growth}	Void growth rate
$f_{nucleation}$	Void nucleation rate
g_{kj}	Metric tensor
G	Crack extention rate
G_c	Elastic energy release rate
I_n	Integration constant

SYMBOLS	MEANING
J	J-integral
K	Acceleration factor
K_I	Stress intensity factor
K_{IC}	Plane stress fracture toughness
q	Multi-axiality quotient
q_1, q_2, q_3	Modifying parameters
Q	Triaxiality indexing parameter
r	Radius vector
R	Mean current void radius
R_0	Initial void radius
s^{ij}	stress deviator
T_i	Traction vector
U	Strain energy stored in a body
U_c	Area under load deflection curve
$U_{c(el)}$	Elastic portion of U_c
$U_{c(pl)}$	Plastic portion of U_c
V_v	Volume fraction of voids
ΔU_p	Change in potential energy
w	Specimen thickness
α	Ramberg-Osgood coefficient, constant
ε	Strain
ε_c	Strain corresponding to critical void growth ratio
$\delta\,\varepsilon^p$	Plastic strain increment
Γ	Arbitrary contour around crack tip
Θ	Angle in polar coordinate
σ	Stress
$\sigma_1, \sigma_2, \sigma_3$	Principal stresses
σ_y	Yield stress

CHAPTER: 1

INTRODUCTION

1.1 Nuclear Reactor

Most nuclear electricity is generated using reactors which were developed in the 1950s and improved since. New designs are coming forward and some are in operation as the first generation reactors come to the end their operating lives. Over 16% of the world's electricity is produced from nuclear energy.

A nuclear reactor produces and controls the release of energy from splitting the atoms of certain elements. In a nuclear power reactor, the energy released is used to make steam to generate electricity. In a research reactor the main purpose is to utilize the actual neutrons produced in the core. In most naval reactors, steam drives a turbine directly for propulsion. The principles for using nuclear power to produce electricity are the same for most types of reactor. The energy released from continuous fission of the atoms of the fuel is harnessed as heat in either a gas or water, and is used to produce steam. The steam is used to drive the turbines which produce electricity.

There are several components common to most types of reactors:-

1. Fuel- Usually pellets of uranium oxide (UO_2) arranged in tubes to form fuel rods. The rods are arranged into fuel assemblies in the reactor core.

2. Moderator- This is material which slows down the neutrons released from fission so that they cause more fission. It is usually water, but may be heavy water or graphite.

3. Control rods- These are made with neutron-absorbing material such as cadmium or boron, and are inserted or withdrawn from the core to control the rate of reaction, or to halt it.

4. Coolant- A liquid or gas circulating through the core so as to transfer the heat from it. . In light water reactors the water moderator functions also as primary coolant.

5. Pressure vessel or pressure tubes- Usually a robust steel vessel containing the reactor core and moderator/coolant, but it may be a series of tubes holding the fuel and conveying the coolant through the moderator.

6. Steam generator- Part of the cooling system where the heat from the reactor is used to make steam for the turbine.

7. Containment- The structure around the reactor core which is designed to protect it from outside intrusion and to protect those outside from the effects of radiation in case of any malfunction inside. It is typically a metre-thick concrete and steel structure.

1.2 Reactor Pressure Vessel

A typical RPV is shown in Figure 1.1. The RPV is cylindrical with a hemispherical bottom head and a flanged and gasketed upper head. The bottom head is welded to the cylindrical shell while the top head is bolted to the cylindrical shell via the flanges. The cylindrical shell course may or may not utilize longitudinal weld seams in addition to the girth (circumferential) weld seams. The body of the vessel is of low-alloy carbon steel. To minimize corrosion, the inside surfaces in contact with the coolant are clad with a minimum of some 3 to 10 mm of austenitic stainless steel. Numerous inlet and outlet nozzles, as well as control rod drive tubes and instrumentation and safety injection nozzles penetrate the cylindrical shell. The number of inlet and outlet nozzles is a function of the number of loops or steam generators.

1.3 Fabrication of RPVs

Fabrication of RPVs has also been an evolving technology, and later vessels were fabricated using knowledge gained from the surveillance

programmes and more modern methods such as the use of large forgings to reduce the number of welds in the beltline

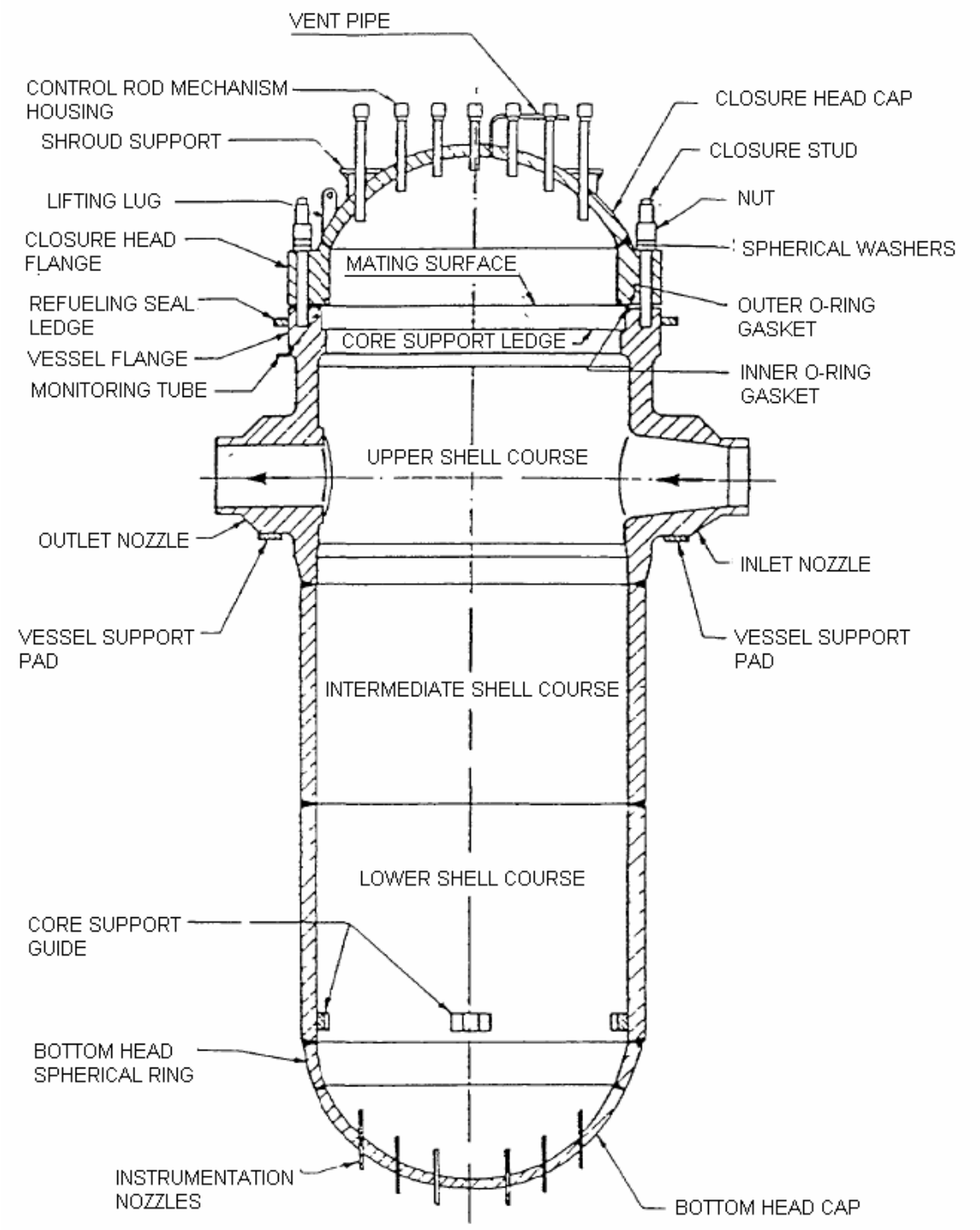

Figure 1.1 A typical Nuclear reactor pressure vessel

Large vessels are generally fabricated by two methods. In the first method, rolled and welded plates are used to form separate steel courses. Such a vessel has both longitudinal and circumferential weld seams (Figure 1.8a). In the second method, large ring forgings are used (Figure 1.8b). This method improves component reliability because of the lack of longitudinal welds. Weld seams are located to avoid intersection with nozzle penetration weldments. Weldments within the beltline region were minimized once research showed that weld metal could be more sensitive to neutron radiation than base material. In general, parts of the longitudinal shell course welds are within the beltline region when the RPV is fabricated using plate material.

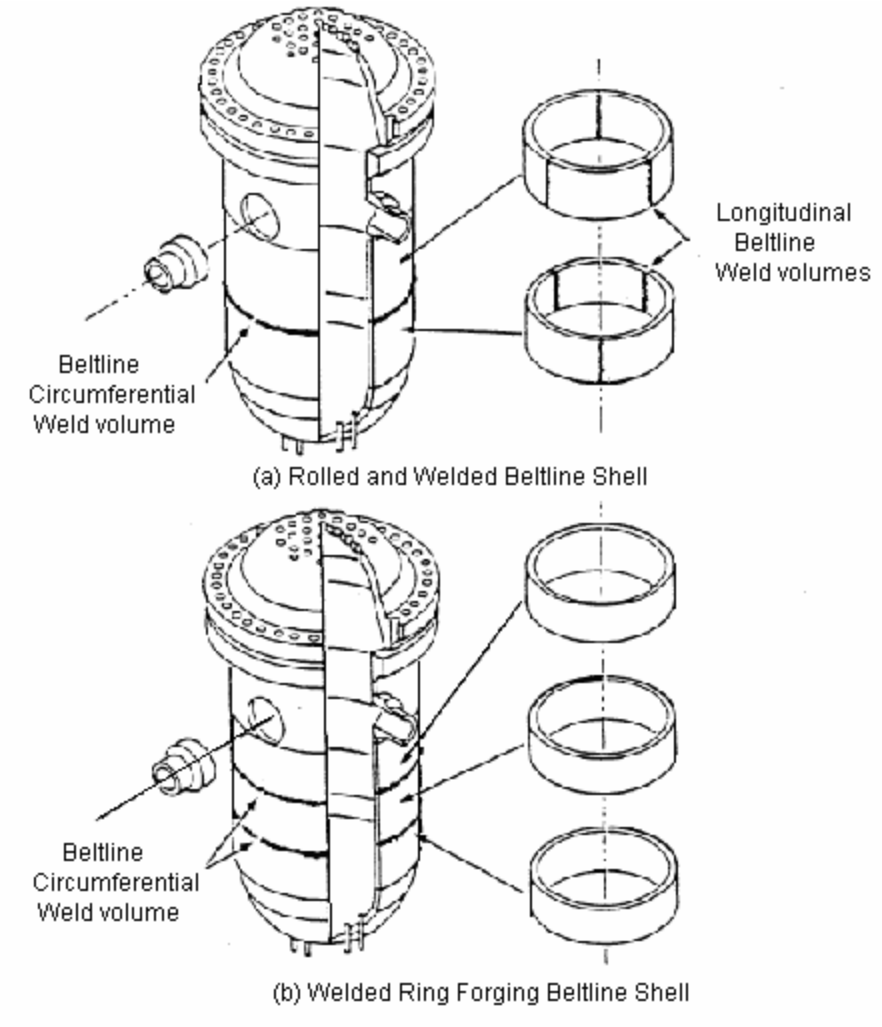

Figure 1.2 Fabrication configurations of PWR beltline shells

1.4 Reactor Pressure Vessel material

In RPVs different materials are used for the different components (shells, nozzles, flanges, studs, etc.). Moreover, the choices in the materials of construction changed as the PWR products evolved. For example, the Westinghouse designers specified American Society for Testing and Materials (ASTM) SA 302 Grade the shell plates of earlier vessels and ASTM SA 53 Grade B Class 1 for later vessels. Other vessel materials in common use include American Society of Mechanical Engineers (ASME) SA 508 Class 2 plate in the USA, 22NiMoCr37 and 20MnMoNi55 in Germany, and 16MnD5 in France. SA-302, Grade B is a manganese-molybdenum plate steel used for a number of vessels made through the mid-1960s. Its German designation is 20MnMo55. As commercial nuclear power evolved, the sizes of the vessels increased. For the greater wall thicknesses required, a material with greater hardening properties was necessary. The addition of nickel to SA-302, Grade B in amounts between 0.4 and 0.7 weight per cent provided the necessary increased hardening properties to achieve the desired yield strength and high fracture toughness across the entire wall thickness. This steel was initially known as SA-302, Grade B Ni Modified.

Forging steels have also evolved since the mid-1950s. The SA-182 F1 Modified material is a manganese-molybdenum-nickel steel used mostly for flanges and nozzles in the 1950s and 1960s. Another forging material used then was a carbon-manganese-molybdenum steel, SA- 336 Fl. Large forgings of these materials had to undergo a cumbersome, expensive heat treatment to reduce hydrogen blistering. Eventually these steels were replaced with a steel, first described as ASTM A366 Code Case 1236 and is now known as SA-508 Class 2, that did not require this heat treatment. This steel has been widely used in ring forgings, flanges and nozzles. It was introduced into Germany with the designation 22NiMoCr36 or 22NiMoCr37. With slight modifications, this steel became the most important material for German reactors for a long time. In addition, SA-508 Class 3 (20MnMoNi55 in Germany and 16 MnD5 and 18MnD5 in France) is used in the fabrication of RPVs.

CHAPTER 2

LITERATURE REVIEW

2.1 Fracture mechanics

Fracture mechanics is the field of solid mechanics that deals with the behavior of cracked bodies subjected to stresses and strains. These can arise from primary applied loads or secondary self-equilibrating stress fields (e.g. residual stresses).

Fracture (definition**) -** “It is defined as separation or fragmentation of body into two or more parts under the action of stress. The process of fracture can be considered to be made up of two components i.e. crack initiation and crack propagation. Fractures can occur under all service conditions. Material subjected to cyclic loading fail due to fatigue and material used at high temperature can fail due to creep rupture.”

From investigating fallen structures, engineers found that most failure began with cracks. These cracks may be caused by material defects (dislocation, impurities...), discontinuities in assembly and/or design (sharp corners, grooves, nicks, voids...), harsh environments (thermal stress, corrosion...) and damages in service (impact, fatigue, unexpected loads...). Most microscopic cracks are arrested inside the material but it takes one run-away crack to destroy the whole structure.

To analyze the relationship among stresses, cracks, and fracture toughness, Fracture Mechanics was introduced. The first milestone was set by Griffith in his famous 1920 paper that quantitatively relates the flaw size to the fracture stresses. However, Griffith's approach is too primitive for engineering applications and is only good for brittle materials.

For ductile materials, the milestone did not come about until Irwin developed the concept of strain energy release rate *G* in 1950s.When the strain energy release

rate reaches the critical value, the crack will grow. Later, the strain energy release rate was replaced by the stress intensity factor K with a similar approach by other researchers. After the fundamentals of fracture mechanics were established around 1960, scientists began to concentrate on the plasticity of the crack tips. In 1968, Rice modeled the plastic deformation as nonlinear elastic behavior and extended the method of energy release rate to nonlinear materials. He showed that the energy release rate can be expressed as a path-independent line integral, called the J- integral. Rice's theory has since dominated the development of fracture mechanics in Unite States. Meanwhile, Wells proposed a parameter called crack tip opening displacement (CTOD), which led the fracture mechanics research in Europe. Thereafter, many experiments were conducted to verify the accuracy of the models of fracture mechanics. Significant efforts were devoted to converting theories of fracture mechanics to fracture design guidelines. Recent trends of fracture research include dynamic and time-dependent fracture on nonlinear materials, fracture mechanics of microstructures, and models related to local, global, and geometry- dependent fractures. Unlike existing major theories with a single-parameter approach (G, K, J, or CTOD), these recent research trends usually require more than one parameter to describe the behavior of the crack growth, which we will discuss later on.

2.2 Classification of Fracture Mechanics

Fracture mechanics can be classified in three types:

1. Linear Elastic Fracture Mechanics (LEFM) e.g. Glass.
2. Elastic Plastic Fracture Mechanics (EPFM) e.g. Mild steel.
3. Net Section Collapse (NSC) e.g. Aluminum.

In the regime where the global stress-strain response of the body is linear and elastic (LEFM), the stress intensity factor K is used. In the plastic collapse region, design can be done on the basis of ensuring that net section yield does not occur, whilst in the elastic-plastic region EPFM, nowadays called yielding fracture mechanics YFM, is applicable. The fracture characterizing parameters in YFM

are the J-integral and the crack opening displacement, COD. All these fracture characterizing parameters meet both the Griffith energy criterion for fast crack growth, and the critical stress/strain criterion. For simple cases, fracture problems can be approached via the Griffith equation, which is particularly suitable for sharp cracks/defects in brittle materials.

2.2.2 **Linear Elastic Fracture Mechanics (LEFM)**

Linear Elastic Fracture Mechanics (LEFM) first assumes that the material is isotropic and linear elastic. Based on the assumption, the stress field near the crack tip is calculated using the theory of elasticity. When the stresses near the crack tip exceed the material fracture toughness, the crack will grow. In Linear Elastic Fracture Mechanics, most formulas are derived for either plane stresses or plane strains, associated with the three basic modes of loadings on a cracked body: opening, sliding, and tearing. Again, LEFM is valid only when the inelastic deformation is small compared to the size of the crack, what we called small-scale yielding. If large zones of plastic deformation develop before the crack grows, Elastic Plastic Fracture Mechanics (EPFM) must be used.

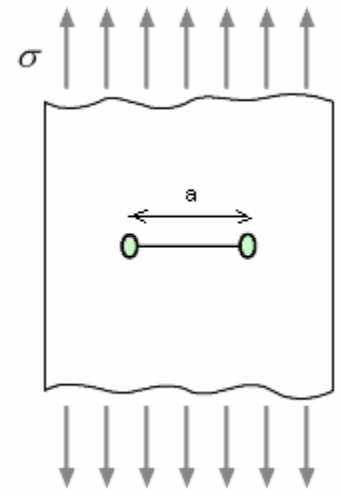

Figure 2.1: Linear elastic crack in tensile specimen

In case of Linear Elastic Fracture Mechanics (LEFM) we uses Stress Intensity Factor *K* or Stress Release Rate G.

Most metallic alloys and thermo set polymers are considered isotropic, where by definition the material properties are independent of direction. Such materials have only two independent variables (i.e. elastic constants) in their stiffness and compliance matrices. The two elastic constants are usually expressed as the Young's modulus E and the Poisson's ratio ν. However, the alternative elastic constants K (bulk modulus) and/or G (shear modulus) can also be used. For isotropic materials, G and K can be found from E and ν by a set of equations, and vice-versa.

2.2.6.1 Plane stresses and Plain strains

For the simplification of plane stress, where the stresses in the *z* direction are considered to be negligible, $\sigma_{zz} = \sigma_{yz} = \sigma_{xz} = 0$, the stress-strain compliance relationship for an isotropic material becomes,

$$\begin{bmatrix} \varepsilon_{xx} \\ \varepsilon_{yy} \\ \varepsilon_{zz} \\ \varepsilon_{yz} \\ \varepsilon_{zx} \\ \varepsilon_{xy} \end{bmatrix} = \frac{1}{E} \begin{bmatrix} 1 & -\nu & -\nu & 0 & 0 & 0 \\ -\nu & 1 & -\nu & 0 & 0 & 0 \\ -\nu & -\nu & 1 & 0 & 0 & 0 \\ 0 & 0 & 0 & 1+\nu & 0 & 0 \\ 0 & 0 & 0 & 0 & 1+\nu & 0 \\ 0 & 0 & 0 & 0 & 0 & 1+\nu \end{bmatrix} \begin{bmatrix} \sigma_{xx} \\ \sigma_{yy} \\ 0 \\ 0 \\ 0 \\ \sigma_{xy} \end{bmatrix} \tag{2.1}$$

For the case of plane strain, where the strains in the *z* direction are considered to be negligible, $\varepsilon_{zz} = \varepsilon_{yz} = \varepsilon_{xz} = 0$, the stress-strain stiffness relationship for an isotropic material becomes,

$$\begin{bmatrix}\sigma_{xx}\\ \sigma_{yy}\\ \sigma_{zz}\\ \sigma_{yz}\\ \sigma_{zx}\\ \sigma_{xy}\end{bmatrix} = \frac{E}{(1+\nu)(1-\nu)}\begin{bmatrix}1-\nu & \nu & \nu & 0 & 0 & 0\\ \nu & 1-\nu & \nu & 0 & 0 & 0\\ \nu & \nu & 1-\nu & 0 & 0 & 0\\ 0 & 0 & 0 & 1-2\nu & 0 & 0\\ 0 & 0 & 0 & 0 & 1-2\nu & 0\\ 0 & 0 & 0 & 0 & 0 & 1-2\nu\end{bmatrix}\begin{bmatrix}\varepsilon_{xx}\\ \varepsilon_{yy}\\ 0\\ 0\\ 0\\ \varepsilon_{xy}\end{bmatrix} \quad (2.2)$$

Three basic modes of loadings on a cracked body: opening, sliding, and tearing

There are three basic modes of crack tip deformation, the opening (Mode I), the in-plane shear (Mode II), and the out-of-plane shear (Mode III):

Mode I (Tension, Opening)

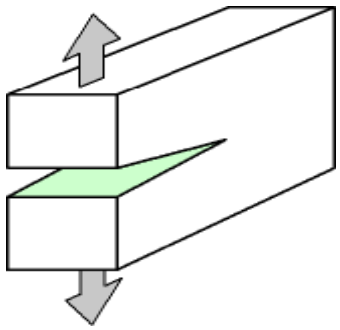

Figure 2.2: Opening mode deformation

Mode II (In-Plane Shear, Sliding)

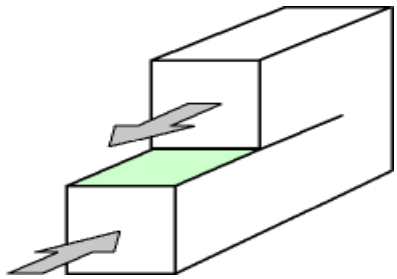

Figure 2.3: Sliding mode deformation

Mode III (Out-Of-Plane Shear, Tearing)

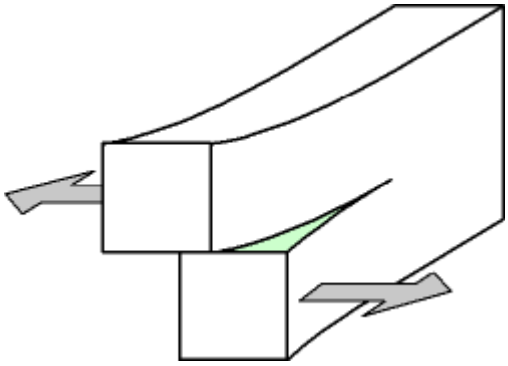

Figure 2.4: Tearing mode deformation

2.2.1.2 Stress Intensity Factor and Crack Tip Stresses

Crack tips produce a $\frac{1}{\sqrt{r}}$ singularity. The stress fields near a crack tip of an isotropic linear elastic material can be expressed as a product of $\frac{1}{\sqrt{r}}$ and a function of θ with a scaling factor K:

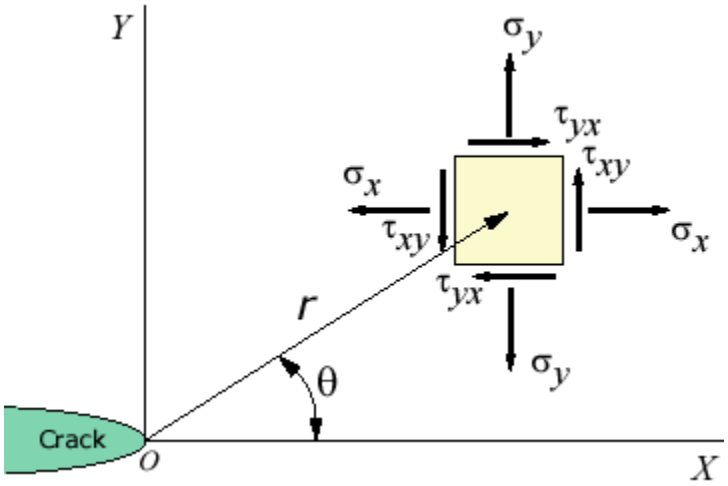

Figure 2.5: Stress field near crack tip of an isotropic linear elastic material

$$\lim_{y\to 0} \sigma_{ij}^{(I)} = \frac{K_I}{\sqrt{2\pi r}} f_{ij}^{(I)}(\theta) \qquad (2.3)$$

$$\lim_{y\to 0} \sigma_{ij}^{(II)} = \frac{K_{II}}{\sqrt{2\pi r}} f_{ij}^{(II)}(\theta) \tag{2.4}$$

$$\lim_{y\to 0} \sigma_{ij}^{(III)} = \frac{K_{III}}{\sqrt{2\pi r}} f_{ij}^{(III)}(\theta) \tag{2.5}$$

Where the superscripts and subscripts *I*, *II*, and *III* denote the three different modes that different loadings may be applied to a crack. The factor K is called the Stress Intensity Factor.

2.2.1.3 Stress Intensity Factor and Fracture Toughness

Based on the linear theory the stresses at the crack tip are infinity but in reality there is always a plastic zone at the crack tip that limits the stresses to infinite values. It is very difficult to model and calculate the actual stresses in the plastic zone and compare them to the maximum allowable stresses of the material to determine whether a crack is going to grow or not.

An engineering approach is to perform a series of experiments and reach at a critical stress intensity factor Kc for each material, called the fracture toughness of the material. One can then determine the crack stability by comparing K and Kc directly.

2.2.1.4 Relationship between G and K

These two factors are directly related by the following formulas:

$$G = \frac{K^2}{E} \quad \text{(Plane stress)} \tag{2.6}$$

$$G = \frac{K^2}{E}\left(1-\nu^2\right) \quad \text{(Plane strain)} \tag{2.7}$$

The value of K for CT specimen:

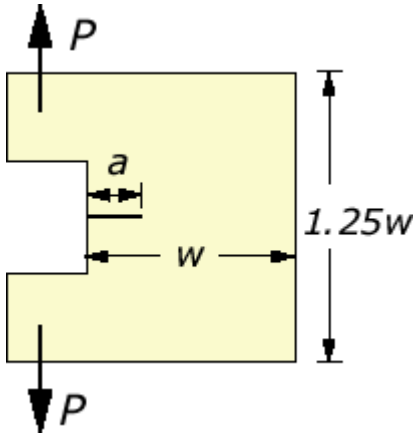

Figure 2.6: CT specimen with initial crack of length a

$$f(\frac{a_i}{W}) = \frac{[(2+\frac{a_i}{W})(0.886+4.64(\frac{a_i}{W}) \ -13.32(\frac{a_i}{W})^2+14.72(\frac{a_i}{W})^3-5.6(\frac{a_i}{W})^4)]}{(1-\frac{a_i}{W})^{3/2}} \qquad (2.8)$$

2.2.2 Elastic Plastic Fracture Mechanics (EPFM)

Linear Elastic Fracture Mechanics (LEFM) applies when the nonlinear deformation of the material is confined to a small region near the crack tip. For brittle materials, it accurately establishes the criteria for catastrophic failure. However, severe limitations arise when large regions of the material are subject to plastic deformation before a crack propagates. Elastic Plastic Fracture Mechanics (EPFM) is proposed to analyze the relatively large plastic zones.

Elastic Plastic Fracture Mechanics (EPFM) assumes isotropic and elastic-plastic materials. Based on the assumption, the strain energy fields or opening displacement near the crack tips are calculated. When the energy or opening exceeds the critical value, the crack will grow.

Although the term elastic-plastic is used in this approach, the material is merely nonlinear-elastic. In others words, the unloading curve of the so called elastic-

plastic material in EPFM follows the original loading curve, instead of a parallel line to the linear loading part which is normally the case for true elastic-plastic materials.

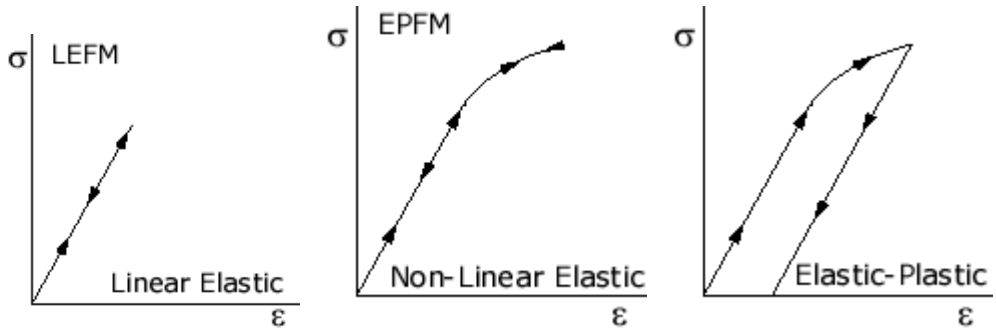

Figure 2.7: Difference between LEFM, EPFM

In case of Elastic Plastic Fracture Mechanics (EPFM) we use the J Integral or Crack Tip Opening Displacement (CTOD). Crack Tip Opening Displacement (CTOD) suggested by Wells, popular in Europe, and the J Integral proposed by Rice, widely used in the United States.

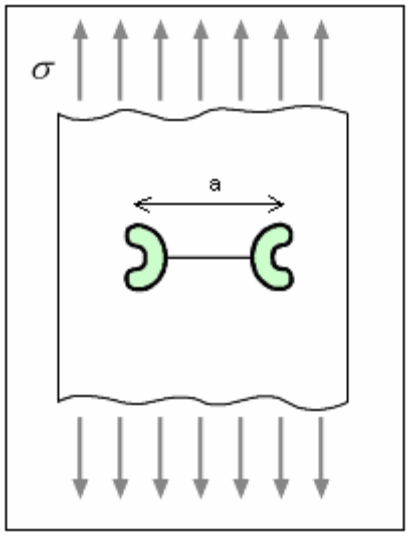

Figure 2.8: Elastic-plastic crack in tensile specimen

However, Shih provided evidence that a unique relationship between J and CTOD exists for a given material. Thus, these two parameters are both valid in characterizing crack tip toughness for elastic-plastic materials.

The basic EPFM analysis can be summarized as follows:

1. Calculate the J-integral or crack tip opening displacement (CTOD) δ as a function of the loading and the geometry.

2. The critical J-integral J_c or the critical CTOD δ can be determined empirically.

3. The J-integral J should NOT exceed J_c, or, the CTOD δ should not exceed the critical CTOD δ.

2.2.3 J-Integral

The *J*-Integral is employed as a fracture characterizing parameter for materials having elasto-plastic deformation idealized as *non-linear elastic* behaviour. Rice applied deformation plasticity (i.e., non-linear elasticity) to the analysis of a crack in a non-linear material. He showed that the non-linear energy release rate, *J* could be written as a path independent line integral. Rice also showed that *J* uniquely characterizes crack tip stresses and strains in non-linear material. Thus the *J*-integral can be viewed as both energy parameter (strain energy release rate, *G*) and a stress intensity parameter (*K*) in the following fashion:

$$J = \frac{K_I{}^2}{E} = G \qquad \text{(Plane stress)}$$

$$J = \frac{K_I^2}{E}(1-\nu^2) = G(1-\nu^2). \qquad \text{(Plane strain)} \qquad (2.9)$$

Definition of *J*-Integral

Rice presented a path independent contour integral for the analysis of cracks. He then showed that the value of this integral, which he called *J*-Integral, is equal to the energy release rate in a non-linear elastic body that contains crack. Consider a non-linear elastic body containing a crack as shown in Fig. 2.9. Rice showed that the decrease in potential energy ΔU_P associated with the development of crack or void is given by,

$$-\Delta U_P = \int_{\Delta V} W dV - \int_{\Delta S} \vec{T} \Delta \vec{u} dS \,. \tag{2.10}$$

For infinitesimal crack-extension, (co-ordinate system as per Fig. 2.8*)* the *J*-Integral is defined as:

$$J = \int_{\Gamma} w dy - T_i \frac{\partial u_i}{\partial x} ds \,, \tag{2.11}$$

where, $w = \int_0^{\varepsilon_{ij}} \sigma_{ij} d\varepsilon_{ij}$ is the strain energy density, $T_i = \sigma_{ij} n_j$ is the traction vector, Γ is an arbitrary contour around the tip of the crack, *n* is the unit vector normal to Γ . σ , ε and *u* are the stress, strain, and displacement field, respectively.

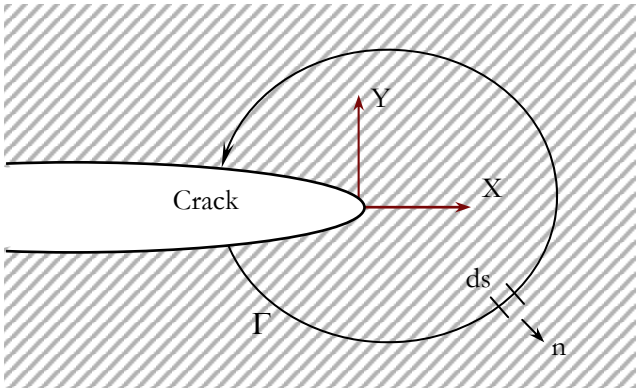

Figure 2.9 Crack in an arbitrary body—definition of *J*-integral

Rice, J. R showed that the *J*-integral is a path independent line integral and it represents the strain energy release rate of non-linear elastic materials:

$$J \equiv -\frac{d\Pi}{dA}, \tag{2.12}$$

where, $\Pi = U - W$ is the potential energy, *U is* the strain energy stored in the body, *W* is the work done by external forces and *A* is the crack area.

In General, the *J*-integral for a variety of configuration can be written in the following form:

$$J = \frac{\eta U_C}{Bb}, \tag{2.13}$$

where η is dimensionless constant, B is specimen width, $b=B-a$, a is crack length and U_c is the area under load-displacement curve.

The above equation can be separated into elastic and plastic components:

$$J = \frac{\eta_{el} U_{C(el)}}{Bb} + \frac{\eta_P U_{C(P)}}{Bb} \tag{2.14}$$

The J-integral, represents a way to calculate work (energy) per unit fracture surface area in a material, Defines the point at which large-scale plastic yielding during propagation takes place under mode one loading. This value is difficult to determine experimentally, however in 1968 Jim Rice developed the J-integral test that allows one to calculate fracture toughness for materials in which sample sizes are too small (on the order of < 1 meter) for direct determination of Fracture toughness. Physically the J-integral is related to the area under curve of a load versus load point displacement.

2.2.4 Crack Tip Opening Displacement (CTOD)

Definition of Crack Tip Opening Displacement-

There are two common definitions of the crack tip opening displacement (CTOD):

1. The opening displacement of the original crack tip.

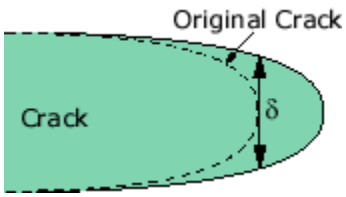

Figure 2.10a: CTOD of original crack tip

2. The displacement at the intersection of a 90° vertex with the crack flanks.

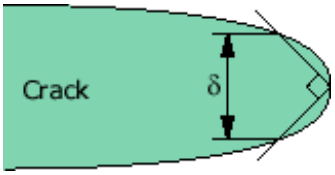

Figure 2.10b: CTOD of crack tip at intersection of 90 vertex

These two definitions are equivalent if the crack blunts in a semicircle.

2.2.5 Relationship between J and CTOD

Consider a linear elastic body containing a crack, the J-integral and the crack tip opening displacement (CTOD) has the following relationship

$$J = \frac{K^2}{E} = m\sigma_{ys}\delta \tag{2.15}$$

Where σ_{ys} is the small scale yielding stress and m is a dimensionless constant that depends on the material properties and the stress states. For plane stress and non hardening materials, m = 1. Hence, for a through crack in an infinite plate subjected to a remote tensile stress σ (Mode I), the crack tip opening displacement δ is

$$\delta = \frac{G}{\sigma_y} = \frac{J}{\sigma_y} \tag{2.16}$$

2.2.6 J-R Curve

The J- resistance curves are used for characterizing the elastic-plastic fracture behavior of metallic components. They are usually determined from ASTM slandered specimens. The stress multiaxiality, 'q', ahead of the crack tip plays an important role in determining fracture resistance behavior of components. The J-R curve depends on component level. The J-R curve is mainly influenced by the multiaxiality of stress state across the ligament. The multiaxiality can be

determined by finite element calculations for specimen and component, it is possible to assess component fracture behaviour correctly.

2.3 Limitations of Single Parameter Characterization

Under small scale yielding conditions a single parameter (i.e. J-integral) characterizes the crack tip conditions and can be used as geometry independent fracture criterion. However, the single parameter assumption is rigorously correct only in an infinite body. In a finite body, the single parameter assumption is suspect when the plastic zone size is significant compared to the dimensions of the body or crack. The breakdown of single parameter fracture mechanics is gradual from low to higher load levels in highly constraint geometries such as deeply cracked bend specimens. But it occurs at relatively low load levels in low constraint geometries such as cracked specimens in uniaxial tension. Now, there is general agreement that single parameters approach is limited to high constraint geometries.

In most cases, standard ASTM specimens maintained high constraint even up to high load levels. ASTM standards require both sufficient thickness to ensure predominantly plane strain conditions at the crack tip and a crack depth of at least half the specimen width. Within certain limits on load level and crack growth, these restrictions ensure the existence of high constraint conditions for fracture and the single parameter characterization is valid. However, actual structures are generally low constraint geometries. This difference between crack tip constraint between specimens and structures indicates that structures can often carry greater loads without failure predictions using fracture toughing values which are measured from laboratory specimens. This introduces a high degree of conversation into the design of load carrying of components. Experiment techniques have been developed for measuring the apparent fracture toughness of low constraint geometries. This work has shown that slope of the J-R curve. The slope of the J-R curve will effect on the load and associated crack growth of components. As crack tip constraint plays important role in explaining

geometric dependence of J-R curve, it seems worthwhile to discuss the underlying idea and physical significance of constraint.

2.4 Physical Significance of Crack Tip Constraint

Constraint is a structural feature that inhibits plastic flow and causes a higher triaxiality of stresses. Therefore, it promotes because the input of external work, for example, measured by J will to a lesser part be dissipated by plastic deformation but be available to enhance material degradation and damage. High crack tip constraint is often found in specimens with sufficiently deep crack under predominantly bending load. Low constraint is often associated with specimen of relatively shallow cracks under predominantly tensile loading. Low constraint generally manifests itself in high crack tip ductility and high fracture toughness.

Although there is no doubt that the resistance against ductile tearing depends on crack tip constraint, the problem still to be solved in how to define and quantify this parameter significant, reliable and reproducible manner. Different definitions and measures are in use and two parameter fracture mechanics has emerged in which second parameter is used to quantify crack tip constraint.

2.5 Two Parameter Fracture Mechanics

The development and confirmation of proper fracture criteria fro crack initiation and stable crack growth has been one of the most important objectives in the study of elastic plastic fracture mechanics. The J-integral has played an important role in fracture mechanics and engineering application over the past 20 years as a single parameter to characterize the crack tip stress field. It was considered the most appealing parameter for crack initiation and stable crack growth. Deformation plasticity solutions which elucidate the behavior of a stationary crack under plane stress or plane strain solutions were given by the Hutchinson and Rice and Rosengren model, known as HRR singularity fields. The amplitude of these is given by J-integral. The conditions under which the HRR fields correspond to those found in small scale yielding (SSY) as

characterized by the J-integral are referred to as the conditions of J- dominance characterized of the crack tip field.

Crack initiation and stable crack growth in ductile material are usually described by J-R curves obtained from standard fracture specimens. The original idea was that J-integral can be used to characterize the crack tip stress field and one unique fracture resistance is sufficient to characterize the material. However, there is growing evidence showing that the J-R curve depends on specimen size, geometry and loading mode. Therefore, the transferability of specimen J-R curve to component level is an unresolved issue that receives a lot of attention among researchers. The J-R curve is mainly influenced by the multiaxiality of stress state across the ligament. The multiaxiality can be determined by finite element calculations for specimen and components. By comparing the multiaxiality values of specimen and components, it is possible to assess component fracture behavior correctly.

2.5.1 J-T approach

The J-T approach was proposed by Hancock et al. Williams showed that the crack tip stress field in an isotropic elastic material can be expressed as an infinite power series, where the leading term exhibits a $\frac{1}{\sqrt{r}}$ (r is the distance from the crack tip) singularity, the second term is constant with respect to r, the third term is proportional to $\sqrt{r}$ and so on. Classical fracture mechanics theory considers the leading term in the Williams solution and neglect all other terms, which results in a single parameter (K or J-integral) description of the near-tip fields. It was found that the second term (constant T stress) have a profound effect on the plastic zone shape and the stresses deep inside the plastic zone. This constant T-stress was identified as constraint indexing parameter. Detailed finite element analysis by Hancock and co-workers confirm that a negative T-stress reduces the crack opening mode stresses relative to that of an infinite body i.e. T=0. Further they reported that a negative T-stress is associated with low constraint geometries while zero or positive T-stress corresponds to high

constraint geometries. However, this methodology has limitations, because T is an elastic parameter. It was found that errors in stress fields inferred from T-stress increase with plastic deformation.

2.5.2 J-h approach

One of the most widely used constraint indexing parameter is the triaxiality factor (h) which is defined by the ratio of hydrostatic or mean stress (σ_m) which does not cause any plastic deformation, to the Misses equivalent stress (σ_e) which is being responsible for plastic flow.

$$h = \frac{\sigma_m}{\sigma_e} \tag{2.17}$$

Where $\sigma_m = \frac{\sigma_1 + \sigma_2 + \sigma_3}{3}$

$$\sigma_e = \frac{\sqrt{\sum(\sigma_1 - \sigma_2)^2}}{\sqrt{2}}$$

$\sigma_1, \sigma_2, \sigma_3$ are principal stresses.

The physical meaning of this ratio was substantiated by the investigation of Mclintock and Rice and Tracey, who found that the growth rate of cavities in perfectly plastic materials is proportional to $e^{1.5h}$. Despite the fact that various authors [11& 12] use the ratio $h = \frac{\sigma_m}{\sigma_e}$ as a measure of stress triaxiality or crack tip constraint, there are still some unresolved problems.

2.5.3 J-A2 approach

J-A2 approach was proposed by Chao and Ji. In this approach J-integral represents the level of loading and A2 quantifies the level of crack tip constraint.

2.5.4 J-Q approach

J-Q theory was proposed by O'dowd and Shih. In this theory, Q is used as constraint indexing parameter. As per this theory, the laboratory specimen must match the constraint of the structure i.e. two geometry must have the same Q-value at failure in order to have same J values. The non dimensional parameter Q is basically the deviation in hoop stress with respect to a reference stress divided by the yield stress.

A negative (positive) Q-value means that the hydrostatic stress is lower (higher) than the reference field (Q=0 state)**.** Geometries with negative Q-value show low stress triaxiality ahead of crack tip (low constraint) and loss of J-dominance. Thus Q-value provides a framework for quantifying the evolution of constraint as plastic flow progresses from small scale yielding to full yielding conditions.

2.6 Micromechanical Modelling / Damage mechanics

The fundamental difference between fracture mechanics and damage mechanics is that in damage mechanics we consider the void, nucleation and coalescence while in fracture mechanics we do not consider any voids formation in metal matrix. The distance between the nucleuses of two voids is of micro level that's why it comes under micro mechanical Modeling.

In any engineering material, a number of microscopic voids are present initially in the metal matrix. These voids may be present due to the manufacturing process of the material itself or these may nucleate from the inclusions and second phase particles. The ductile fracture (damage mechanics) is a process, which consist of nucleation, growth, and coalescence of these microscopic voids. The void coalescence leads to stable crack growth by merging of voids in the material. Void nucleation may arise from particle cracking. Void may also be formed by pipe-up of dislocations at highly disordered grain boundaries. In the first instance, the particle cracks and thereby separates itself from the matrix, leaving a void. In the later situation, the particle and the matrix separate at their interface without any cracking of the particle. Once formed, the voids grow under the applied loads also the growth rate depends on the size and shape of the

voids & ligaments between the voids. At some point, stresses in the ligament become high to the point where an unstable necking of the ligament takes place, this leads to the merging of two voids. The merging of two voids is known as the void coalescence or stable crack growth.

Application of micromechanical models should enable attunement of so-called transferability of model parameters to different geometries. Application of micromechanical models should not have specific requirements related to test geometries, as the model parameters solely depend on material. If this is really so then the advantage of such a way of analysis over the traditional process is obvious.

So far developed models for ductile fracture may be broadly classified in two groups: uncoupled micromechanical models and coupled micromechanical models.

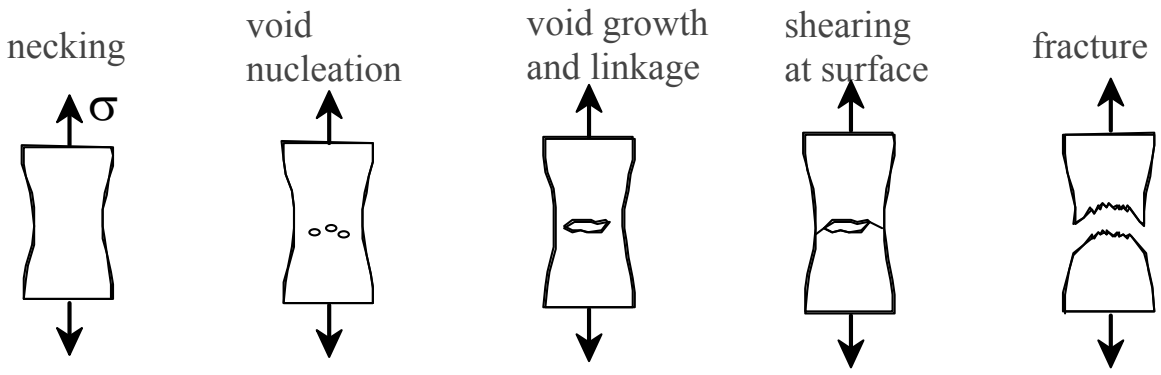

Figure 2.11 Void nucleation and growth in a tensile specimen of ductile material

These types of models aim to model ductile fracture by local approach – correlating the stress triaxiality with damage, which occurs in three stages: nucleation, growth & coalescence of voids. Constraint effects do not enter the problem as a separate issue as triaxiality of stresses enters the problem directly. Crack initiation & propagation occur with local degradation of the material losing completely its load carrying capacity. Micromechanical modelling or local approach has been extensively used in the last decade in order to analyze & predict ductile fracture behavior of different alloys. A large number of models

have been developed, application of which should enable analysis of ductile fracture in a way that is to the largest extent in accordance with the natural phenomena in a material.

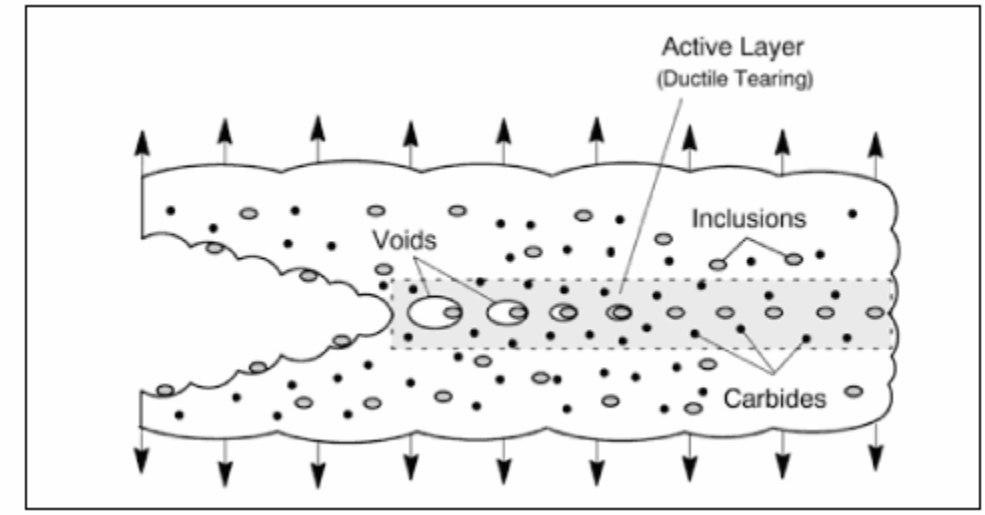

Figure 2.12 Schematic path of a growing crack in a ductile material

Application of micromechanical models should enable attunement of so-called transferability of model parameters to different geometries. Here model parameters do not mean only so called damage parameters (referring mostly to the size & number of nucleated voids in the material), but local stress & strain as well. Applications of micromechanical models should not have specific requirements related to test geometries, as the model parameters solely depend on the material. If this is really so then the advantage of such a way of analysis over the traditional process is obvious.

So far developed models for ductile fracture may be classified in two broad groups: uncoupled micromechanical models & coupled micromechanical models.

2.6.1 Uncoupled Micromechanical Models

This type of models is relatively simple & damage variable does not participate in the constitutive behaviour of the material. Here the damage & the yielding

behaviour are uncoupled. The material is assumed to follow the von-Mises yield criteria with the appropriate flow & strain hardening rules (elasto-plastic properties). A damage potential symptomatic of void growth is calculated in post processing manner at large number of sampling points near the crack tip with increase in applied loads. A critical value of this parameter signifying the crack initiation in a given material is determined comparing the computed value with the experimental result for a fracture specimen. The critical value is then used to ascertain crack initiation in other real life plant components made up of same materials. This category of Modelling is called uncoupled damage Modelling. Some of these models are:

1. Rice & Tracey's cavity-growth model.
2. Budiansky *et al*'s model.
3. Tai & Yang's model.
4. Huang model.
5. Chaouadi *et al*'s model.
6. Dutta & Kushwaha's Ψ -integral model

2.6.2 Coupled Micromechanical Models

On the past two decades, more & more attention has been paid to & research work directed towards the so-called coupled models for damage. Coupled approach to the material damage & the ductile fracture initiation considers alloy as a porous medium where the influence of nucleated voids on the stress/strain rate & plastic flow cannot be avoided. In the coupled micromechanical models, one or more damage parameters are calculated to predict ductile fracture initiation. Thus, the FE analysis must include procedure for calculation for these parameters & optionally fracture initiation criterion.

These approaches have been extensively studied to different materials. In order to apply these models, there is need to find out the critical values of these parameters for the given materials. The major advantage of these models is that initiation & propagation of cracks occur naturally when the local softening due to

void growth & coalescence results in the formation of a region, transmitting negligible stresses. It is not even necessary to assume an initial crack in a specimen or component, as is done in conventional fracture mechanics. Crack initiation & propagation occur when the local degradation of material has exceeded some critical value of void volume fraction over a characteristic distance. Two of the most frequently used models are:

1. Rousellier Seidenfuss Model.
2. Gurson model.

In next section, the Gurson model & its modified version Gurson Tvergaard Needleman model have been discussed in a detail which is the subject matter of this dissertation work.

2.7 Gurson Tvergaard Needleman model

Based on the work of Berg (which shows that a porous medium is governed by the normality rule), Gurson developed an approximately yield criterion & flow rule for porous ductile materials, showing the role of hydrostatic stress in plastic yield & void growth. Gurson idealized the voids as spherical or cylindrical in shape & the matrix material as rigid-perfectly-plastic material obeying von-Mises yield criterion. He calculated the stress field required for yield using a distribution of macroscopic flow fields & working through dissipation integral. The derived model originally given by Gurson is:

$$\phi(\sigma^{ij}, \sigma_m, f) = \left(\frac{\sigma_e}{\sigma_m}\right)^2 + 2f\cosh\left(\frac{\sigma_k^k}{2\sigma_m}\right) - 1 - f^2 = 0, \qquad (2.18)$$

Where, σ_m = tensile flow strength of the material, $\sigma_e = \sqrt{\frac{3}{2} s_{ij} \cdot s^{ij}}$, $s^{ij} = \sigma^{ij} - \sigma_k^k \cdot \bar{g}^{ij}$ represents the stress deviator, $\sigma_k^k = \bar{g}_{kj}\sigma^{kj}$, $\bar{g}_{kj} = \bar{g}_k \cdot \bar{g}_k$ is the metric tensor, σ^{kj} is the contravariant component of the macroscopic Cauchy stress tensor.

It can be noticed that for $f = 0$, the Gurson yield equation becomes von-Mises yield criterion, $\sigma_e/\sigma_m - 1 = 0$.

Or, $$\sqrt{(\sigma_1 - \sigma_2)^2 - (\sigma_2 - \sigma_3)^2 - (\sigma_3 - \sigma_1)^2/2} = \sigma_m$$

The original model considers that there were no interactions between voids which are not justified for modelling the final stage of void growth when coalescence of voids by localized internal necking of the matrix occurs. Tvergaard & Needleman therefore introduced an empirical modification of Gurson's yield function:

$$\phi(\sigma^{ij}, \sigma_m, f^*) = \left(\frac{\sigma_e}{\sigma_m}\right)^2 + 2 f^* q_1 \cosh\left(q_2 \frac{\sigma_k^k}{\sigma_m}\right) - 1 - q_3 (f^*)^2 = 0 \qquad (2.19)$$

The parameter q_1 was introduced by Tvergaard who analyzed the microscopic behavior of doubly periodic array of voids using a model which fully accounts for the non-uniform stress field around each void & which also accounts for the interaction between voids.

Further modifications of the plastic flow rule, made by Tvergaard & Tvergaard & Needleman , are associated with modelling the complete loss of stress carrying capacity accompanying at void coalescence occurring at void spacing of the order of void length. According to Tvergaard & Needleman, the modified void volume fraction is taken as:

$$f^*(f) = \begin{cases} f & \text{When, } f \le f_c \\ f_c + K(f - f_c) & f > f_c, \end{cases} \qquad (2.20)$$

where, $K = \dfrac{f_u^* - f_c}{f_f - f_c}$; f_c is the critical value of void volume fraction at which the material stress carrying capacity starts to decay more rapidly due to void coalescence; f_f is the actual void volume fraction associated with the complete loss of stress carrying capacity. At this point f^* becomes f_u^*. The parameter K defines slope of the sudden drop of load on the load-ΔD curve & is often referred as the 'accelerating factor'.

2.7.1 Flow rule

The strain increment ($\dot{\eta}_{ij}$) in a ductile solid can be written as the sum of the elastic part ($\dot{\eta}^{e}_{ij}$) & plastic part ($\dot{\eta}^{p}_{ij}$):

$$\dot{\eta}_{ij} = \dot{\eta}^{e}_{ij} + \dot{\eta}^{p}_{ij} . \tag{2.21}$$

The elastic part ($\dot{\eta}^{e}_{ij}$) is obtained from Hook's law. Since the material satisfies the normality rule based on the von-Mises yield criterion, the macroscopic plastic strain increment satisfies

$$\dot{\eta}^{p}_{ij} = \Lambda \frac{\partial \phi}{\partial \sigma_{ij}} . \tag{2.22}$$

The scalar quantity (Λ) is determined by the strain hardening behavior of the matrix material. The equivalent plastic strain-rate in the matrix material is obtained from the plastic work expression & the work hardening properties of the matrix by the relation:

$$\sigma^{ij}\dot{\eta}^{p}_{ij} = (1-f)\sigma_{M}\dot{\varepsilon}^{p}_{M} \tag{2.23}$$

Where,

$$\dot{\varepsilon}^{p}_{M} = \left(\frac{1}{E_{t}} - \frac{1}{E}\right)\dot{\sigma}_{M} . \tag{2.24}$$

Here 'E' is the Young's modulus & 'E_t' is the current tangent modulus of the matrix material.

The uniaxial stress-strain behavior of the material is to be presented by a piecewise power-law of the form:

$$\varepsilon = \begin{cases} \dfrac{\sigma}{E} \\ \dfrac{\sigma_{y}}{E}\left(\dfrac{\sigma}{\sigma_{y}}\right)^{n} \end{cases} \quad \text{for,} \quad \begin{cases} \sigma \le \sigma_{y} \\ \sigma > \sigma_{y} . \end{cases} \tag{2.25}$$

Here σ & ε are the true stress & true strain in uniaxial tension, respectively, & σ_{y} is the initial matrix yield strength. Accordingly, E_t is given in the terms of matrix flow strength σ_{M} by:

$$E_t = \frac{E}{n}\left(\frac{\sigma_M}{\sigma_y}\right)^{1-n}. \tag{2.26}$$

The increase in the void-volume-fraction, '*f*' arises partly from the growth of existing voids & partly from the nucleation of the new voids, so that:

$$\dot{f} = \dot{f}_{growth} + \dot{f}_{nucleation}. \tag{2.27}$$

Since the matrix material is plastically incompressible,

$$\dot{f}_{growth} = (1-f)\bar{g}^{ij}\,\dot{\eta}^{p}_{ij}. \tag{2.28}$$

The void nucleation rate can be described by the simple two-parameter relation as suggested by Chu & Needleman

$$\dot{f}_{nucleation} = A\left(\frac{EE_t}{E-E_t}\right)\dot{\varepsilon}^{p}_{M} + \frac{1}{3}B(\sigma^k_k) \tag{2.29}$$

Where *A* gives the dependence of the void rate on the matrix effective plastic strain increment & *B* gives the dependence on the rate of increase of the hydrostatic stress.

For nucleation controlled by plastic strain the parameters are specified by:

$$A = \left(\frac{1}{E_t} - \frac{1}{E}\right)\frac{f_N}{S_N\sqrt{2\pi}}\exp\left\{-\frac{1}{2}\left(\frac{\varepsilon^p_M - \varepsilon_N}{S_N}\right)^2\right\}$$
$$B = 0 \tag{2.30}$$

& for nucleation controlled by stress the parameters are specified by

$$A = B = \left(\frac{1}{E_t} - \frac{1}{E}\right)\frac{f_N}{S_N\sqrt{2\pi}}\exp\left\{-\frac{1}{2}\left(\frac{\sigma_M + \frac{1}{3}\sigma^k_k - \sigma_N}{S_N\sigma_y}\right)^2\right\} \tag{2.31}$$

Where f_N is the volume fraction of void nucleating particles, ε_N is the mean strain for nucleation & S_N is the corresponding standard deviation. Using the consistency condition $\phi = 0$,

$$\dot{\eta}_{ij}^{p} = \frac{1}{h} P_{ij} Q_{kl} \overset{\Delta}{\sigma}^{kl} \tag{2.32}$$

Here,

$$P_{ij} = \frac{\partial \phi}{\partial \sigma^{ij}}$$

$$Q_{kl} = \frac{\partial \phi}{\partial \sigma^{ij}} + \frac{1}{3}\frac{\partial \phi}{\partial f} B \bar{g}_{ij}$$

$$h = -[(1-f) + \frac{\partial \phi}{\partial f}\bar{g}_{ij}\frac{\partial \phi}{\partial \sigma^{ij}} + \frac{EE_t(A\frac{\partial \phi}{\partial f} + \frac{\partial \phi}{\partial \sigma_M})}{(E-E_t)\sigma_M(1-f)}]\sigma^{ij}\frac{\partial \phi}{\partial \sigma^{ij}} \tag{2.33}$$

The Algorithms & mathematical expressions for finding the FE solution for this model can be found in reference. It was reported by many investigators that the prediction by the Gurson model depends on size of mesh near the crack tip. Brocks et al. Showed that even in a tensile specimen where the stress state is quite uniform, the mesh-size affects the results. Before crack formation the stress & strain fields are quite homogeneous. But as crack appears, high stress & strain gradient occur in the vicinity of crack tip & the results obtained from different mesh-size deviate from each other. The prediction of ductile fracture initiation will be therefore strongly dependant on the mesh-size at crack tip, which is rather an unpleasant effect & has hence become a popular argument against the use of damage models in fracture mechanics.

The mesh dependency may be overcome by the introduction of 'localization limiters' in the model. The basic idea is that the evaluation of the internal variables at a given material point does not only depend on the local values of state variables at this very point but also on their values in some vicinity of that point. The influence of neighboring points is limited by some weight functions

decreasing with the distance. A number of proposals exist how to do this, which have proved their ability of reducing mesh sensitivity. They all require the introduction of a new material parameter – a characteristic length (l_c) or a critical volume, which determines the region of influence & which physically, characterizes micromechanical features such as the average distance (mean free path) of inclusions.

2.8 GTN MODEL PARAMETERS & THEIR DETERMINATION

Following are the GTN model parameters & their method of determination is given below briefly. The detailed procedure for determination of these parameters is explained in details in the next section of this chapter.

1. Initial void volume fraction ´f_0´: It represents the initial void fraction of the inclusions in the material which are not strongly adhered to the matrix. It is determined by metallographic examination in SEM. But analysis of notched tensile test confirms the parameter.

2. Critical length parameter 'l_c': It represents the mean spacing of inclusion which is responsible for void nucleation. It is determined by some standard relationships given in literature.

3. Mean strain of void nucleation: ε_n: It is determined by conducting tensile tests & subsequent metallographic examination..

4. Standard deviation of nucleation strain 'S_N': The process of nucleation follows statistical distribution. Chu & Needleman suggested a Gaussian distribution for the instantaneous volume fraction of nucleated voids with different values of strain. ε_N represents mean strain of this nucleation & S_N represents the standard deviation of nucleation strain. S_N is assumed generally as 0.1 for steel. It doesn't have much effect on the results of analysis. It represents the scatter of nucleation strain. It can be determined from metallographic study of nucleation process of voids & finding the statistical distribution.

5. Void volume fraction at saturated nucleation ´f_N´: It is determined by metallographic examination as well as fitting of numerical analysis data with experimental data

6. Final void volume fraction at fracture 'f_f': It is determined by metallographic examination.

7. 'q_1' = 1.5, 'q_2' = 1.0, 'q_3' = 2.25: These values are usually not changed. But some studies suggest that these parameters are also material dependent. For this dissertation work, the values are assumed constant.

8. Critical Void volume fraction ´f_c´: It is determined by numerical fitting of the point of drop of experimental load-deflection curve of the notched tensile specimen.

2.9 Work reviewed

Several centuries' earlier experiments performed by Leonardo de Vinci provided some clues as to the root cause of fracture. He measured the strength of iron wires and found that the strength varied inversely with wire length. These results implied that flaws in material controlled the strength; a longer wire corresponded to a larger sample volume and a higher probability of sampling a region containing flaw. These results were qualitative in nature.

A quantitative connection between fracture stress and flaw size came from the work of **Griffith [1],** which was published in 1920. He applied a stress analysis of an elliptical hole to the unstable propagation of a crack. Griffith invoked the first law of thermodynamics to formulate a fracture theory based on a simple energy balance. Griffith's model correctly predicted the relationship between strength and flaw size in glass specimens. Subsequent efforts to apply Griffith model to metals were unsuccessful. Since this model assumes the work of fracture exclusively comes from the surface energy of material, the Griffith approach only applies only to ideally brittle solids.

Then came the famous liberty ship incident during World War II. These ships were completely welded. There was large number of failures of these ships. Some of the ships broke into two parts. Investigation revealed the ship failures were combination of three factors: weld defects, stress concentration at some locations and poor material used. Once the reasons of failure were identified. Corrective actions were taken whine manufacturing these Liberty ships in future. However, it led to a more detailed fracture research program in US Naval

Research Laboratory in Washington DC under the leadership of Dr. G.R. Irwin. The first major contribution of Irwin was to modify the Griffiths approach to metals by including the energy dissipated by local plastic flow. In 1956, **Irwin [2]** developed energy release rate concept, which is related to Griffith theory, but in a form, which is more useful to solve engineering problems. Afterwards, Irwin developed the equation of the stress and strain field around a crack in an infinite plate using the Westergaard stress function approach. This paved the way for the development of a new field, known as Fracture Mechanics. A number of successful applications of fracture mechanics bolstered the standing of this new field in the engineering community.

The original motivation for development of fracture mechanics was to be able to account for materials that fracture with limited plastic deformation- that is, at applied stress levels less than those producing net section yielding. The discipline was initially focused on linear elastic brittle behavior. But, with the successes that were achieved with LEFM, materials for which such an approximation would be invalid also became of interest. To address the integrity of components made of these type of ductile materials in the presence of crack like defects, an alternative fracture mechanics model named as 'Elastic Plastic Fracture Mechanics' (EPFM) developed in late sixties and at later decades. Major thrust in the development of EPFM came in the late seventies and eighties when it was being extensively used to assess the integrity of piping of various nuclear power plants all over the world.

Rice [3] proposed a new parameter named *J-integral*, which has enjoyed great success as a fracture characterizing parameter for non-linear materials. By idealizing elastic –plastic deformation as nonlinear elastic, he provided the basis for extending fracture mechanics methodology well beyond the validity of LEFM.

Ductile tearing is normally controlled by micro void nucleation, growth, and coalescence mechanisms. Micro-mechanical model based approaches have shown promise when tackling the ductile fracture problem. Within these approaches, a model originally introduced by **Gurson [4,5]** and later modified by **Tvergaard [6,7]** and **Tvergaard and Needleman [8]** is attractive in that it is

endowed with a yield function, a flow law and rules for void nucleation and growth. In recent years, much pioneer work has demonstrated that the Gurson model can be applied for the prediction of plastic localization and ductile fracture. Besides the distinct material characteristic length dependent problem, there are two important aspects in applying the Gurson model. One is how to implement accurately and efficiently the model into a computer, the other one is how to interpret the material parameters for the Gurson model. Until now, how to select the material parameters for the Gurson model in a practical application has been an open question, and in practice the determination of the material parameters is often made arbitrarily. Efforts have been made recently for the practical application of the Gurson model by developing a special numerical scheme for implementing the Gurson model in ABAQUS via a user material subroutine, and developing a new failure criterion for the Gurson model. The new failure criterion, which is based on **Thomason's [9]** void coalescence mechanism, is novel in that it could be used for the establishment of damage parameters and also for reducing the non-uniqueness of damage parameters. With the convincing demonstration of its predictive power and the advance of the numerical algorithms for implementing the model, the time has perhaps come to study the selection of realistic material parameters for the Gurson model, and to relate the parameters for the Gurson model to the toughness of homogenous as well as inhomogeneous materials such as weldments. In this study, the problems of selecting material parameters for the Gurson model are outlined. Two kinds of void nucleation have been considered. In the first case, the voids were nucleated at the beginning of plastic deformation from the primary inclusions. In the second case, the voids were assumed to nucleate from the secondary inclusions. It has been found that the selection of the initial void volume fraction or the volume fraction of void nucleating particles is not unique in parameter fitting when using finite element models.

A European round-robin on micro-mechanical models has recently been completed **[10]**. One of the purposes of the round-robin was to characterize the material and identify the critical damage parameters for ductile tearing at room

temperature. In the round-robin, an initial void volume fraction of 0.002 was assumed for the ductile tearing. No void nucleation of secondary particles was considered for the sake of comparison.

Current research trends in damage mechanics are to find out damage characteristics materials experimentally as well as analytically, so that fracture behavior of materials is predicted.

S TARAFDER, et al. [11] in their work, they have studied the ductile fracture behavior of primary heat transport piping material of nuclear reactor. In this paper, the fracture resistance of SA333, Grade 6 steel – the material used for Indian PHWR – under monotonic and cyclic tearing loading has been documented. An attempt has also been made to understand the mechanism responsible for the high fracture toughness of the steel through determination of the effect of constraint on the fracture behaviour and fractographic observations. From *J –R* tests over a range of temperatures, it was observed that SA333 steel exhibits embrittlement tendencies in the service temperature regime. The fracture resistance of the steel is inferior in the longitudinal direction with respect to the pipe geometry as compared to that in the circumferential direction. Imposition of cyclic unloading during ductile fracture tests for simulation of response to seismic activities results in a dramatic decrease of fracture resistance. It appears, from the observations of effects of constraint on fracture toughness and fractographic examinations, that fracture resistance of the steel is derived partly from the inability of voids to initiate and grow due to a loss of constraint in the crack-tip stress field.

Xiaosheng Gao , et al. [12] In this paper void coalescence is regarded as the result of localization of plastic flow between enlarged voids. We obtain the failure criterion for a representative material volume (RMV) in terms of the macroscopic equivalent strain (Ec) as a function of the stress triaxiality parameter (T) and the Lode angle (h) by conducting systematic finite element analyses of the void-containing RMV subjected to different macroscopic stress states. A series of parameter studies are conducted to examine the effects of the initial shape and volume fraction of the primary void and nucleation, growth, and coalescence of

secondary voids on the predicted failure surface Ec(T,h). As an application, a numerical approach is proposed to predict ductile crack growth in thin panels of a 2024-T3 aluminum alloy, where a porous plasticity model is used to describe the void growth process and the expression for Ec is calibrated using experimental data. The calibrated computational model is applied to predict crack extension in fracture specimens having various initial crack configurations and the numerical predictions agree very well with experimental measurements.

Alan T. Zehnder, Ph.D. [13] In these lecture notes the emphasis is on mechanics models for crack tip fields and energy flows with discussion of how these results affect observed fracture behavior. A brief discussion of computational fracture methods is given along with additional practical aspects such as fracture toughness testing and fracture criteria. The notes do not contain much on the understanding of material behavior or on fracture at the micromechanical level. Both the mechanics and the materials sides of fracture should be studied in order to obtain a balanced and more complete picture of the field. These notes grow out of my experience teaching fracture at Cornell and taking fracture mechanics in graduate school at Caltech with Ares Rosakis.

Z. L. ZHANG [14] Following a convincing demonstration of the prediction power of the Gurson model for ductile fracture, it is now required to select realistic material parameters for practical applications of the model. **In** this paper, using studies on a smooth tensile specimen, a notched tensile specimen, a centre-cracked tensile panel and an analytical cell model, a sensitivity analysis of the material parameters is performed that includes the initial void volume fraction of the primary inclusions and the void volume fraction of the secondary inclusions when fitting the critical void volume fraction. Voids that nucleated from primary and secondary inclusions have been considered separately. It has been found that in either case the selection of material parameters for the finite element analyses is not unique, and the most significant parameter for the predictions is the nucleation burst strain. Some general conclusions concerning the selection of material parameters for the Gurson model have also been made.

J. Chattopadhyay et al [15], In the present paper, limit load based general expressions functions are proposed. These expressions are validated by deriving the known functions of pipe with throughwall circumferential crack under four point bending load. The general expressions are then used to derive the functions of elbow with throughwall circumferential crack configurations under in-plane bending moment, for which no solutions are available in the literature. Finally, experiments have been carried out on 200mm NB (Nominal Bore) elbows with throughwall circumferential crack under in-plane bending moment. The proposed new expressions for this geometry are used to obtain the *J-R* curve from the experimental load vs. loadline- displacement and load vs. crack growth data.

J. Chattopadhyay et al [16], Component Integrity Test Program was initiated in 1998 at Reactor Safety Division (RSD) of Bhabha Atomic Research Centre (BARC), India in collaboration with MPA, Stuttgart, Germany through Indo-German bilateral project. In this program, both theoretical and experimental investigations were undertaken to address various issues related to the integrity assessment of pipes and elbows. The important results of the program are presented in this two-part paper. In the part II of the paper, the experimental investigations are discussed.

Part I covered the theoretical investigations. Under the experimental investigations, fracture mechanics tests have been conducted on pipes and elbows of 200–400 mm diameter with various crack configurations and sizes under different loading conditions. Tests on small tensile and three point bend specimens, machined from the tested pipes, have also been done to evaluate the actual stress–strain and fracture resistance properties of pipe/elbow material. The load– deflection curve and crack initiation loads predicted by non-linear finite element analysis matched well with the experimental results. The theoretical collapse moments of throughwall circumferentially cracked elbows, predicted by the recently developed equations, are found to be closer to the test data compared to the other existing equations. The role of stress triaxialities ahead of

crack tip is also shown in the transferability of J–resistance curve from specimen to component.

J. Chattopadhyay et al [17], In their work a number of fracture tests have been carried out on elbows with through wall circumferential/axial cracks subjected to in-plane closing/opening bending moment. These test data are then thoroughly analysed numerically through non-linear finite element analyses, analytically through limit load comparison and also through comparison of crack initiation loads by finite element and R6 methods. These test data may be utilized in future for validation of new theoretical developments in the integrity assessment of through wall cracked elbows.

B. Nedjar [18] describes the Elastoplastic-damage Modelling including the gradient of damage: formulation and computational aspects. Given a framework for continuum elastoplastic-damage Modelling, which employs irreversible thermodynamics and internal state variables, is investigated. The damage part of the Modelling involves the gradient of damage quantity which, together with the equations of motion, was issued from a new formulation of the principle of virtual power recently proposed. It is shown how the plastic part of the Modelling takes its standard format. Next, we consider in detail the variational formulation and subsequent numerical implementation of the elastoplastic-damage models. The development of an algorithm consistent with the present formulation is given where, for the plastic part, it leaves the standard return mapping algorithms unchanged. Application is made to different classical rate-independent and rate-dependent plastic models with the presence of a damage mechanism.

J. Oliver et al [19] discuss about the aspect of “From continuum mechanics to fracture mechanics: the strong discontinuity approach”. The paper deals with the strong discontinuity approach and shows the links with the decohesive fracture mechanics provided by that approach. On the basis of 1-D continuum damage models it is shown that, by introducing some few ingredients like the strong discontinuity kinematics, discrete constitutive models (traction vs. displacement jumps) are automatically induced. For the general 2D–3D cases it is shown that the weak discontinuity concept is an additional ingredient, necessary in order to

fulfill the strong discontinuity conditions, which allows to establish additional links with the fracture process zone concept. Also classical fracture mechanics properties as the fracture energy are related to the continuum model properties in a straightforward manner.

A. A. Benzerga [20] describes the Micromechanics of coalescence in ductile fracture. Significant progress has been recently made in modelling the onset of void coalescence by internal necking in ductile materials. The aim of this paper is to develop a micro-mechanical framework for the whole coalescence regime, suitable for finite-element implementation. The model is defined by a set of constitutive equations including a closed form of the yield surface along with appropriate evolution laws for void shape and ligament size. Normality is still obeyed during coalescence. The derivation of the evolution laws is carefully guided by coalescence phenomenology inferred from micromechanical unit-cell calculations. The major implication of the model is that the stress carrying capacity of the elementary volume vanishes as a natural outcome of ligament size reduction. Moreover, the drop in the macroscopic stress accompanying coalescence can be quantified for many initial microstructures provided that the microstructure state is known at incipient coalescence. The second part of the paper addresses a more practical issue that is the prediction of the acceleration rate δ in the Tvergaard–Needleman phenomenological approach to coalescence. For that purpose, a Gurson-like model including void shape effects is used. Results are presented and discussed in the limiting case of a non-hardening material for different initial microstructures and various stress states. Predicted values of δ are extremely sensitive to stress triaxiality and initial spacing ratio. The effect of initial porosity is significant at low triaxiality whereas the effect of initial void shape is emphasized at high triaxiality.

T. D. Righiniotis et al [21] presents the simplified crack model for weld fracture in steel moment connections. This paper presents a simplified two-dimensional crack model for assessing the fracture of bottom flange welds in steel beam-to-column connections. The formulation of the model includes the determination of

approximate expressions for stress intensity factors related to the cracked geometry, accounting for typical stress conditions and taking due consideration of the presence of the backing bar. Idealized residual stress distributions are also incorporated in the model to examine their influence on the behaviour. Particular attention is given to typical connection configurations, which have suffered considerable damage in the Northridge earthquake. Comparisons are made between the results obtained from the proposed model and those available from a number of experimental investigations as well as two-dimensional finite element analyses. Within the range of results examined in this study, the proposed model is shown to provide good, and generally conservative, predictions in terms of both the fracture moments and reduction in stiffness.

E. Schnack and W. Weikl [22] give the Shape optimization under fatigue using continuum damage mechanics. An introduction and overview of the developments in shape optimization for fatigue problems is given, beginning with the main ideas in the field of static shape optimization. The use of numerical tools together with the incorporation of non-linear material properties in the continuum mechanics design has led to new possibilities for the analysis of fatigue behaviour in mechanical engineering structures. Based on publications by Lemaitre and Chaboche, the material behaviour is described by defining different partial differential equation systems on micro-scale and meso-scale. From this an optimal algorithm results for the shape optimization of mechanical engineering structures using continuum damage mechanics. Our numerical and experimental tests show a significant increase of lifetime in comparison to classical shapes.

C. S. Chang et al [23] presents the Fracture modeling using a micro-structural mechanics approach—I, Theory and formulation. Stress–strain relationships used for modeling the mechanical behavior of materials have been traditionally derived following a phenomenological approach, without explicit considerations of the micro-structures of material. Here, we adopt a micro-structural mechanics approach to model the development of fracture in concrete. The continuum is assumed to have an underlying micro-structure of lattice type, which has been

demonstrated as a useful description for concrete fracture. A finite element formulation is also described that incorporates the developed stress–strain relationship. In an accompanying paper, we will show the results of finite element analyses, discuss its characteristics with respect to mesh size independency, and evaluate the applicability of this method.

C. S. Chang et al [24] presents the Fracture modeling using a micro-structural mechanics approach—II, Finite element analysis. In the accompanying paper [C.S. Chang, T.K. Wang, L.J. Sluys, J.G.M. van Mier, J. Eng. Fract. Mech.], the theoretical aspects of a stress–strain model are described based on a micro-structural approach. A finite element formulation was presented that incorporates the developed stress–strain relationship. In this paper the results of finite element analyses are described. The paper is focused on two main issues: the difference between the micro-polar and the non-polar micro-structural model, and the performance of the model respect to mesh size dependence. Specimens in uniaxial tension test and in biaxial tension–shear tests have been analyzed. To evaluate the applicability of this method, the finite element results are also compared with measured experimental results.

M. Yatomi et al [25] have presented about the Creep crack growth prediction using a damage based approach. This paper presents a numerical study of creep crack growth (CCG) in a fracture mechanics specimen. The material properties used are representative of carbon–manganese steel at 360 °C and the constitutive behaviour of the steel is described by a power law creep model. A damage-based approach is used to predict the crack propagation rate in a compact tension specimen and the data are correlated against an independently determined C parameter. Elastic–creep and elastic–plastic–creep analyses are performed using two different crack growth criteria to predict crack extension under plane stress and plane strain conditions. The plane strain crack growth rate predicted from the numerical analysis is found to be less conservative than the plane strain upper bound of an existing ductility exhaustion model, for values of C within the limits of the present CCG testing standards. At low values of C the

predicted plane stress and plane strain crack growth rates differ by a factor between 5 and 30 depending on the creep ductility of the material. However, at higher loads and C values, the plane strain crack growth rates, predicted using an elastic–plastic–creep material response, approach those for plane stress. These results are consistent with experimental data for the material and suggest that purely elastic–creep Modelling is unrealistic for the carbon–manganese steel as plastic strains are significant at relevant loading levels.

J. Besson et al [26] formulate the Modeling of plane strain ductile rupture. The formation of slanted fracture under plane strain conditions is studied using the finite Element (FE) method. Constitutive models proposed by Rousselier and by Gurson are used. Rice's condition for localization is checked at every point of the FE mesh for each time step. The role of mesh design (element size, element aspect ratio, symmetry) is first studied. The different constitutive models are then compared. It is in particular shown that the use of the f function in the Gurson model favors flat fracture.

Yingbin Bao and Tomasz Wierzbicki [27] focused on fracture locus in the equivalent strain and stress triaxiality space. The stress triaxiality is, besides the strain intensity, the most important factor that controls initiation of ductile fracture. In this study, a series of tests including upsetting tests, shear tests and tensile tests on 2024-T351 aluminum alloy providing clues to fracture ductility for a wide range of stress triaxiality was carried out. Numerical simulations of each test was performed using commercial finite element code ABAQUS. Good correlation of experiments and numerical simulations was achieved. Based on the experimental and numerical results, the relation between the equivalent strain to fracture versus the stress triaxiality was quantified and it was shown that there are three distinct branches of this function with possible slope discontinuities in the transition regime. For negative stress triaxialities, fracture is governed by shear mode. For large triaxialities void growth is the dominant failure mode, while at low stress triaxialities between above two regimes, fracture may develop as a combination of shear and void growth modes.

Jinkook Kim et al [28] described the Modeling of crack growth in ductile solids: a three-dimensional analysis. A population of several spherical voids is included in a three-dimensional, small scale yielding model. Two distinct void growth mechanisms, put forth for the case of a two-dimensional model containing cylindrical voids, are well contained in the model developed in this study for spherical voids. A material failure criterion, based on the occurrence of void coalescence in the unit cell model, is established. The critical ligament reduction ratio, which varies with stress triaxiality and initial porosity, is used to determine ligament failure between the crack tip and the nearest void. A comparison of crack initiation toughness of the model containing cylindrical voids with the model containing spherical voids reveals that the material having a sizeable fraction of spherical voids is tougher than the material having cylindrical voids. The proposed material failure determination method is then used to establish the fracture resistance curve (J–R curve) of the material. For a ductile material containing a small volume fraction of microscopic voids initially, the void by void growth mechanism prevails, which results in a J–R curve having steep slope. On the other hand, for a ductile material containing a large volume fraction of initial voids, the multiple voids interaction mechanism prevails, which results in a flat J–R curve. Next, the effect of T-stress on fracture resistance is examined. Finally, nucleation and growth of secondary micro-voids and their effects on void coalescence are briefly discussed.

I. Einav et al [29] discussed about the Coupled damage and plasticity models derived from energy and dissipation potentials. A theoretical framework is defined that allows plasticity and damage models of inelastic behaviour to be combined within a consistent approach.

CHAPTER 3

PROBLEM DEFINITION

3.1 Introduction

Safe operation of nuclear power plants is one of the major concerns of Reactor Safety Division. It focuses its programme on the development of expertise on materials behaviour. Safe operation of nuclear power plants relies primarily on the integrity of the reactor pressure vessel. Neutron exposure induces temperature dependent embrittlement of the vessel and alters the mechanical properties of the vessel materials.

The part of the vessel of primary concern with regard to age related degradation is the core beltline-the region of shell material directly surrounding the effective height of the fuel element assemblies. The low alloy steels making up the beltline are subject to irradiation embrittlement that can lead to loss of fracture toughness.

3.2 Aim of thesis

Different materials used for RPVs are described in section 1.4, although many materials are acceptable for reactor pressure vessels, the special considerations pertaining to fracture toughness and radiation effects effectively limit the basic materials acceptable for most parts of reactor pressure vessels.

The J-resistance curves are used for characterising the elasto-plastic fracture behaviour of metallic components. They are usually determined from ASTM standard specimens. However, there is a problem in transfering the specimen J-R curves to components because crack tip plays an important role in determining fracture resistance behaviour of components. In order to get rid of the effect of the effect of the effect of geometry, one has to consider the phases of the microscopic failure processes and incorporate it in the mathematical or constitutive model. In ductile fracture, the microscopic processes are void initiation, growth and coalescence to form microscopic crack. In the frame work of continuum mechanics, Gurson first derived the yield potential for porous

material with voids and introduced the model for analysis of ductile fracture which was later modified by Tvergaard and Needleman. If one uses this model, he can simulate the crack initiation and growth as this happens in the material without resorting to artificial numerical technique. So, the effect of stress multiaxiality on the fracture resistance behaviour is automatically taken care of and one can predict fracture behaviour of any component with any geometry and loading conditions.

In this work BARC in house code MADAM (Material Damage Modelling) based on GTN model was used to determine fracture characteristics of RPV steel 20MnMoNi55.

CHAPTER: 4

EXPERIMENTAL RESULTS

4.1 Introduction

The Gurson parameters are usually determined by curve fitting of experimental and analytical results. The curve fitting is generally done using load-ΔD curves of round notched tensile specimens. In curve fitting the Gurson parameters are varied so that the analytical curve approximates the experimental one in terms of load droping point and slope of curve at sudden load drop. All experiments were performed at BARC and data was provided. This chapter describes the results of tests conducted for damage mechanics analysis.

4.2 Material Properties

The material studied is German steel, used in reactor pressure vessel of Indian PHWR and designated as 20MnMoNi55. The mechanical properties of material are given in Table 4.1 and chemical composition is given in Table 4.2.

Material Properties	Value
Young's Modulus	2.05×10^5 MPa
Ultimate Tensile Strength	627.6575
Yield strength	498.0412
Poisson's Ratio	0.29
% Elongation	22%

Table: 4.1 Mechanical properties of 20MnMoNi55 steel at room temperature

Chemical Composition of 20MnMoNi55													
Source	C	Si	Mn	P	S	Cr	Ni	Mo	V	Cu	Al	Sn	As
[Wt-%]	0.21	0.24	1.48	0.008	0.005	0.2	0.8	0.52	0.02	0.07	0.015	0.005	0.02

Table: 4.2 Chemical composition of 20MnMoNi55 steel

Stress train curves for German steel are shown in Figure 4.1 and 4.2.

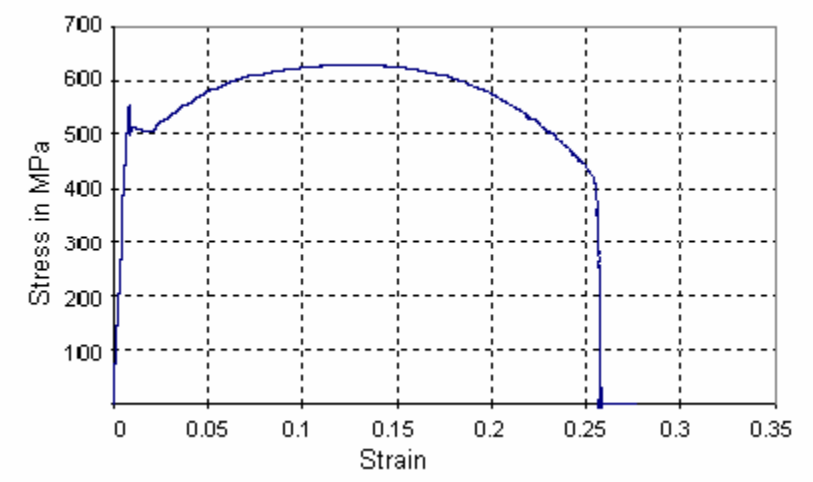

Fig 4.1 Engineering stress-strain curve of 20MnMoNi55 steel

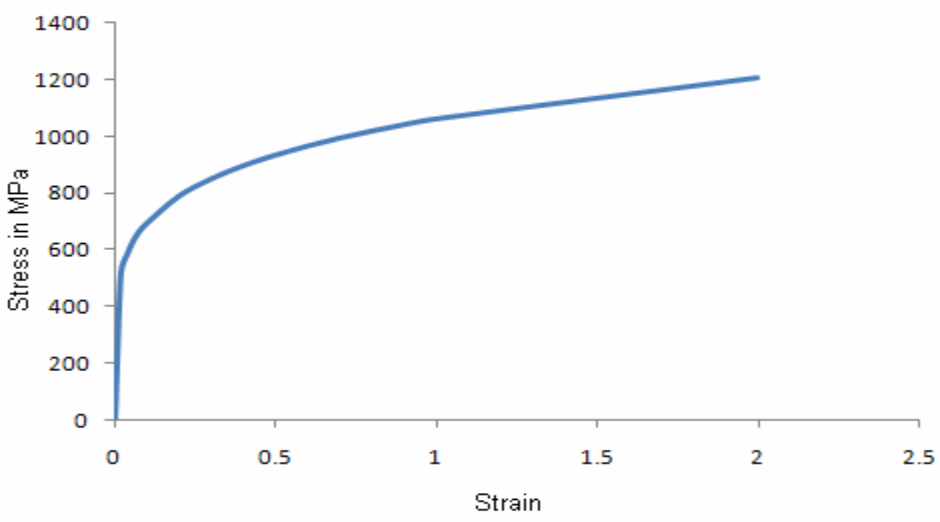

Fig 4.2 True stress strain curve of 20MnMoNi55 steel

4.3 Experimental load – Diametric contraction curves of Round Notched Tensile specimens

Tensile test results of RNTS were taken from RSD, BARC. Results were given in the form of time vs load and material diametric contraction was recorded using digital camera which takes 25 images per second. These images were processed to find diametric contraction of round notch tensile specimen.

4.3.1 Details of the Round Notched Tensile Specimens

There were two notched tensile specimens with notch groove radius 2mm and 4mm, designated as RNTS R2 and RNTS R4. The geometry of specimens is shown in Figure 3.3.

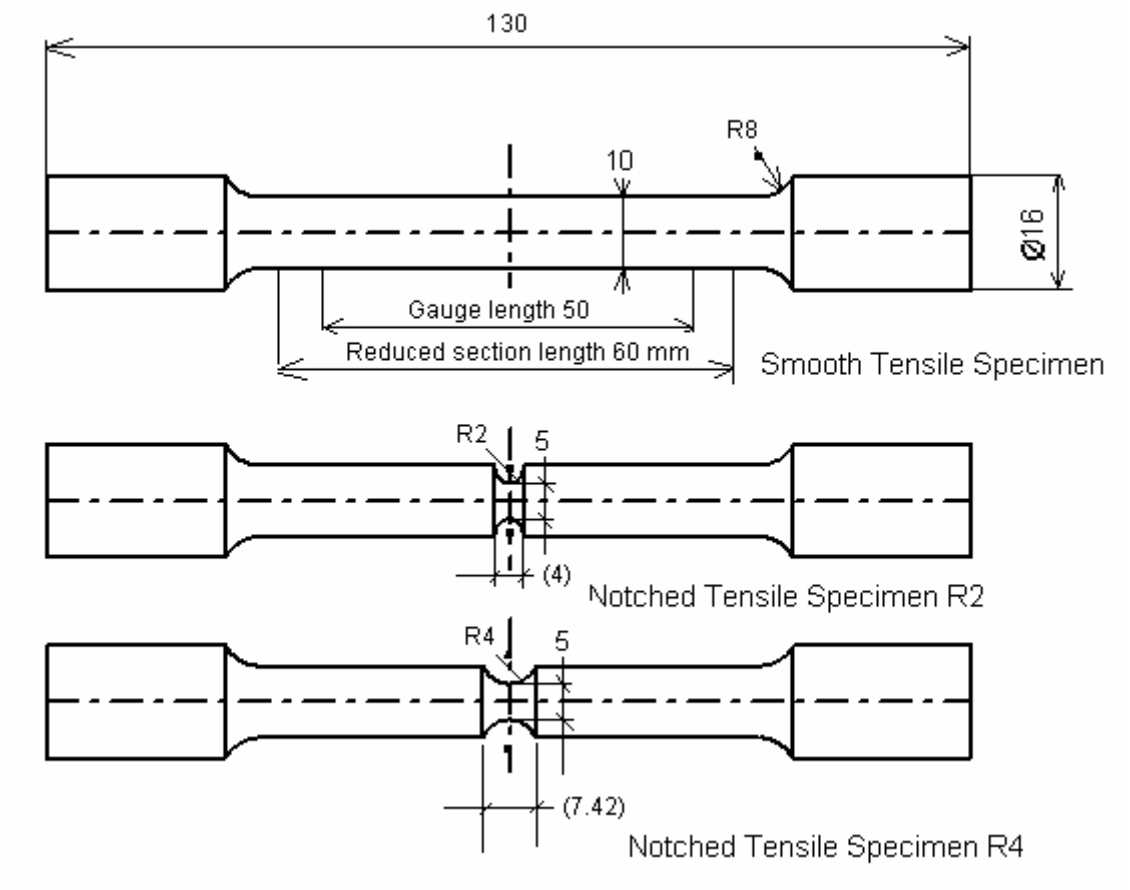

Figure 4.3 Detail of smooth and notched tensile specimens

The results of tests were recorded in the form of images (Figure4.4) and instantaneous load values from the digital display. The images were then post-processed with AutoCAD software (Figure 4.5). The images were copied and pasted in AutoCAD. Then the round piece diameter and notch diameter were measured. The notch diameter was calculated by taking the reference diameter of cylindrical part as 10mm.

Let Measured notch diameter =d

Cylinderical part diameter =D

Now as we know that the diameter of cylindrical part is 10mm

So we can find out notch diameter as:

Notch diameter = (d/D) x 10 mm

Diametric contraction (ΔD) = Initial Notch diameter –Notch diameter

Initial notch diameter was 5mm.

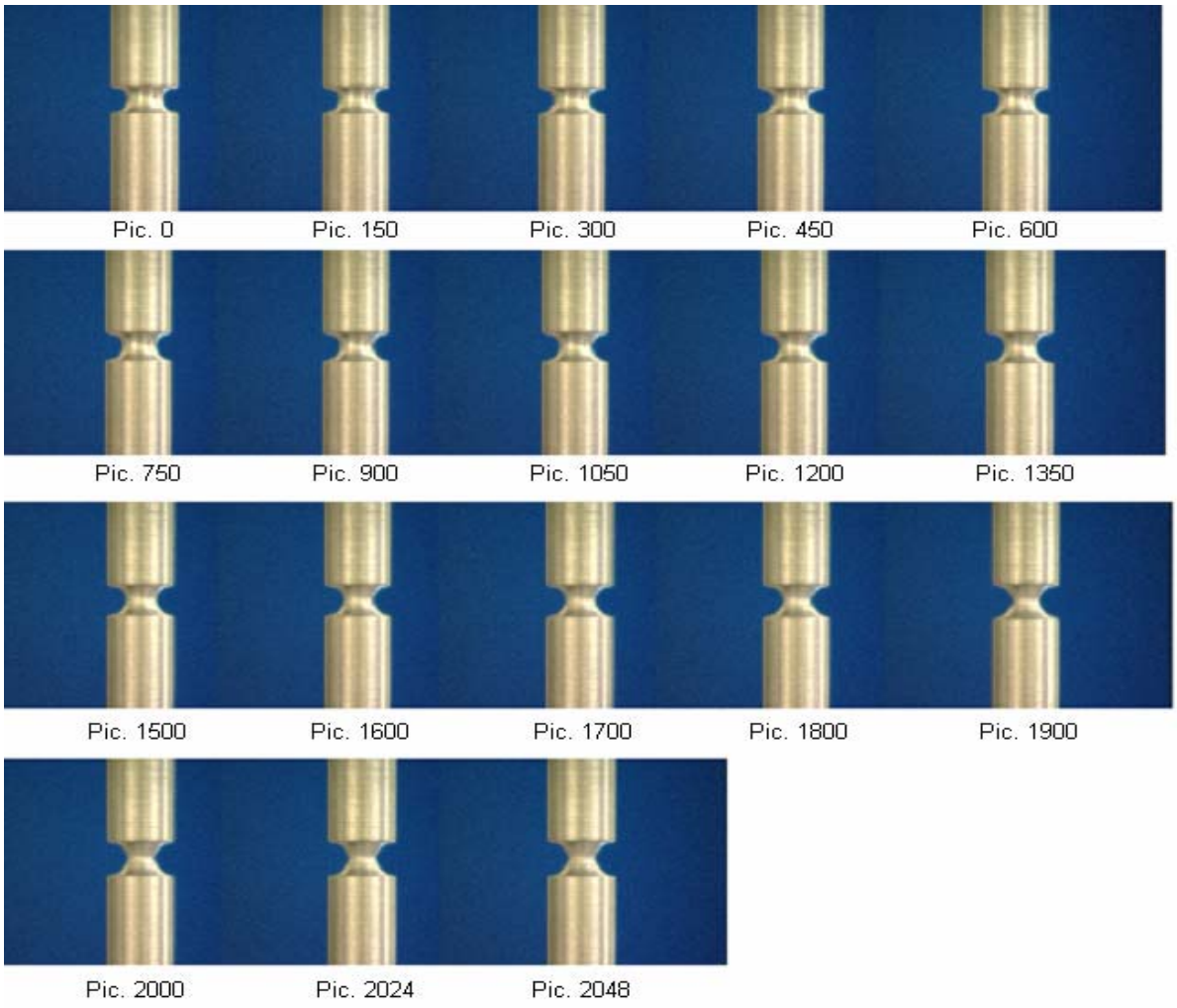

Figure 4.4 Photographs during testing (20MnMoNi55 R2)

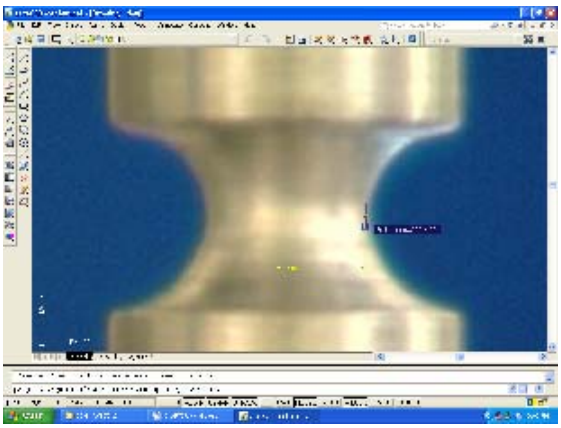

Figure 4.5 The image processing using AutoCAD

4.3.2 Test results for RNTS

The load-ΔD values for R2 & R4 obtained by image processing are given in Table 4.3 & 4.4 and corresponding load – ΔD curves are shown in Figure 4.6 & 4.7 respectively

S.No.	ΔD (mm)	Load (kN)	S.No.	ΔD (mm)	Load (kN)
1	0	0	22	0.49501939	1.88E+01
2	0.000221249	2.03172	23	0.566598386	1.87E+01
3	0.000288177	4.068172	24	0.61509039	1.85E+01
4	0.00195383	5.672121	25	0.631601708	1.84E+01
5	0.002199706	7.448649	26	0.72369926	1.82E+01
6	0.018217264	9.337997	27	0.750406154	1.80E+01
7	0.03574651	11.33834	28	0.790410424	1.78E+01
8	0.037616124	13.33827	29	0.840647647	1.76E+01
9	0.069822725	14.83247	30	0.86001975	1.74E+01
10	0.100600137	15.56288	31	0.898673861	1.72E+01
11	0.118656887	16.35754	32	0.97921178	1.69E+01
12	0.170296376	17.06943	33	0.99895957	1.67E+01
13	0.208827357	17.63526	34	1.375873173	1.31E+01
14	0.212683164	18.13371	35	1.466844738	1.13E+01
15	0.288916651	18.49311	36	1.551431841	1.00E+01
16	0.333742197	1.87E+01	37	1.584568825	9.69E+00
17	0.397612303	1.89E+01	38	1.599264477	9.42E+00
18	0.441090564	1.90E+01	39	1.621176317	9.19E+00
19	0.472342325	1.90E+01	40	1.631935143	8.93E+00
20	0.477876132	1.90E+01	41	1.639960129	8.49E+00
21	0.483035439	1.89E+01	42	1.652880678	8.22E+00

Table: 4.3 Load – ΔD values of RNTS R2 specimen

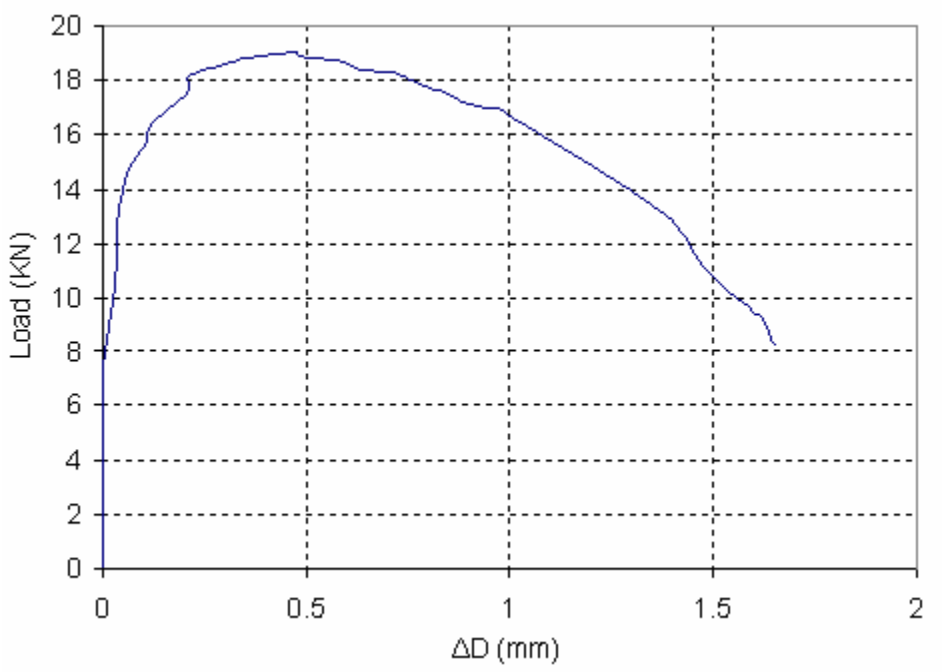

Figure 4.6 Experimental Load-ΔD curve for R2

S.No.	ΔD (mm)	Load (kN)	S.No.	ΔD (mm)	Load (kN)
1	0.00E+00	0.02759695	19	9.81E-01	1.53E+01
2	2.41E-02	2.053809	20	1.09E+00	1.51E+01
3	2.84E-02	4.619539	21	1.05E+00	1.48E+01
4	8.01E-02	6.814802	22	1.18E+00	1.45E+01
5	1.64E-01	9.405863	23	1.23E+00	1.43E+01
6	2.30E-01	11.97699	24	1.42E+00	1.40E+01
7	3.08E-01	13.50231	25	1.51E+00	1.37E+01
8	3.32E-01	14.53658	26	1.52E+00	1.34E+01
9	3.82E-01	15.2546	27	1.61E+00	1.31E+01
10	4.29E-01	15.7011	28	1.71E+00	1.28E+01
11	5.20E-01	16.03286	29	1.78E+00	1.24E+01
12	5.68E-01	16.14389	30	1.84E+00	1.21E+01
13	6.63E-01	16.1551	31	1.87E+00	1.17E+01
14	6.54E-01	16.09221	32	1.96E+00	8.55E+00
15	7.79E-01	16.01033	33	2.04E+00	6.64E-01
16	7.43E-01	1.58E+01	34	2.04E+00	1.87E-02
17	8.39E-01	1.57E+01	35	2.05E+00	3.86E-02
18	8.73E-01	1.55E+01			

Table: 4.4 Load – ΔD values of RNTS R4 specimen

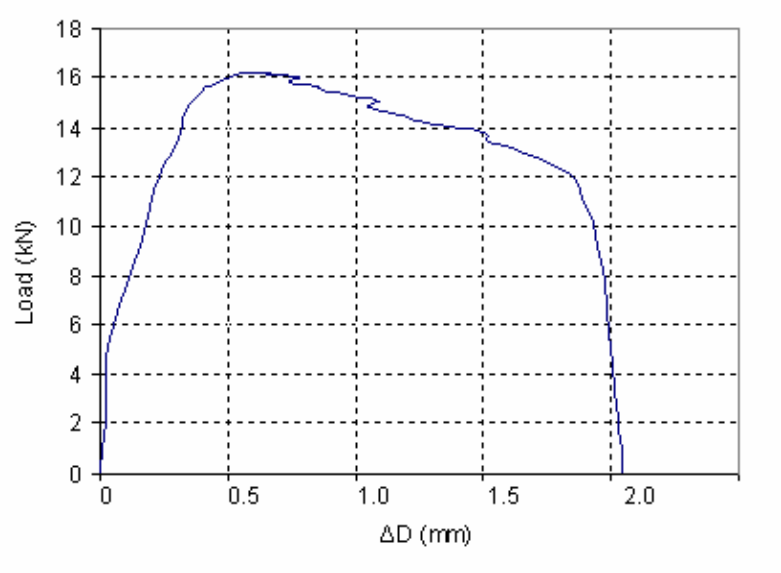

Figure 4.7 Experimental Load-ΔD curve for R4

4.4 Testing of CT Specimen and TPB Specimen

Three identical CT and TPB specimens conforming ASTM standard E1820 were tested at IIT Roorkee. The dimensions and the details of the testing procedure is following:

4.4.1 Details of the Test Specimens

The dimensions of the specimens are shown in Fig. 3.8:

Figure 4.8 CT specimen used for testing

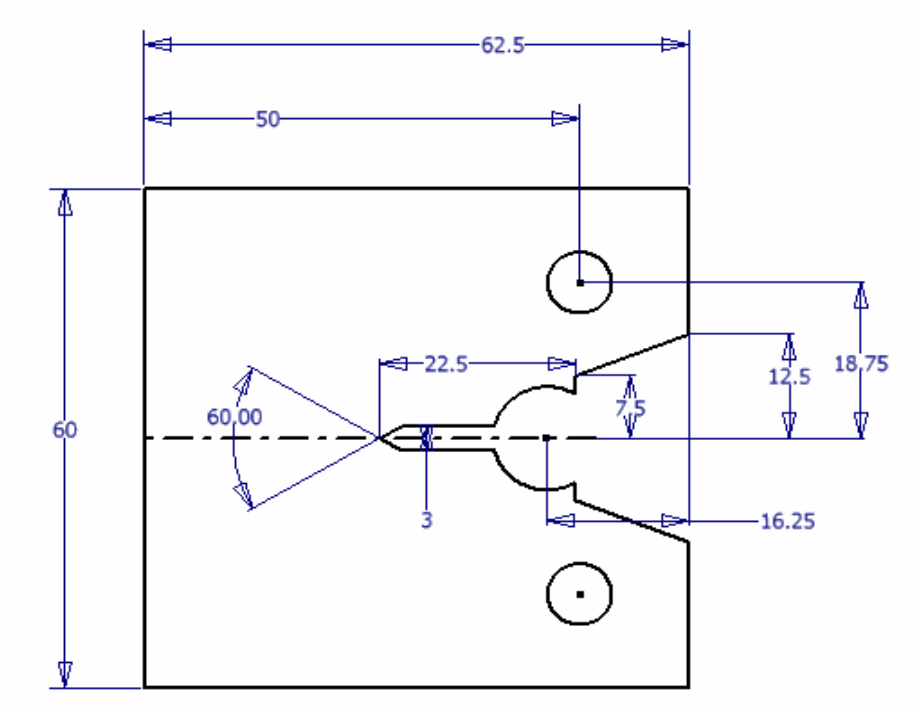

Figure 4.9 Details of the CT specimens

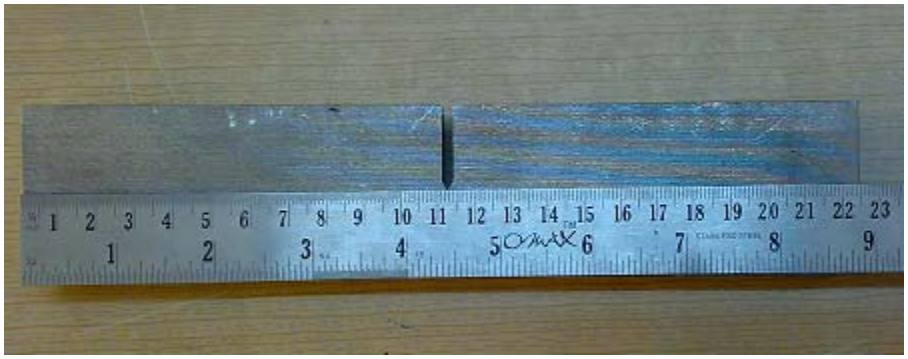

Figure 4.10 TPB specimen used for testing

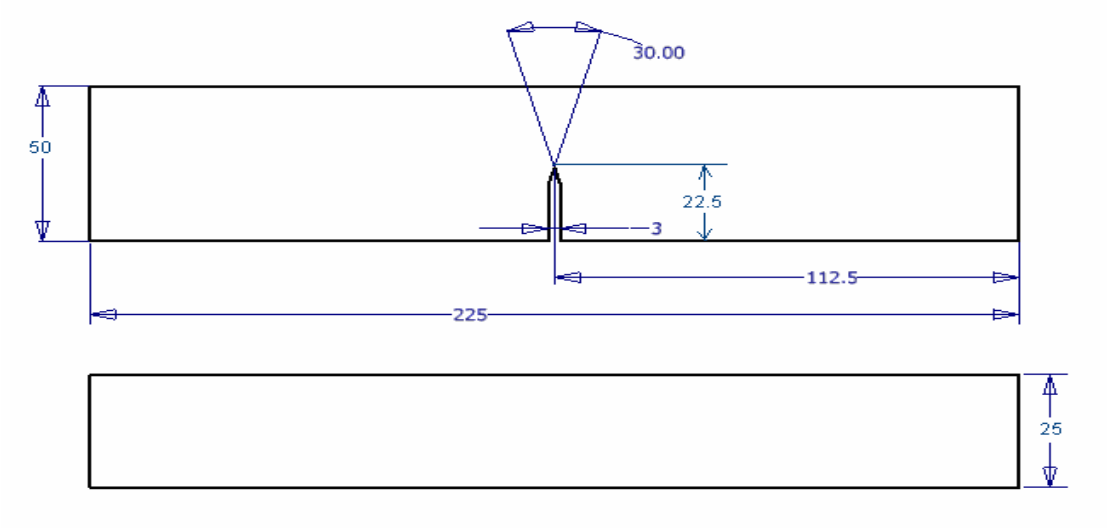

Figure 4.11 Details of the TPB specimen

4.4.2 Details of the Testing Procedure

The testing was done as per ASTM standard E1820. The specimens were pre-cracked (2-2.5mm) by cyclic loading. Crack opening displacement was measured using displacement gauge attached to the knife edge. Crack growth was calculated by monitoring the specimen compliance at each instant of unloading and employing the CCL relations. The load, load-line displacement and crack-growth were processed to obtain the *J*-integral vs. crack growth.
Pre-crack load was calculated as below

For CT Specimen

All specimen s shall be precracked in fatigue at a force value based upon the Maximum force Pm as follows:

$$\text{Maximum load} \quad Pm = \frac{0.4Bb_o^2\sigma_y}{(2W + a_0)} \quad = 36.4 \text{ kN} \tag{4.1}$$

$$f\left(\frac{a_i}{W}\right) = \frac{\left[\left(2+\frac{a_i}{W}\right)\left(0.886 + 4.64\left(\frac{a_i}{W}\right) - 13.32\left(\frac{a_i}{W}\right)^2 + 14.72\left(\frac{a_i}{W}\right)^3 - 5.6\left(\frac{a_i}{W}\right)^4\right)\right]}{\left(1-\frac{a_i}{W}\right)^{3/2}} = 8.34 \tag{4.2}$$

Where,

Specimen Thickness B= 25mm

Width of specimen W =50mm

Crack length a =22.5mm

Remaining width b_o =27.5mm

Yield strength σ_{ys} =552 Mpa

Ultimate Tensile Strength σ_{uts} =628 Mpa

Average yield strength $\sigma_y = (\sigma_{ys} + \sigma_{uts})/2$ = 590 Mpa

Initial Crack Length=26. 951552 mm

For TPB Specimen

$$Pm = \frac{0.5Bb_o^2\sigma_y}{S} \quad = 27.88 \text{ kN} \tag{4.3}$$

$$f(\frac{a_i}{W}) = \frac{3(\frac{a_i}{W})^{1/2}[1.99 - (\frac{a_i}{W})\ (1 - \frac{a_i}{W})(2.15 - 3.93(\frac{a_i}{W}) + 2.7(\frac{a_i}{W})^2)]}{2(1 + 2\frac{a_i}{W})(1 - \frac{a_i}{W})^{3/2}} = 3.08 \tag{4.4}$$

Where,

Specimen Thickness B = 25mm

Width of specimen W =50mm

Crack length a =22.5mm

Support span S= 200mm

Remaining width b_o =27.5mm

Yield strength σ_{ys} =552 Mpa

Ultimate Tensile Strength σ_{uts} =628 Mpa

Average yield strength $\sigma_y = (\sigma_{ys} + \sigma_{uts})/2$ = 590 Mpa

Initial Crack Length=32.952879 mm

4.4.3 Test Results

Test results are in the form of Experimental J-R curve for CT and TPB specimens.

Figure 4.12 Fractured CT specimen.

Figure 4.13 Fractured surface of broken CT specimen.

Figure 4.14 Fractured TPB specimen.

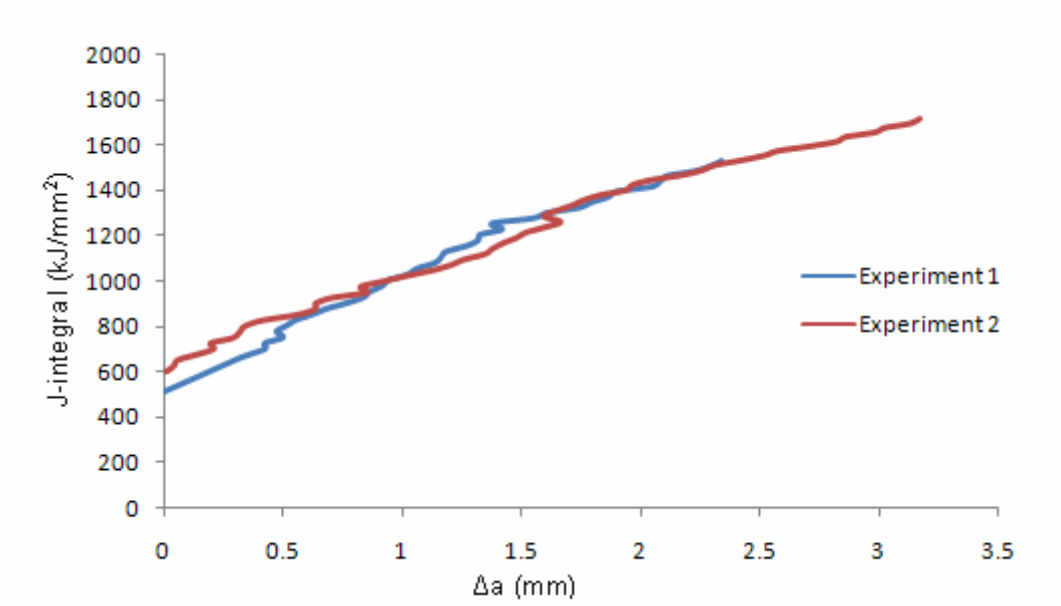

Figure 4.15 Experimental J-R curves for CT specimen (20MnMoNi55 steel)

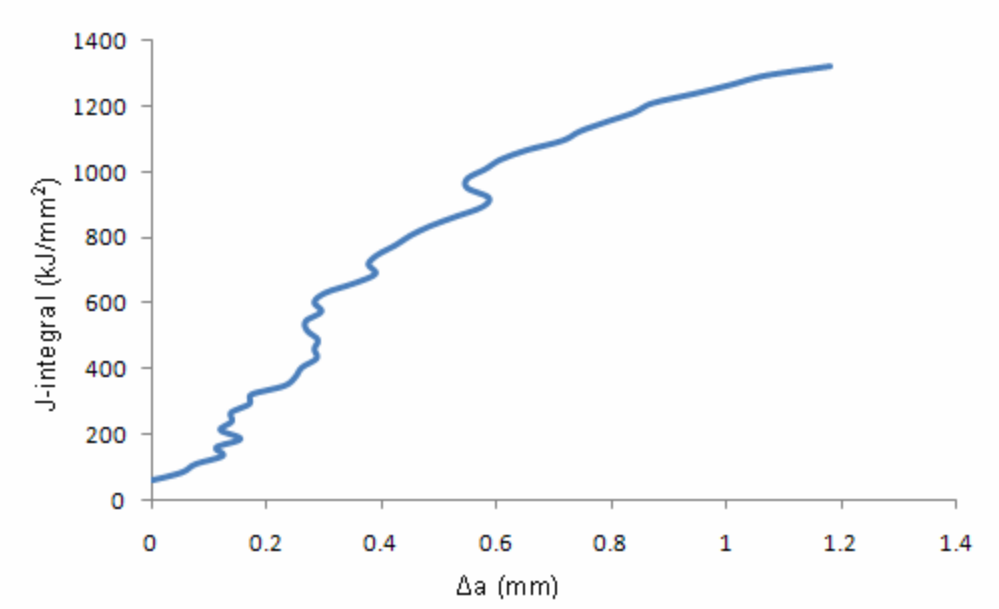

Figure 4.16 Experimental J-R curve for TPB specimen (20MnMoNi55 steel)

CHAPTER: 5

FINITE ELEMENT ANALYSIS METHODOLOGY

5.1 Introduction

FE analysis is divided into four steps:

I. Generation of FE mesh
II. Making the input file
III. Running the FE code MADAM (Material Damage Modelling)
IV. Post-processing the output from code

5.2 Generation of FE mesh

The meshes for Notched Tensile Specimen, Ct and TPB were generated using in house code FEMSHAPE. In case of RNTS as the specimen has two axis of symmetry, only one fourth of the specimen was modeled and in case of CT and TPB specimens have one axis of symmetry , only one half of the specimen was modeled. The geometric models were made such a way that the mesh size near the crack tip was equal to two times the critical length. Meshes away from the crack path were intentionally made large to reduce computational time. All the elements were 2D 8-node isoparametric elements. The output file of fem shape was used to made input file for MADAM code

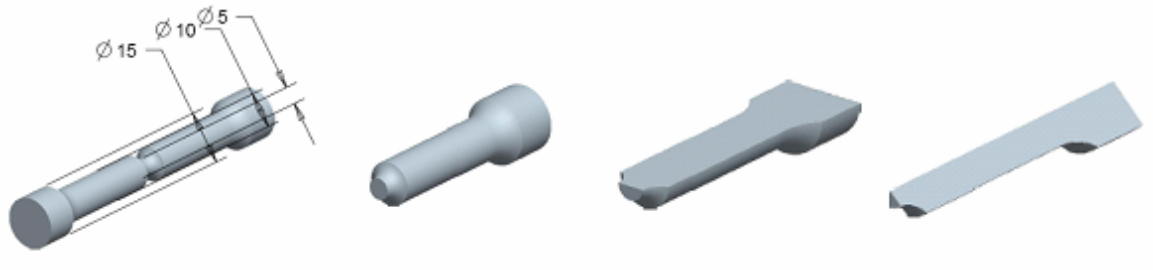

Figure 5.1 Geometry of RNTS specimen

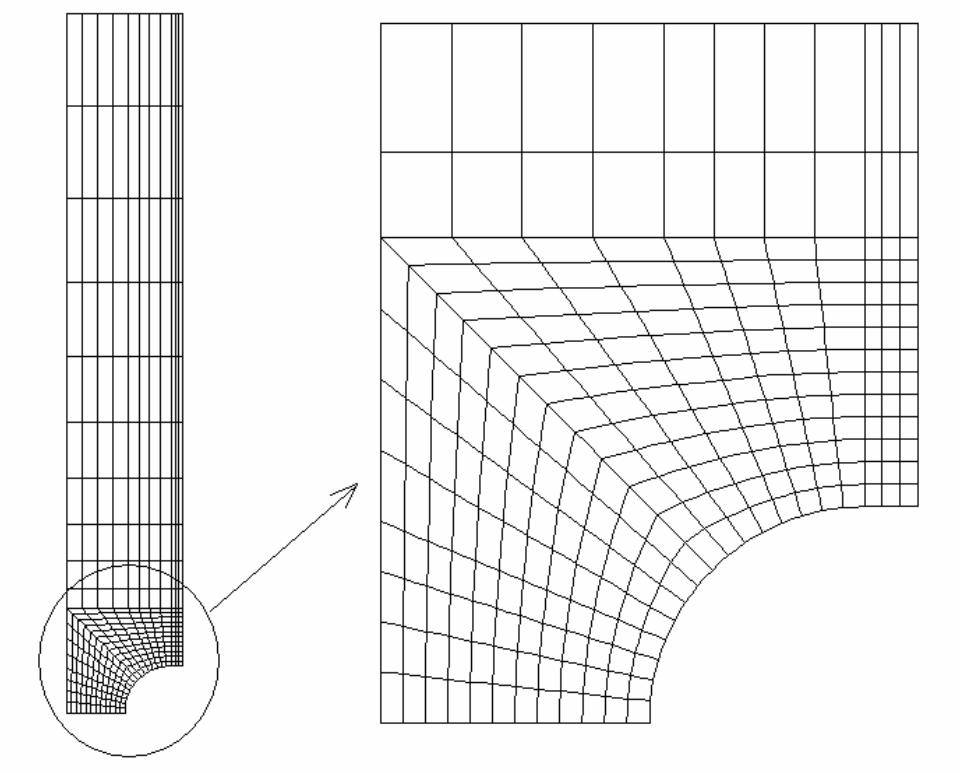

Figure 5.2 FE mesh for RNTS R2 specimen

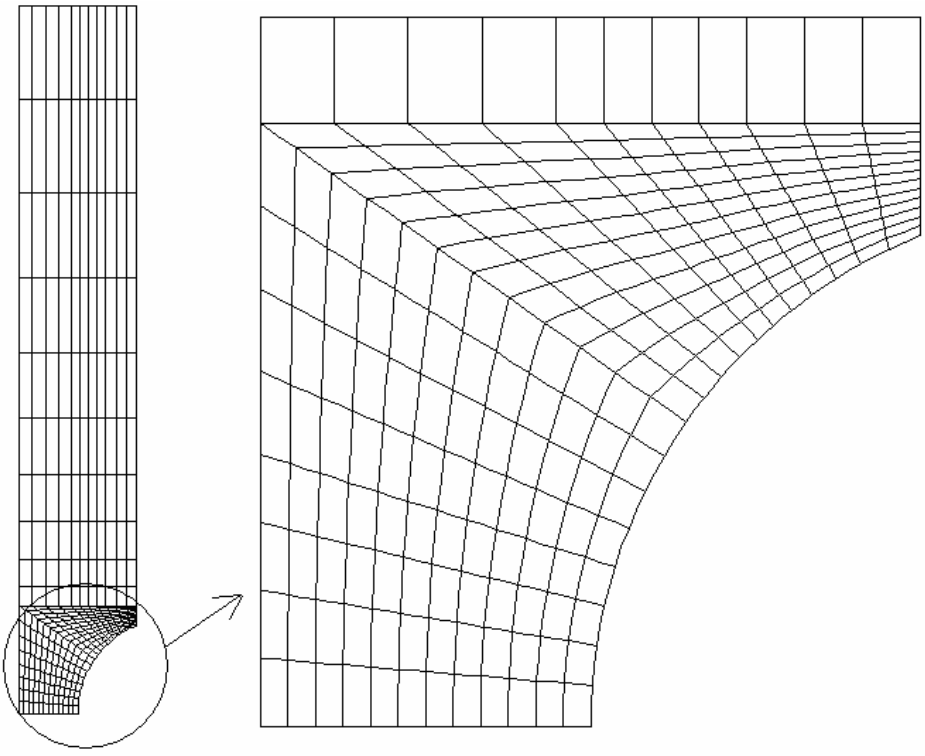

Figure 5.3 FE mesh for RNTS R4 specimen

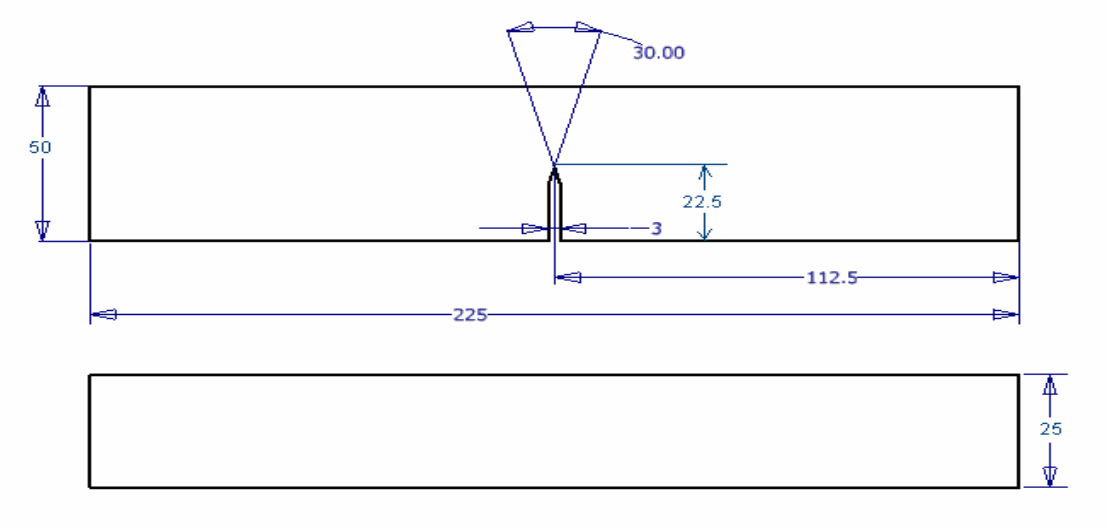

Figure 5.4 Geometry of TPB specimen

In case of TPB and CT as the specimen has one axis of symmetry, so only one half of these specimens are modeled. Geometry of TPB and Ct specimens are given in Figure 5.4 &5.6 respectively and corresponding FE meshes are given in Figure 5.5 & 5.7 respectively.

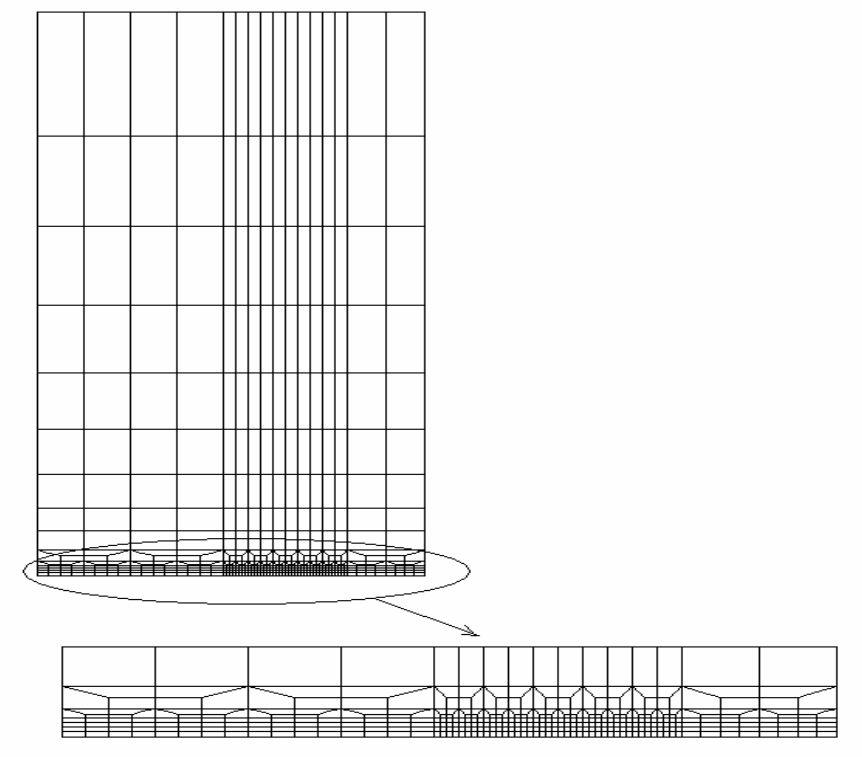

Figure 5.5 FE mesh for TPB specimen

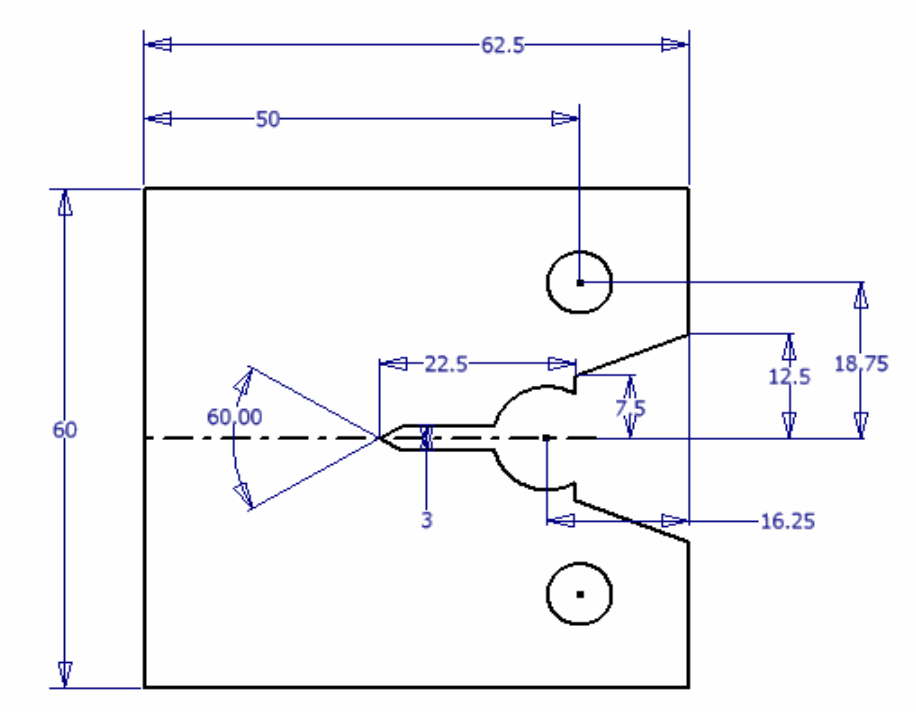

Figure 5.6 Geometry of CT specimen

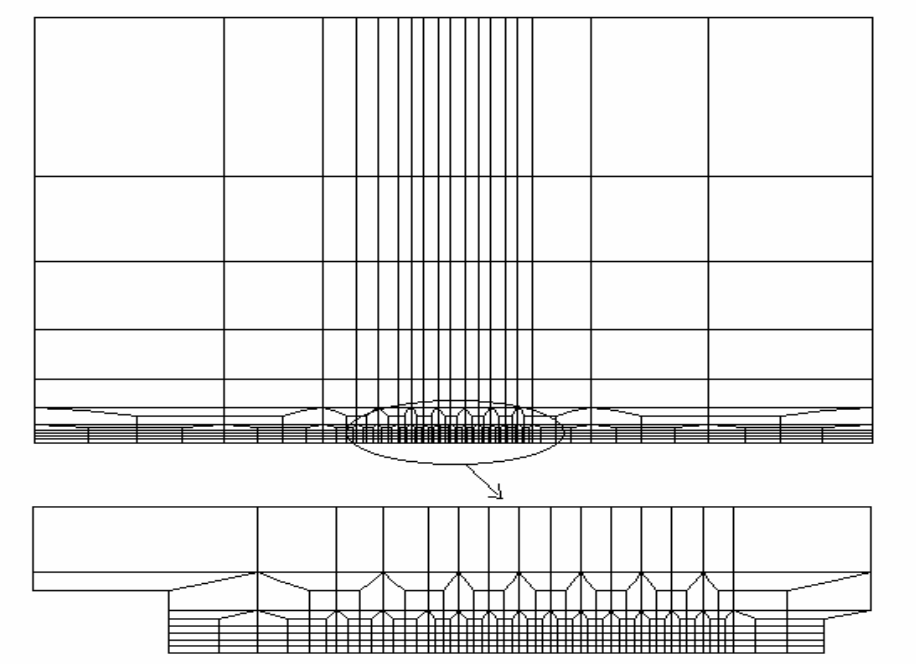

Figure 5.7 FE mesh for CT specimen

5.3 Generation of the input file

Once the mesh has been constructed the next step is to prepare the input file for the component giving every detail that describes actual problem under investigation. The input file is then used by MADAM code. The input file is written in the following format:

Card 1

First word (A10): Name of equation solver- SPRASE, FRONTAL, COLSOL (column solver), LPCG (linear pre-conditioned conjugate gradient solver).
Second word (A10): Solution technique- NEWTON (Newton-Raphson method), RIKS (Modified Rik's method).
Third word (A10): Integration scheme employed- MIDPOINT, BEULER (backward Euler), FEULER (forward Euler).

Card 2

This card set (A80) describes title to the problem.

Card 3

First data (I5): Total number of elements
Second data (I5): Total number of nodes
Third data (I5): Total number of nodes per element
Fourth data (I5): Number of elements for which the node relations are to be provided
Fifth data (I5): Number of nodes for which the coordinates are to be provided
Sixth data (I5): Index for loading condition -1 (Plane stress), 2 (plane strain), 3 (axis- symmetric case), 4 (3-D case).

Card 4

First data (I5): Number of materials
Second data (I5): Type of stress strain curve- 1 (true stress- true strain), 2 (engineering stress engineering strain)

Third data (I5): Type of analysis-0 (elastic –plastic), 12 (damage mechanics)
Fourth data (I5): Index for material hardening-0, (isotropic hardening),1(kinematics hardening

Card 5

First data (I5): Number of group of boundary conditions
Second data (I5): Total number of boundary nodes
Third data (I5): Number of group of loads

Card 6

First data (I5): Index for geometric non-linearity-1(On), 0(Off)
Second data (I5): Number of load increments
Third data (I5): Maximum number of iteration for convergence
Fourth data (I5): Number of group of load fractions
Fifth data (I5): Number of print interval for output files.

Card 7

Here element and node relationship is provided which has been obtained through the mesh generating code or software.

For 2D 4-node iso- parametric quadrilateral element

First data (I5): Elements ID
Second data (I5): Material ID
Third to sixth data (I5): ID of corner nodes

For 2D 8-node iso- parametric quadrilateral element

First data (I5): Elements ID
Second data (I5): Material ID
Third to sixth data (I5): ID of corner nodes (anticlockwise)
Seventh to tenth data (I5): ID of corresponding mid - nodes (anticlockwise)

For 3D 20-node brick element

First data (I5): Elements ID

Second data (I5): Material ID
Third to tenth data (I5): ID of corner nodes
Eleventh to eighteenth data (I5):ID of corresponding mid - nodes

Card 8

Here the co-ordinates in x, y and z direction for each node are provided as obtained through the mesh generating code or software.

Card 9

Depending upon the number of groups of boundary conditions data are to be provided in this card.

Card 10

In this card material properties are given.
First data (E10.3): young's modulus of elasticity in MPa of material
Second data (E10.3): Poisons ratio
Third data (E10.3): Yield stress
Fourth data (I5): Number of data points for stress strain curve

Card 11

This card gives the data for stress-strain curve and immediately follows the card where young's modulus is provided.

Card 12

This card is only to be read when the 3^{rd} data in 4^{th} card is 1. The data are Gurson parameters.

Card 13

This card gives number of group of distributed loads and number of concentrated loads. For displacement controlled loading these parameters are zero.

Card 14

This card is read only when first data in card 13 is non zero. This card provides data for each face.

Card 15

This card is read only when second data in card 13 is non zero. It provides data regarding node number and corresponding loads in x and y direction.

Card 16

Depending on the no. of group of loads and the number of groups of load fraction data is to be provided.

Card 17

Here the data represents no. of elements for which damage mechanics calculations is to be done.

Card 18

The data in this card represents the id of elements for which damage mechanics calculation is required.

Card 19

This card gives data regarding engineering quantity to be found (displacement, reaction etc.) and range of nodes for which it is to be found.

5.4 Running the FE code MADAM (Material Damage Modelling)

Input file was run using BARC in-house finite element code MADAM (Material Damage Modelling). MADAM has been developed based on the principles of continuum damage mechanics (Modified Gurson's model).

Feature's of the code:

1. The code has the ability to solve both two and three dimensional structures. In 2D analysis, 4-noded and 8-noded isoperimetric elements are available. In 3D, 20 noded isoperimetric brick elements are available.
2. It can handle the 2- dimensional case of plain strain, plain stress and axisymmetric structures under thermal-elastic-plastic deformations.
3. The geometric nonlinearity is considered by using the Lagrangian formulation.
4. The deformation and rotation in elastic-plastic analysis is considered by transforming the computed Cauchy stress to Jaumann stress rate using the corresponding spin rate tensor.
5. The frontal solution technique is used for solving linear set of simultaneous equations. The load-deformation equilibrium conditions are obtained by using Modified-Riks Algorithm.
6. For integration of elastic-plastic constitutive equations for the GTN yield model, the generalized mid-point algorithms formulate by Zhang [12] has been used.
7. Both load and displacement controlled formulation.

5.5 Post-processing the output from MADAM code

1. Output file: Gives the damage elements corresponding iteration number and gauss point and also confirms the input data.
2. MADAM-POST.OUT: Stores in detail the deformation history and different stress and strain values.
3. MADAM.DAT: Gives the displacement of each node and reaction of boundary nodes at specified interval.

Post-processing for load-ΔD and load-displacement

For RNTS, CT and TPB specimens the load-displacement values were given in MADAM.DAT file. A program was used to find the load-displacement for all specimens and also load-ΔD value for RNTS specimen.

Post-processing for J-R curve

For calculating J-R values jcg code was used. There were two input files to the code. First *jcg.INP file and second jcg.EXT file. In *jcg.INP file there were data regarding total number of iterations and displacement and load corresponding to each iteration and also data regarding the damage element corresponding gauss point and iteration number. Jcg.EXT file contains data regarding specimen geometry and material properties. From out put file *jcg.DAT we get J-R values and J_i (initiation) value.

CHAPTER: 6

EVALUATION OF GURSON DAMAGE PARAMETERS

6.2 A Study on Effect of Gurson Parameters on Material Behaviour

The effect of Gurson parameters on load-ΔD & J-R curve is studied by varying one parameter at a time and keeping other parameters unchanged. In the study, four criteria were considered extensively:

i. The sudden load dropping point in the RNTS load- ΔD curves
ii. The slope of sudden load drop curve in the RNTS load- ΔD curves
iii. J_i (J-integral at crack initiation) for CT specimen.
iv. Stable slope of J_R curve for CT specimen.

Gurson parameters used in study are given in Table 6.1 and same parameters were used as initial parameters.

Gurson parameters	Value
Initial void volume fraction, 'f_o'	0.00001
Critical void volume fraction, 'f_c'	0.07
Final void volume fraction, 'f_f'	0.252
Void volume fraction at saturated nucleation, 'f_N'	0.007
Mean value of strain for nucleation, 'ε_N'	0.165
Standard deviation of strain for nucleation, 'S_N'	0.1
'q_1'	1.5
Modifying parameters 'q_2'	1.0
'q_3'	2.25
Critical length parameters 'l_c'	0.2
Modified ultimate void volume fraction 'f_u'	0.566

Table 6.1 Initial Gurson parameters and their values

6.2 Effect of Initial void volume fraction (f_0)

It represents the initial void fraction of the inclusions in the material which are not strongly adhered to the matrix. It is determined by metallographic examination and calibrated by analysis of notched tensile test specimens. The primary void portion of $f_{0,}$ grows under increasing stress and strain of the material, while the inclusion part of the initial void volume fraction increases the probability of void nucleation. Figure 6.1 clearly shows the effect of initial void volume fraction on load dropping point for notched tensile specimens. With increase in values of f_0 there is increase in slope of load- ΔD curve. The effect of

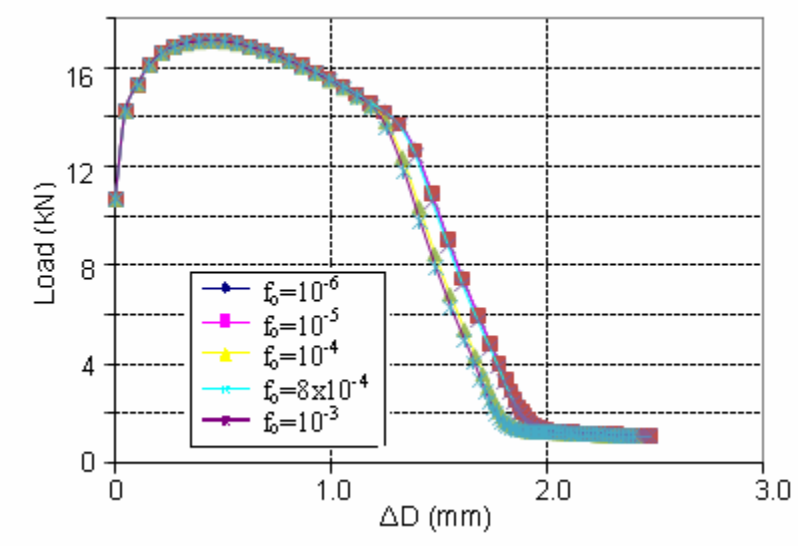

Figure 6.1 Load-ΔD curves for different f_o values

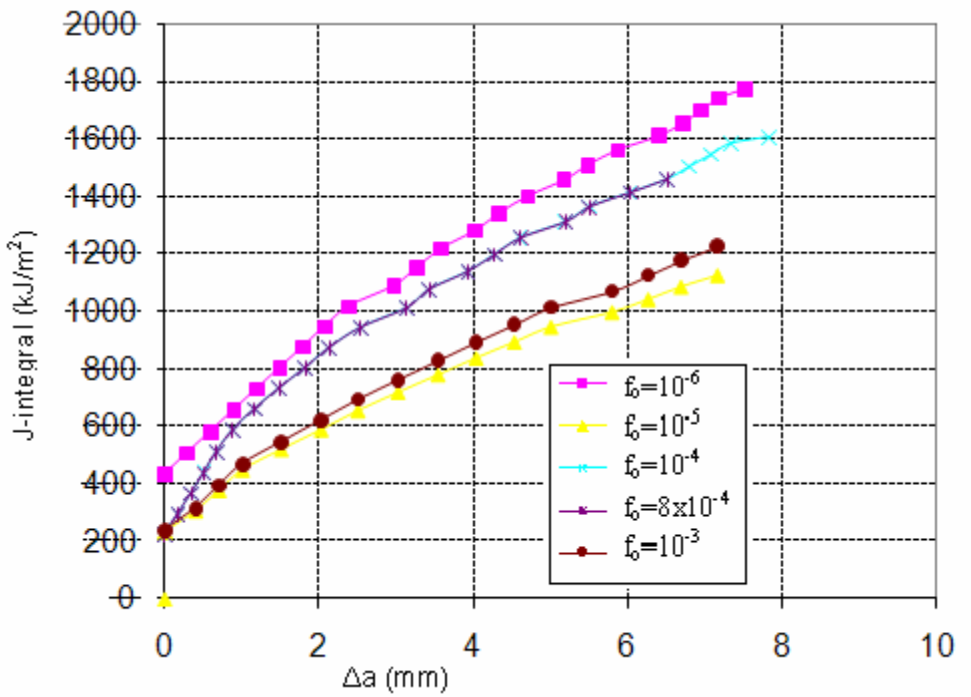

Figure 6.2 J-R curves for different f_o values

f_0 is more prominent in J-R curve as shown in Figure 6.2. The study reveals that through the J-initiation is much affected by initial void volume fraction, the slope also changes significantly with changing this parameter. Table 6.1 gives the ΔD (at sudden load drop), Slope Load-ΔD, Ji (initiation) and slope of J-R curve for different values of f_o

	ΔD	Slope Load-ΔD	Ji	Slope J-R
f_o =10E-6	1.26	21.2	431.7	164.2347
f_o =10E-5	1.2768	21.2	233.74	98.4369
f_o =10E-4	1.154	21.3	223.17	167.5375
f_o =8*10E-4	1.15	20.9	223.17	167.5375
f_o =10E-3	1.12	20.5	237.13	112.3277

Table 6.2 Effect of f_o on ΔD (at sudden load drop), Slope Load-ΔD, Ji (initiation) and slope of J-R curve

6.3 Effect of critical void volume fraction (f_c)

The Critical void volume fraction (f_c) is the critical value of void volume fraction at which the material stress carrying capacity starts to decay more rapidly due to void coalescence. Lower f_c means that the material reaches this point earlier. The load dropping point in the load – diametral contraction curve is mainly influenced by this parameter. The J-R curves (Figure 6.4) shows that J_I and the slope of the J-R curve are significantly affected by the critical void volume fraction. While J_i is affected almost linearly, the 'slope' varies parabolically.

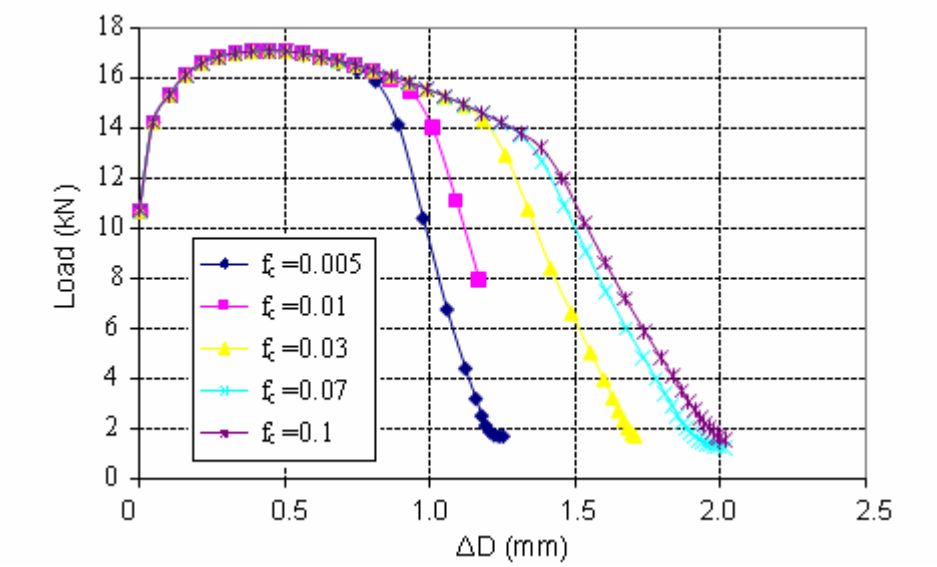

Figure 6.3 Load-ΔD curves for different f_c values

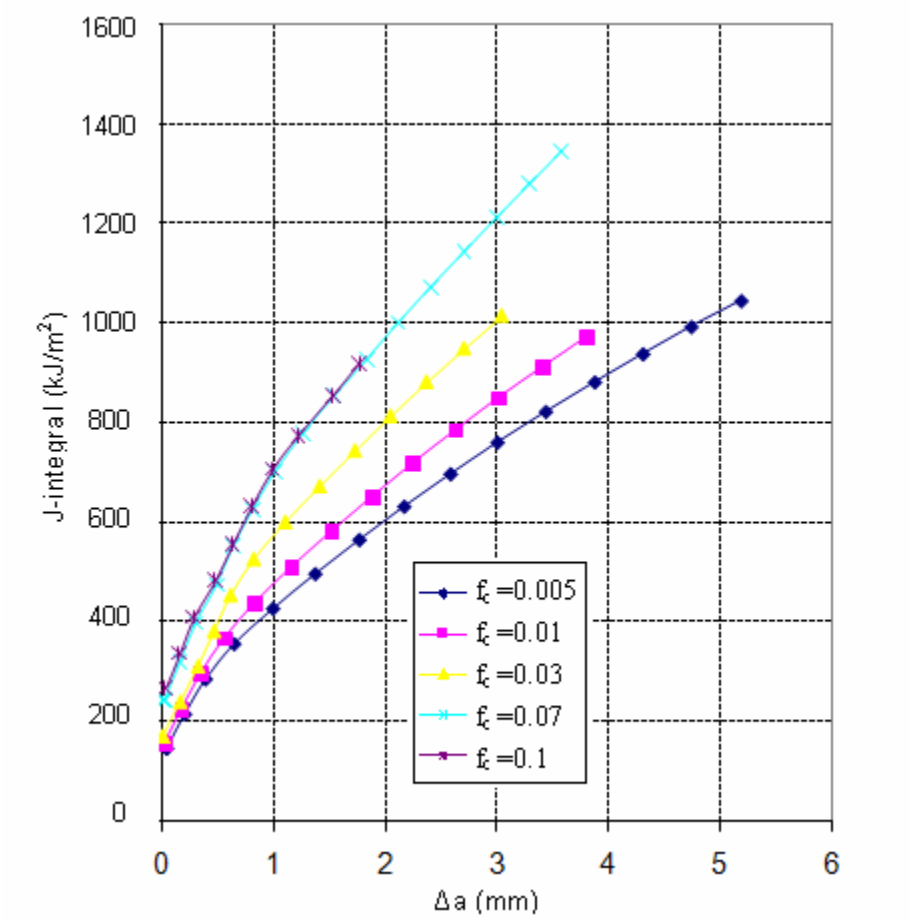

Figure 6.4 J-R curves for different f_c value

	ΔD	Slope Load-ΔD	Ji	Slope J-R
f_c =0.005	0.868	34.77381	144.89	133.8162
f_c =0.01	0.93	33.692	156.1211	155.4224
f_c =0.03	1.18	31.554	169.5724	197.1494
f_c =0.07	1.32	25.8	243.09	241.6448
f_c =0.1	1.34	24.3	265.41	272.356

Table 6.3 Effect of f_c on ΔD (at sudden load drop), Slope Load-ΔD, Ji (initiation) and slope of J-R curve

6.4 Effect of final void volume fraction (f_f)

Final void volume fraction (f_f) is the actual void volume fraction associated with the complete loss of stress carrying capacity of the material matrix. Lower values of f_f force the material to loss the stress carrying capacity earlier and thus a

steeper slope is obtained (Figure 6.5). The load dropping point remains unaffected by f_f, while the slope varies linearly. The J-R curves (Figure 6.6) shows that while the slope is not much affected by varing the f_f the J_i is linearly affected by the final void volume fraction.

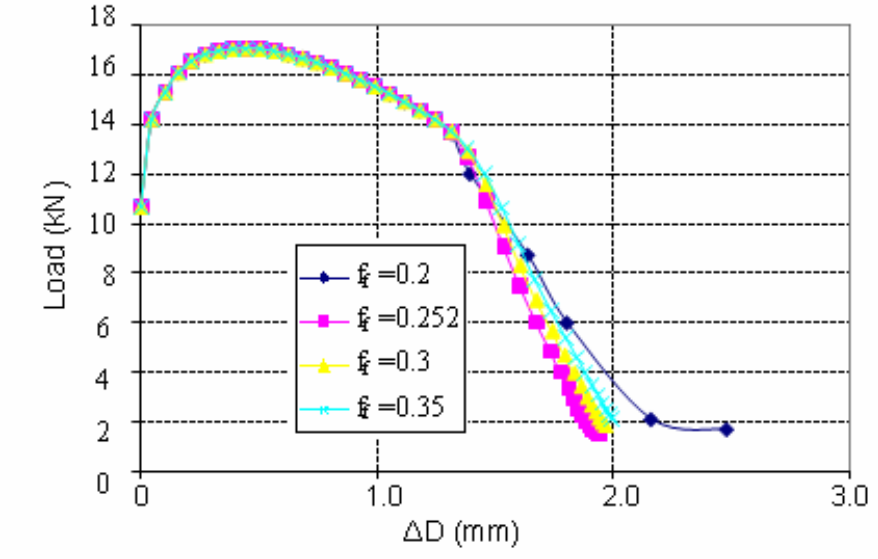

Figure 6.5 Load-ΔD curves for different f_f values

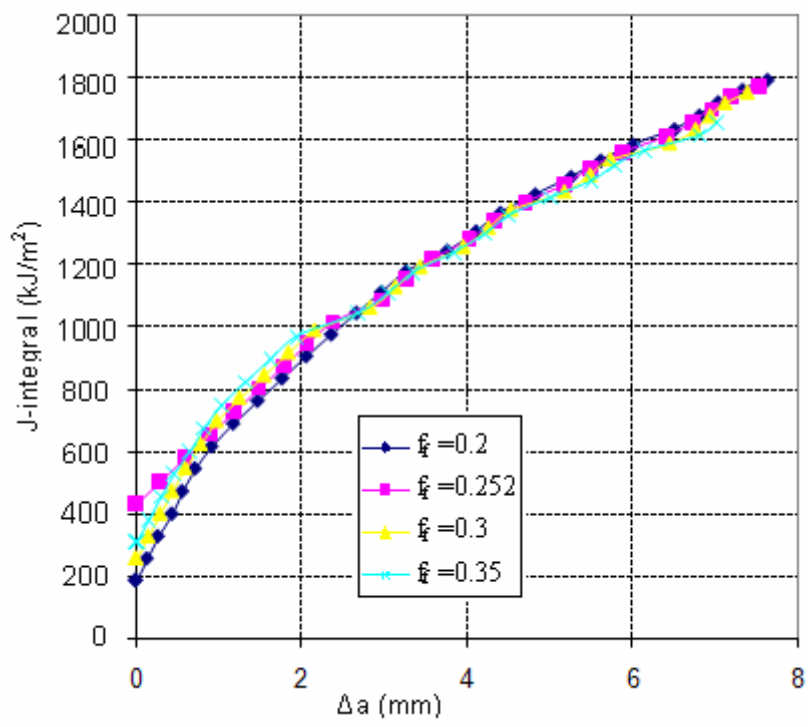

Figure 6.6 J-R curves for different f_f values

	ΔD	Slope Load-ΔD	Ji	Slope J-R
f_f =0.2	1.3758	16.5	187.2626	182.2859
f_f =0.252	1.3760	24.5	431.7313	139.2481
f_f =0.3	1.376	22.5	258.1413	160.2185
f_f =0.35	1.378	18.4	312.5624	149.3879

Table 6.4 Effect of f_f on ΔD (at sudden load drop), Slope Load-ΔD, Ji (initiation) and slope of J-R curve

6.10 Effect of mean strain of void nucleation (ε_n):

It is determined by conducting tensile tests & subsequent metallographic examination. The Figure 6.1 clearly shows the effect of mean strain of void nucleation on load dropping point for notched tensile specimens. With increase in values of ε_n there is decrease in slope of load- ΔD curve. The effect of ε_n is more prominent in J-R curve as shown in Figure 6.2. The study reveals that the J-initiation first decreases and then increases with increase in ε_n and the slope changes significantly with changing this parameter. Table 6.1 gives the ΔD (at sudden load drop), Slope Load-ΔD, Ji (initiation) and slope of J-R curve for different values of ε_n

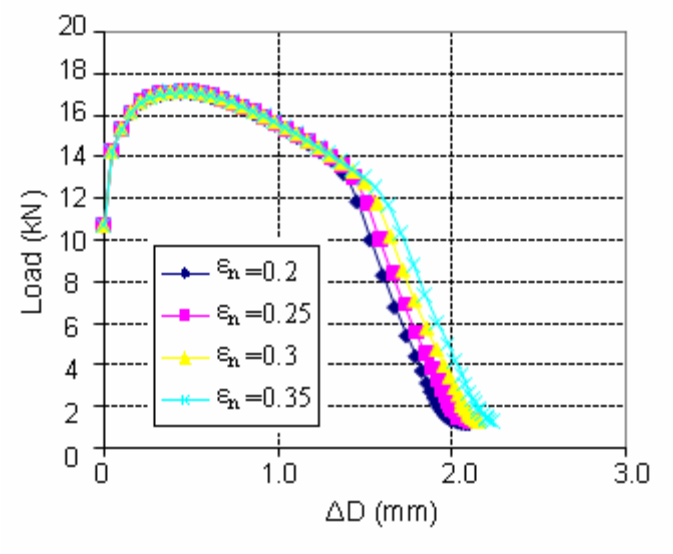

Figure 6.7 Load-ΔD curves for different ε_n values

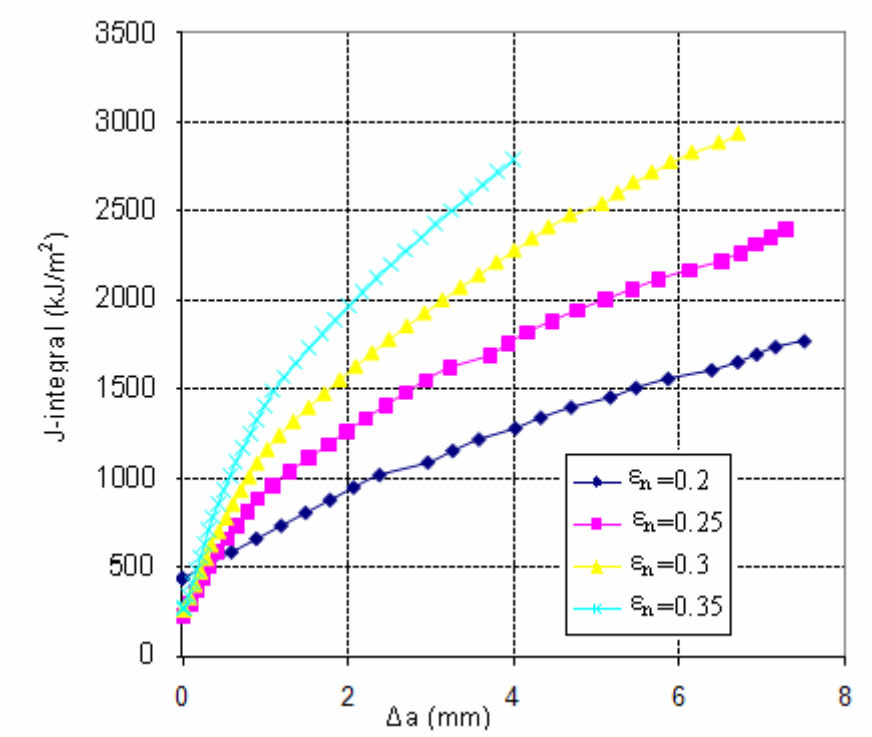

Figure 6.8 J-R curves for different ε_n values

	ΔD	Slope Load-ΔD	Ji	Slope J-R
ε_n =0.2	1.44	20.1	431.7313	139.2481
ε_n =0.25	1.50	18.9	219.0257	313.0222
ε_n =0.3	1.57	18.7	259.5757	456.4039
ε_n =0.35	1.64	18.3	263.7476	764.0117

Table 6.5 Effect of ε_n on ΔD (at sudden load drop), Slope Load-ΔD, Ji (initiation) and slope of J-R curve

6.11 Effect of standard deviation of nucleation strain 'S_N':

The process of nucleation follows statistical distribution. Chu & Needleman suggested a Gaussian distribution for the instantaneous volume fraction of nucleated voids with different values of strain. ε_N represents mean strain of this nucleation & S_N represents the standard deviation of nucleation strain. S_N is assumed generally as 0.1 for steel. It represents the scatter of nucleation strain. It can be determined from metallographic study of nucleation process of voids & finding the statistical distribution. The Figure 6.1 clearly shows

the effect of standard deviation of nucleation strain on load dropping point for notched tensile specimens. With increase in values of S_n there is decrease in slope of load- ΔD curve. The effect of S_n on J-R curve as shown in Figure 6.2. The study reveals that the J-initiation changes significantly with change in S_n. Table 6.1 gives the ΔD (at sudden load drop), Slope Load-ΔD, Ji (initiation) and slope of J-R curve for different values of S_n

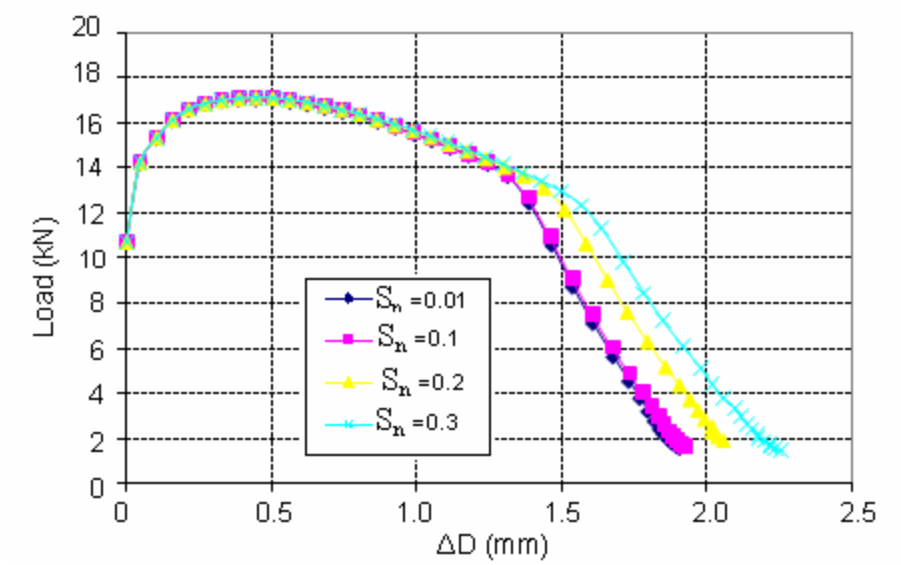

Figure 6.9 Load-ΔD curves for different S_n values

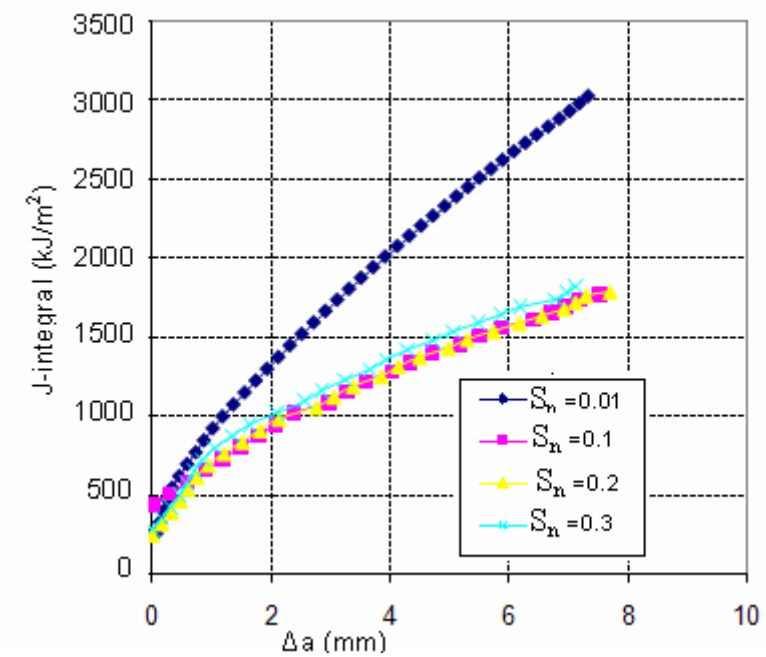

Figure 6.10 J-R curves for different S_n values

	ΔD	Slope Load-ΔD	Ji	Slope J-R
S_n =0.01	1.391	20.4	255.4546	384.2448
S_n =0.1	1.392	19.3	431.7313	139.2481
S_n =0.2	1.43	17.6	252.5209	168.8664
S_n =0.3	1.57	17.7	279.9193	176.784

Table 6.6 Effect of S_n on ΔD (at sudden load drop), Slope Load-ΔD, Ji (initiation) and slope of J-R curve

6.12 Effect of void volume fraction at saturated nucleation, 'f_N'

Effect of void volume fraction at saturated nucleation is shown in Figure 6.11 & 6.12. Overall effect of f_N on ΔD (at sudden load drop), Slope Load-ΔD, Ji (initiation) and slope of J-R curve is given in Table 6.7. slope of Load- ΔD curve increases with increase in value of f_N and load dropping point decreases slightly, while both Ji and slope of J-R decreases with increase in f_N value.

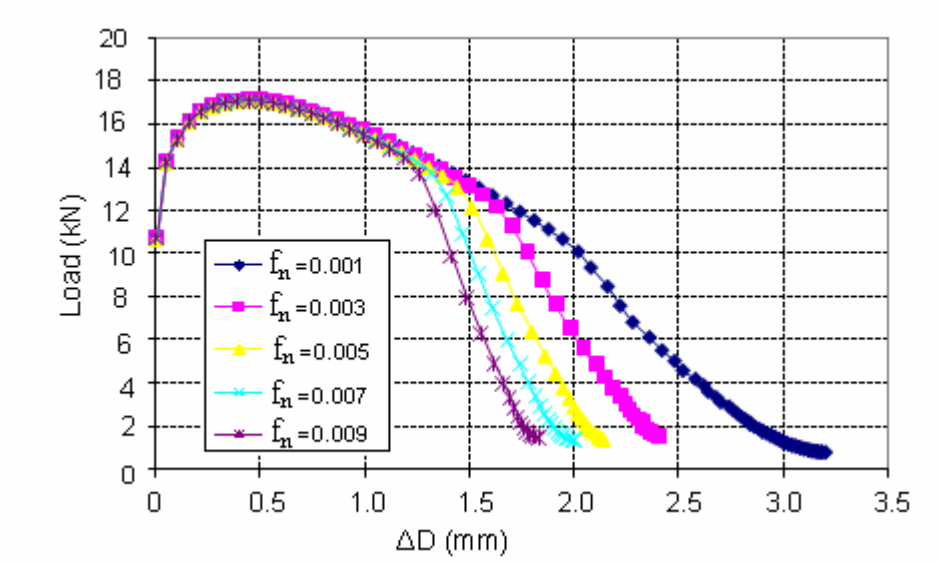

Figure 6.11 Load-ΔD curves for different f_n values

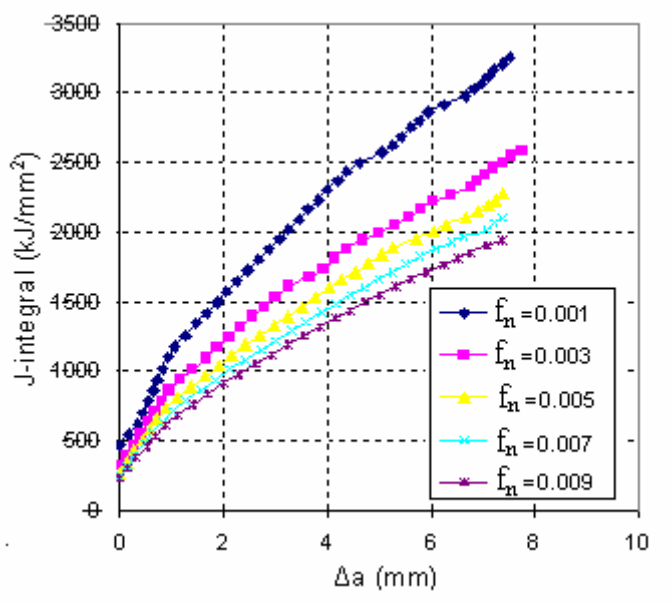

Figure 6.12 J-R curves for different f_n values

	ΔD	Slope Load-ΔD	Ji	Slope J-R
f_n =0.001	1.95	9.7	457.1532	399.568
f_n =0.003	1.63	12.9	313.4159	326.5016
f_n =0.005	1.51	19.8	270.5932	261.4581
f_n =0.007	1.322	29.76	244.811	232.7431
f_n =0.009	1.26	31.05	226.6186	215.55

Table 6.7 Effect of f_n on ΔD (at sudden load drop), Slope Load-ΔD, Ji (initiation) and slope of J-R curve

6.13 Determination of damage parameters from experimental and analytical load- ΔD curves

Effect of various damage parameters on Load-ΔD curve was studied in previous sections. Now the Gurson parameters for the German steel are to be found using experimental and analytical load- ΔD curves of RNTS R2 & R4 by curve fitting of analytical curve to experimental curve by varying Gurson parameters.

6.13.1 Curve fitting of RNTS R2

The experimental and analytical load- ΔD curves for different values of Gurson parameters are shown in following Figure 6.13, 6.14, 6.15, 6.16 & 6.17.

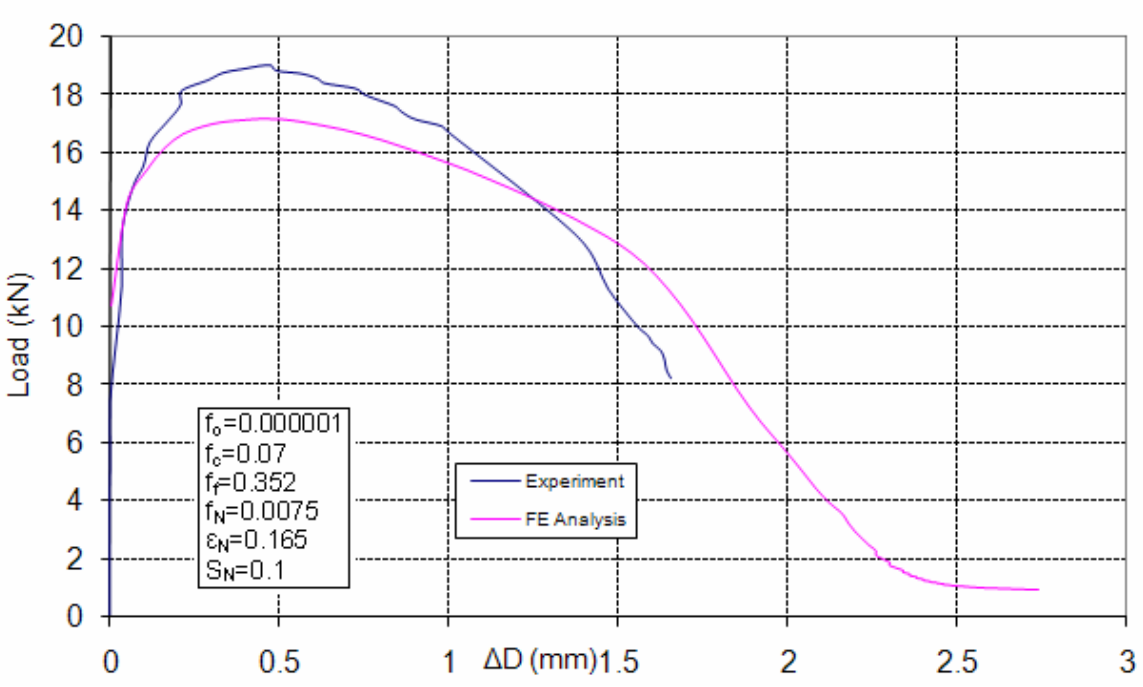

Figure 6.13 Experimental and Analytical load- ΔD curves for RNTS R2

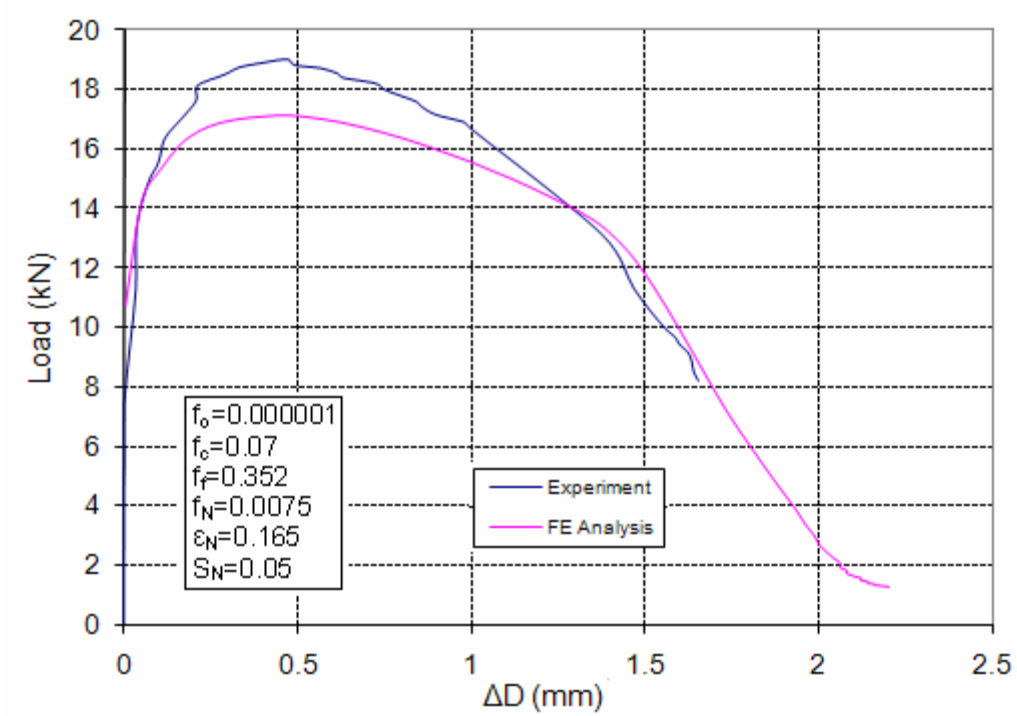

Figure 6.14 Experimental and Analytical load- ΔD curves for RNTS R2

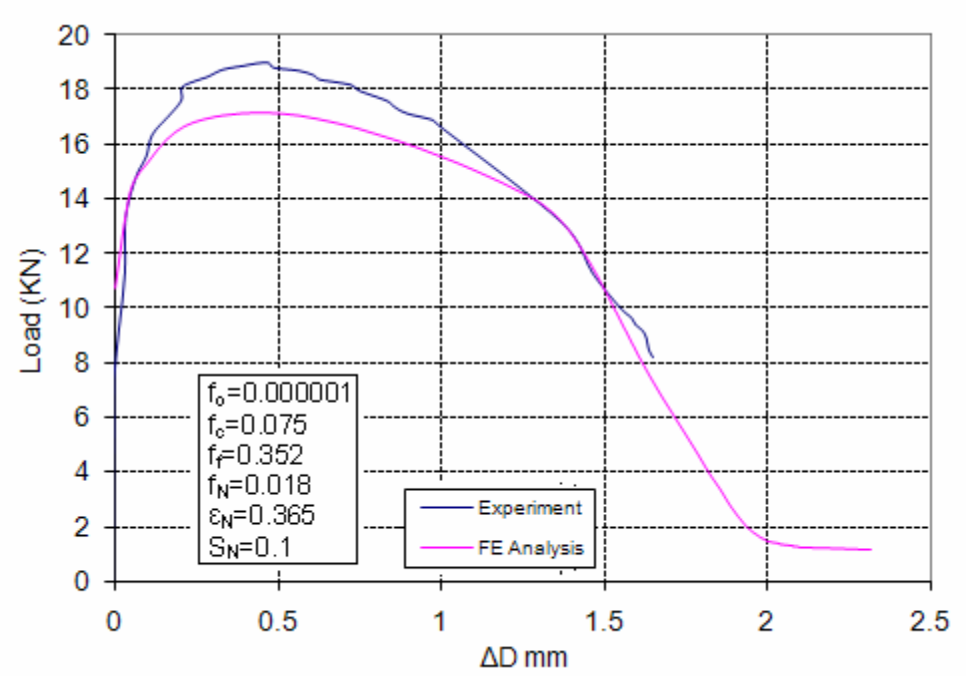

Figure 6.15 Experimental and Analytical load- ΔD curves for RNTS R2

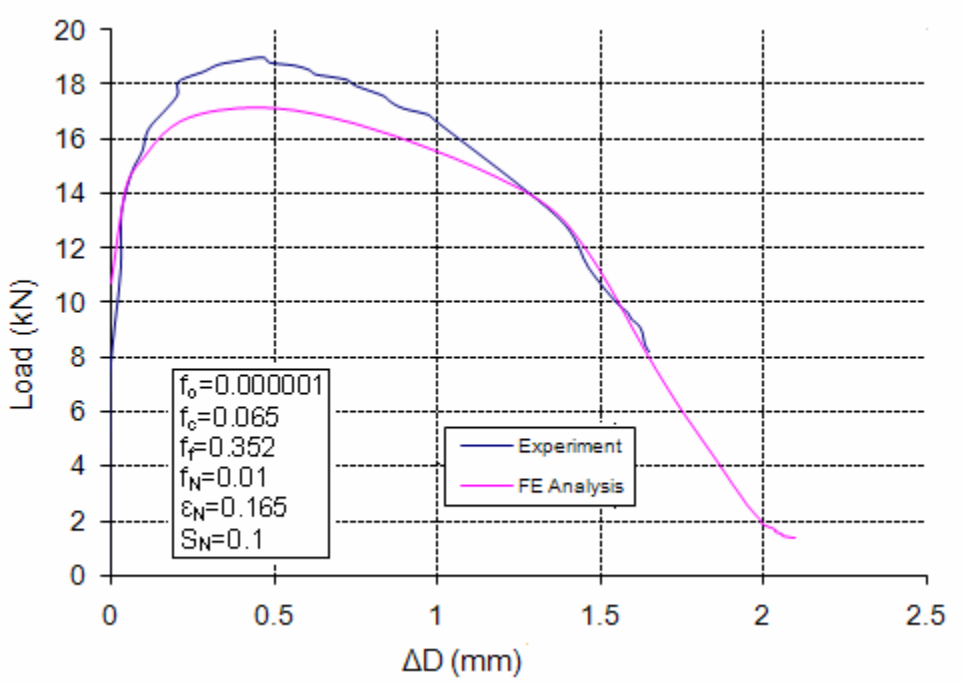

Figure 6.16 Experimental and Analytical load- ΔD curves for RNTS R2

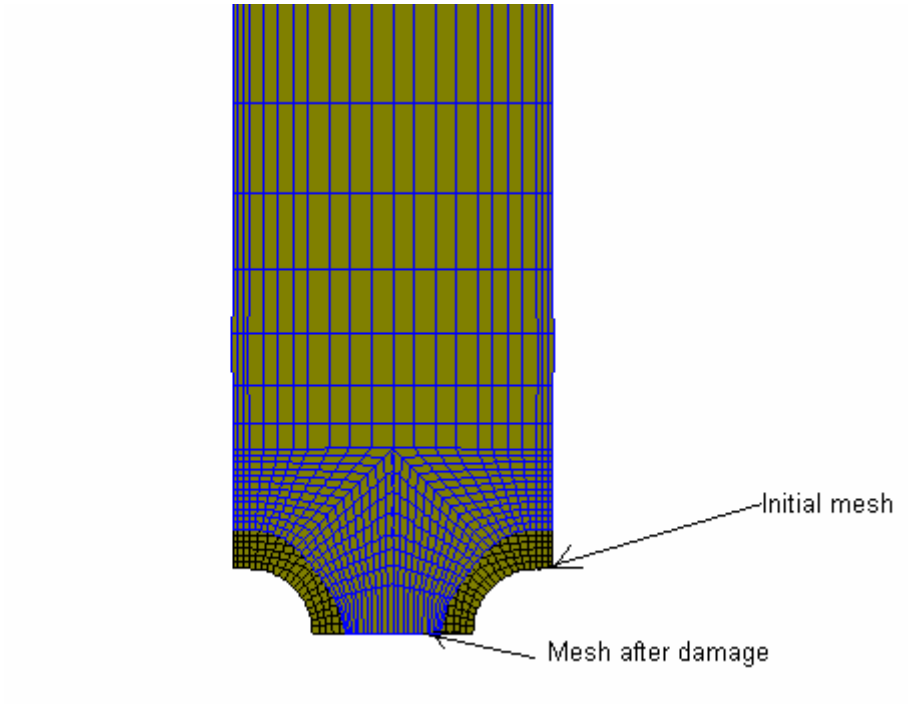

Figure 6.17 FEM mesh of RNTS R2 at load 2.2 KN and displacement 1.8mm

In case of Figure 6.16 analytical load- ΔD curve best approximate the experimental one, so from here we get set of parameters those can best describe the material behaviour.

Gurson parameters	Value
Initial void volume fraction, 'f_o'	0.000001
Critical void volume fraction, 'f_c'	0.065
Final void volume fraction, 'f_f'	0.352
Void volume fraction at saturated nucleation, 'f_N'	0.01
Mean value of strain for nucleation, 'ε_N'	0.165
Standard deviation of strain for nucleation, 'S_N'	0.1
'q_1' Modifying parameters 'q_2' 'q_3'	1.5 1.0 2.25
Critical length parameters 'l_c'	0.2
Modified ultimate void volume fraction 'f_u'	0.566

Table 6.8 Set of Gurson parameters that best approximate material behaviour for R2

6.13.2 **Curve fitting of RNTS R4**

The experimental and analytical load-ΔD curves for different values of Gurson parameters are shown in following Figure 6.18 & 6.19.

In case of RNTS R4 figure 6.19 analytical load- ΔD best matches the experimental one, so from here we take third set of Gurson parameters those best describes the material behaviour.

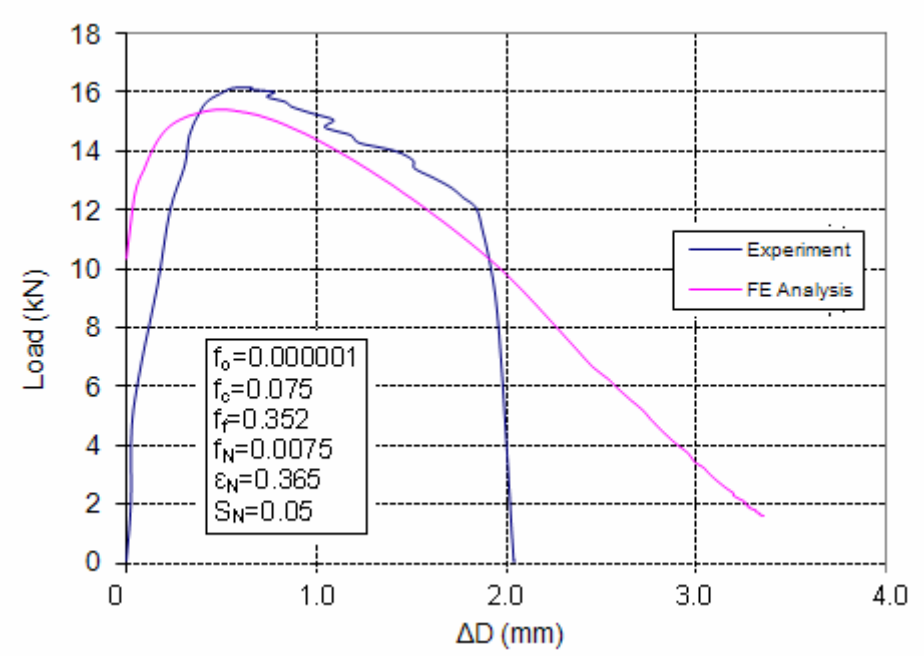

Figure 6.18 Experimental and Analytical load- ΔD curves for RNTS R4

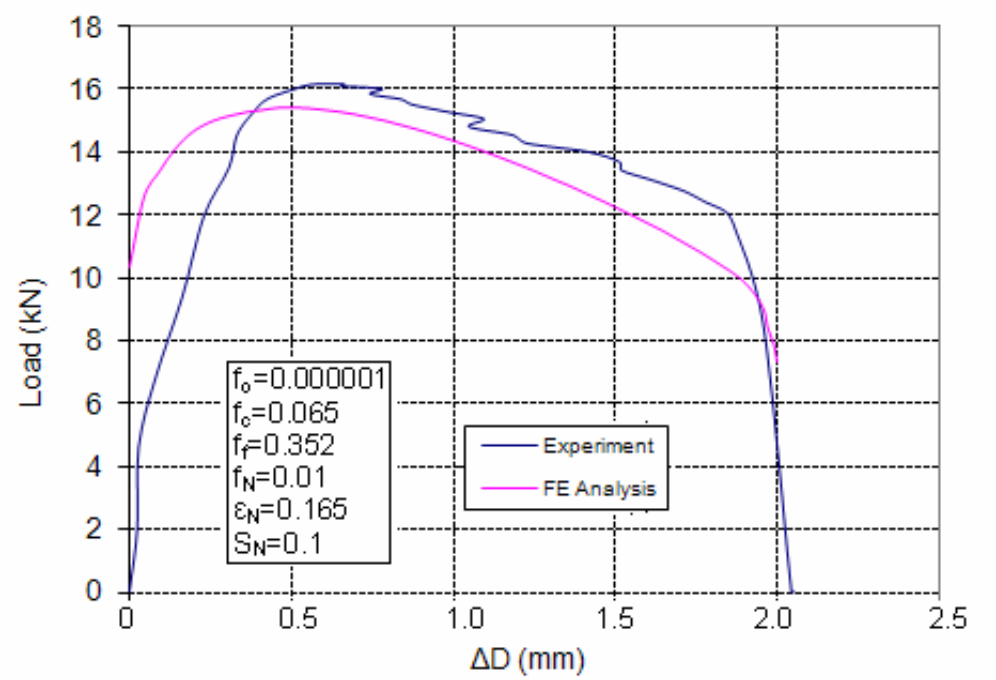

Figure 6.19 Experimental and Analytical load- ΔD curves for RNTS R4

Gurson parameters	Values
Initial void volume fraction, 'f_o'	1.0E-06
Critical void volume fraction, 'f_c'	0.065
Final void volume fraction, 'f_f'	0.35
Void volume fraction at saturated nucleation, 'f_N'	0.01
Mean value of strain for nucleation, 'ε_N'	0.175
Standard deviation of strain for nucleation, 'S_N'	0.1
'q_1'	1.5
Modifying parameters 'q_2'	1.0
'q_3'	2.25
Critical length parameters 'l_c'	0.2
Modified ultimate void volume fraction 'f_u'	0.566

Table 6.9 Set of Gurson parameters that best approximate material behaviour for R4

From above analysis the values of Gurson parameters those best approximate material behavior for R2 & R4 are almost same. So final set of Gurson parameters is given in Table 6.10.

Gurson parameters	Values
Initial void volume fraction, 'f_o'	1.0E-06
Critical void volume fraction, 'f_c'	0.065
Final void volume fraction, 'f_f'	0.352
Void volume fraction at saturated nucleation, 'f_N'	0.01
Mean value of strain for nucleation, 'ε_N'	0.165
Standard deviation of strain for nucleation, 'S_N'	0.1
'q_1' Modifying parameters 'q_2' 'q_3'	1.5 1.0 2.25
Critical length parameters 'l_c'	0.2
Modified ultimate void volume fraction 'f_u'	0.566

Table 6.10 Final set of Gurson parameters that best approximate material behaviour

CHAPTER 7

VERIFICATION OF GURSON PARAMETERS

7.1 Experimental vs Analytical J-R curves for CT specimen

Analytical vs Experimental J-R curves are shown in following figures for CT specimens for final set of Gurson parameters determined for the material.

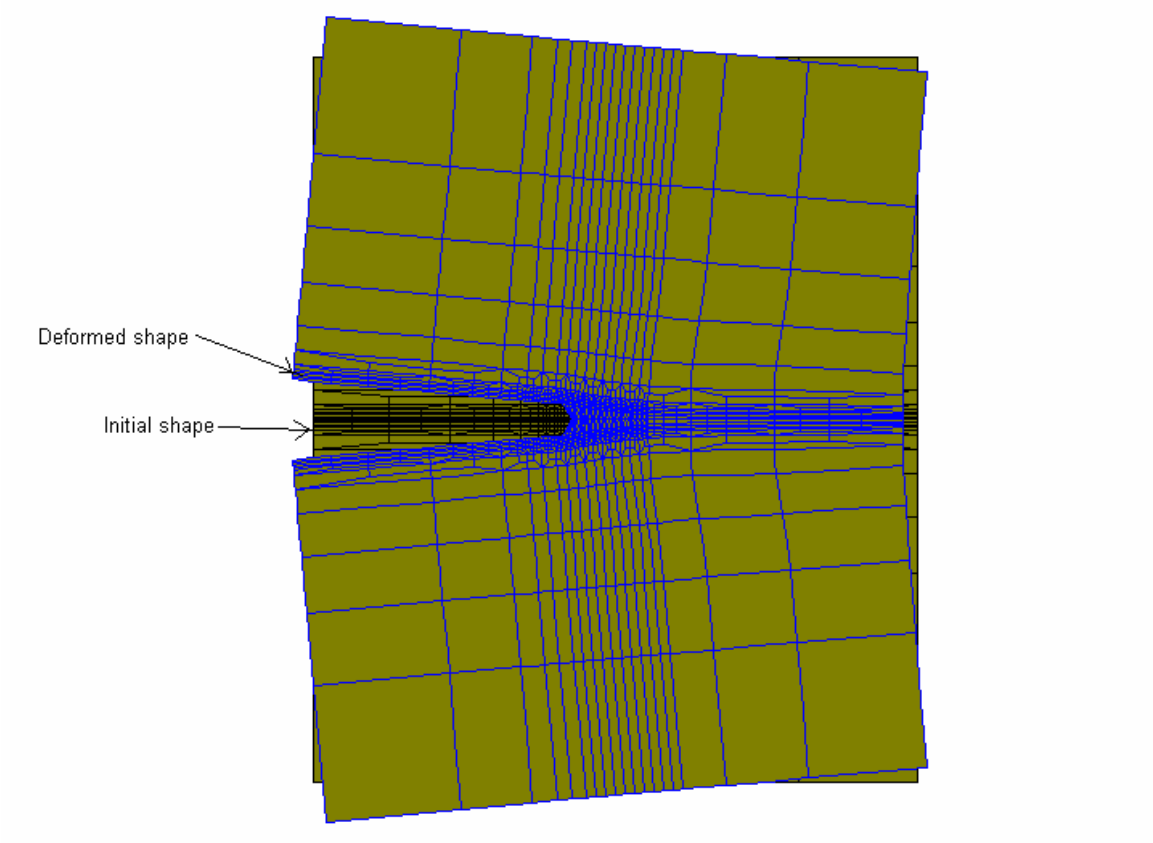

Figure 7.1 FEM mesh of CT specimen at load 3.32 KN and CTOD 3mm

As from Figure 7.2 analytical J-R curve for CT specimen nearly matches the experimental J-R curves. Similar check is also done for Three Point Bend (TPB) specimen as shown in figure 7.3. Here also analytical J-R curve approximates the experimental J-R curve . So the determined set of Gurson Parameters best describe the material damage behavior and can be used to model real life components of this material.

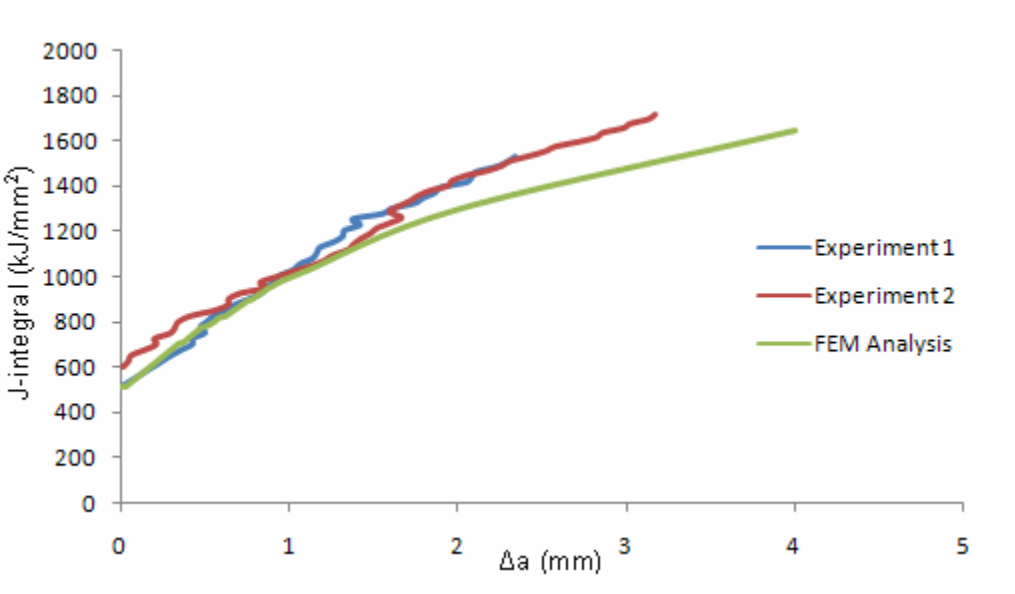

Figure 7.2 Experimental vs Analytical J-R curves for CT Specimen for final set of Gurson parameters

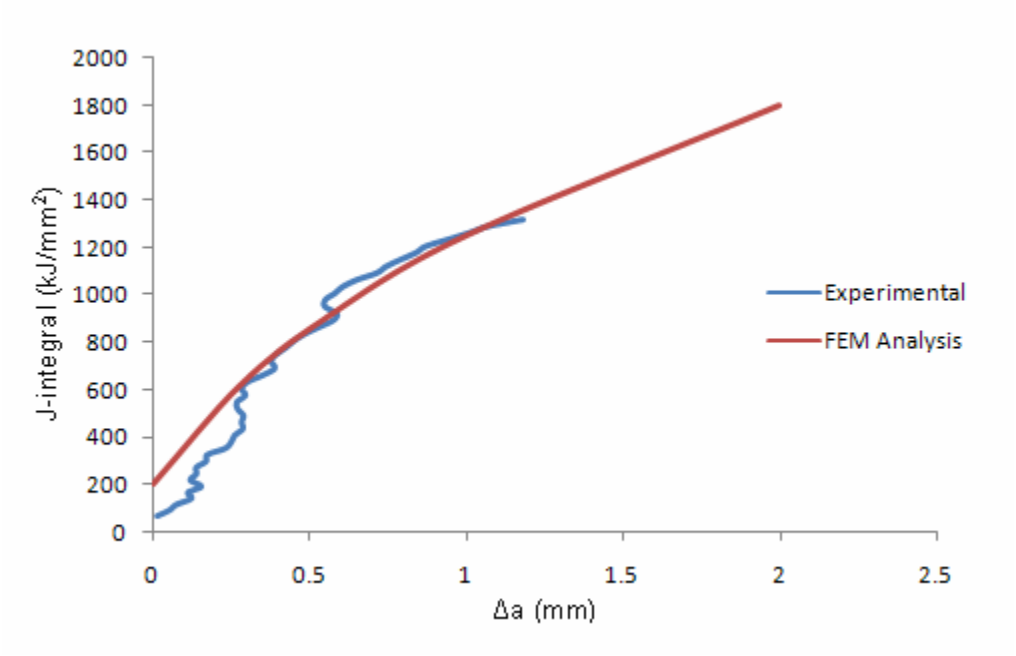

Figure 7.3 Experimental vs Analytical J-R curves for TPB Specimen for final set of Gurson parameters

Superimpose of initial and damaged finite element mesh of CT and TPB specimens are shown in Figure7.1 and Figure 7.4 for particular load and CMOD value

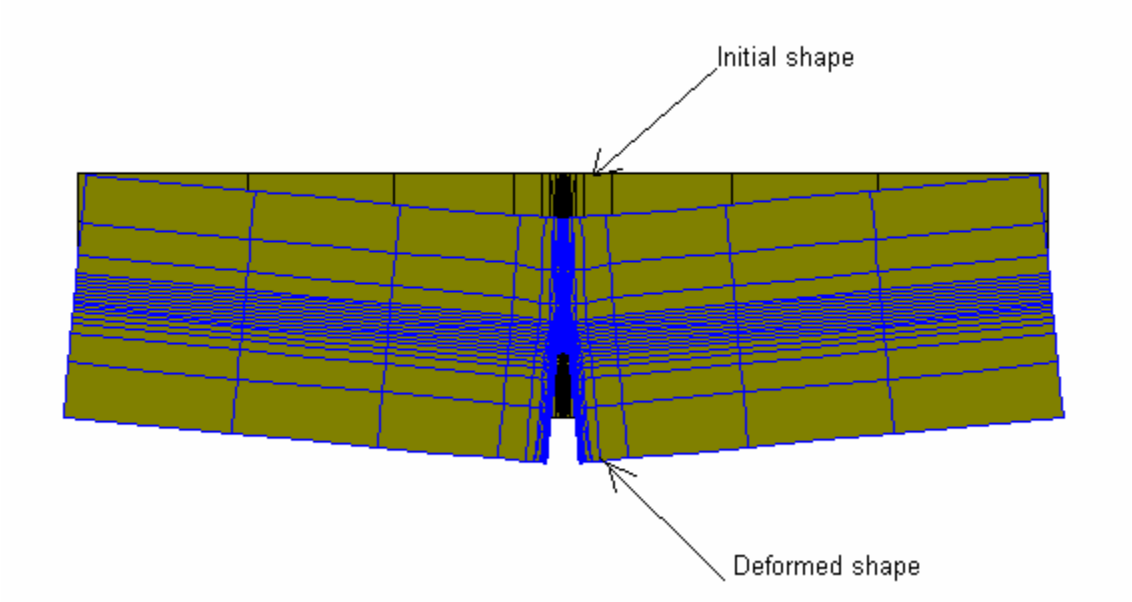

Figure 7.4 FEM mesh of TPB specimen at load 1.3KN and CTOD 2.95mm

CHAPTER 8

CLOSURE

8.1 Conclusions

The work done in thesis leads to following conclusions

1. The values of Gurson parameters for 20MnMoNi55 steel are found these can be used to model any real life component for fracture toughness calculations.
2. The effect of Gurson parameters is also studied.on Load-diametral contraction and J-R curves.

8.2 Recommendations for Future Work

1. The parameters determined from present work can be further checked on real life components to confirm their credibility.
2. In this work mesh size is kept unchanged, so the effect of mesh size on model should be studied and correlation with other factors may be developed to remove mesh dependency completely. This will help modeling with larger mesh size, which in term will reduce valuable computational time.
3. In this work only 2D models are studied, so further work could be done using 3D models.
4. As this work is done at room temperature, so temperature effect can also be studied.
5. In this work Gurson parameters are determined for 20MnMoNi55 steel so the same work could be done for other materials.

REFERENCES

[1] **Griffith, A.A**., “The phenomena of rupture and flow in solids”, Philosophical Transactions, Series A, Vol. 221, 1920, pp163-198

[2] **Irwin, G.R**., “Fracture Dynamics”, Fracturing of Metals, American society of metals, Cleveland, 1948,p 147-166

[3] **Rice J.R.**,” a path independent integral and approximate analysis of strain concentration by notches and cracks”, Journal of Applied Mechanics, Vol.35, 1968, pp379-386

[4] **Gurson A.L.** (1975) Plastic flow and fracture behavior of ductile materials incorporating void nucleation,

[5] **Gurson A. L.** (1977) Continuum theory of ductile rupture by void nucleation and growth: part I-yield

[6] **Tvergaard V**. (1981) Influence of voids on shear band instabilities under plane strain conditions. *Int.* J.

[7] **Tvergaard V.** (1982) On localization in ductile materials containing spherical voids. *Znt.* J. of *Fract.*

[8] **Tvergaard V. and Needleman A**. (1984) Analysis of the cup-cone fracture in a round tensile bar. *Acta Metall. 32,* 157-169.

[9] **Thomason P. F.** (1990) *Ductile Fracture of Metals.* Pergamon Press, Oxford.

[10] **Brocks W.** (1995) *Numerical round robin on micromechanical models (Phase!) .* IWM Reports T 8/95, FhIWM Freiburg, Germany

[9] **TARAFDER S., RANGANATH V. R., SIVAPRASAD S. and JOHRI P.,** "Ductile fracture behaviour of primary heat transport piping material of nuclear reactors", Sadhana, Volume 28, part 1 & 2, February/April 2003, Pages 167–186.

[12] **Xiaosheng Gao , Jinkook Kim,** " Modeling of ductile fracture: Significance of void coalescence", Department of Mechanical Engineering, The University of Akron, 302 Buchtel Mall, Akron, OH 44325, USA

[13**] Alan T. Zehnder,** "Lecture Notes on Fracture Mechanics", Dept. of Theoretical and Applied Mechanics, Cornell University, Ithaca, NY 14853 (607) 255-9181

[14] **ZHANG Z. L.**, "A sensitivity analysis of material parameters for the Gurson constitutive model", SINTEF Materials Technology, N-7034 Trondheim, Norway.

[15] **Chattopadhyay J., Dutta B.K. and Kushwaha H.S.** , "Evaluation of J-R Curve of Throughwall Cracked Elbow Under In-plane Bending Moment " RSD, Hall-7, Bhabha Atomic Research Centre, Mumbai - 400085, India

[16] **Chattopadhyay J. a,*, Kushwaha H.S. a, Roos E. b, "**Some recent developments on integrity assessment of pipes and elbows" Part II: Experimental investigations a Reactor Safety Division, Hall-7, Bhabha Atomic Research Centre, Mumbai 400085, India ,b Material Testing Institute, MPA, Pfaffenwaldring 32, University of Stuttgart, D-70569 Stuttgart, Germany

[17] **Chattopadhyay J.*, Pavankumar T.V., Dutta B.K., Kushwaha H.S.,** "Fracture experiments on through wall cracked elbows under in-plane bending moment: Test results and theoretical/numerical analyses" 'Reactor Safety Division, Hall-7, Bhabha Atomic Research Center, Mumbai 400085, India

[18] **Nedjar B.,** "Elastoplastic-damage Modelling including the gradient of damage: formulation and computational aspects", International Journal of Solids and Structures, Volume 38, Issues 30-31**,** July 2001, Pages 5421-5451.

[19] **Oliver J., Huespe A. E., Pulido M. D. G. and Chaves E., "**Continuum mechanics to fracture mechanics: the strong discontinuity approach", Engineering Fracture Mechanics**,** Volume 69, Issue 2, January 2002, Pages 113-136.

[20] **Benzerga A. A., "**Micromechanics of coalescence in ductile fracture", Journal of the Mechanics and Physics of Solids**,** Volume 50, Issue 6, June 2002, Pages 1331-1362.

[21] **Righiniotis T. D., Omer E. and Elghazouli A. Y.,** "A simplified crack model for weld fracture in steel moment connections", Engineering Structures**,** Volume 24, Issue 9, September 2002, Pages 1133-1140.

[22] **Schnack E., and Weikl W., "**Shape optimization under fatigue using continuum damage mechanics", Computer-Aided Design**,** Volume 34, Issue 12, October 2002, Pages 929-938.

[23] **Chang C. S., Wang T. K., Sluys L. J. and Mier J. G. M.,** "Fracture modeling using a micro-structural mechanics approach—I. Theory and formulation", Engineering Fracture Mechanics **,**Volume 69, Issue 17, November 2002, Pages 1941-1958.

[24] **Chang C. S., Wang T. K., Sluys L. J. and Mier J. G. M., "**Fracture modeling using a micro-structural mechanics approach—II. Finite element analysis", Engineering Fracture Mechanics**,** Volume 69, Issue 17, November 2002, Pages 1959-1976.

[25] **Yatomi M., Nikbin K. M., and O'Dowd N. P., "**Creep crack growth prediction using a damage based approach", International Journal of Pressure Vessels and Piping, Volume 80, Issues 7-8, July-August 2003, Pages 573-583.

[26] **Besson J., Steglich D. and Brocks W., "**Modelling of plane strain ductile rupture", International Journal of Plasticity, Volume 19, Issue 10, October 2003, Pages 1517-1541.

[27] **Yingbin Bao and Tomasz Wierzbicki, "**fracture locus in the equivalent strain and stress triaxiality space", International Journal of Mechanical Sciences, Volume 46, Issue 1, January 2004, Pages 81-98.

[28] **Kim Jinkook, Gao Xiaosheng and Srivatsan T. S., "**Modeling of crack growth in ductile solids: a three-dimensional analysis", International Journal of Solids and Structures, Volume 40, Issue 26, December 2003, Pages 7357-7374.

[29] **Einav I., Houlsby G.T. and Nguyen G.D.**, "Coupled damage and plasticity models derived from energy and dissipation potentials", International Journal of Solids and Structures**,** Volume 44, Issues 7-8, April 2007, Pages 2487-2508.

[30] **Roylance David,** "Introduction to Fracture Mechanics", Department of Materials Science and Engineering, Massachusetts Institute of Technology, Cambridge, MA 02139 June 14, 2001

[31] **Wang C.H** ."Introduction to Fracture Mechanics", Airframes and Engines Division, Aeronautical and Maritime Research Laboratory

[32] **TARAFDER S., RANGANATH V R, SIVAPRASAD S and JOHRI P**, "Ductile fracture behaviour of primary heat transport piping material of nuclear reactors", Fatigue & Fracture Group, National Metallurgical Laboratory, Jamshedpur 831 007, India

[33] **Chattopadhayay J**.,"Linear Elastic Fracture Mechanics (LEFM)", Lecture notes on fracture mechanics, RSD. Hall-7, BARC, Mumbai 400085, India

[34] **George E. Dieter**, "Mechanical Metallurgy", university of Maryland